12-16-2020

Development of esterase-sensitive persulfide prodrugs and studies of CO-independent reactivities from ruthenium-based CO-releasing molecules

Zhengnan Yuan

DEVELOPMENT OF ESTERASE-SENSITIVE PERSULFIDE PRODRUGS AND STUDIES OF CO-INDEPENDENT REACTIVITIES FROM RUTHENIUM-BASED CO-RELEASING MOLECULES

by

ZHENGNAN YUAN

Under the Direction of Binghe Wang, PhD

ABSTRACT

As endogenously produced small molecules, hydrogen sulfide (H_2S) and carbon monoxide (CO) have been demonstrated in extensive studies to mediate cellular signaling. More importantly, the therapeutic effects of these small molecules have been validated *in vitro* and *in vivo*. As such, development of H_2S- and CO-based therapeutic agents have attracted great interests in recent years.

H_2S is known to undergo redox transformations in biological systems to produce various sulfur species such as glutathione persulfide (GSSH) and cysteine persulfide (CysSSH). Several studies have indicated the enhanced ability for persulfides to modify protein through S-

persulfidation and to quench reactive oxygen species (ROS) as compared with H_2S. These findings raised the potential importance of persulfide species in as a signaling molecule. Generally speaking, persulfides are not chemically stable for storage under near physiological conditions. This lack of stability presents difficulties in formulating and delivering such molecules for research and therapeutic purposes. In Chapter 1, we describe the development of stable prodrug forms of persulfide for various applications. In doing so, we explored the stability issues of persulfides under near physiological conditions. The biological activities of these prodrugs were also examined and compared with that of H_2S.

In the field of developing CO as therapeutic agent, ruthenium-based CO releasing molecules (CO-RMs), CORM-2 and CORM-3, have been widely used as CO surrogates. However, several previous studies have revealed the ability for such CO-RMs to chemically modify proteins through CO-independent mechanisms, raising concerns of the suitableness for CORM-2, 3 as CO surrogates in biological studies. In Chapter 2, we reported our findings on CO-independent reactivities of CORM-2, 3 toward representative reagents commonly used in various bioassays. These results suggest the need to carefully de-convolute and interpret the biological data from relevant experiments using ruthenium-based CO-RMs as surrogates of CO for probing its biological effects.

INDEX WORDS: Prodrugs, Persulfide species, S-persulfidation, Carbon monoxide, CORM-2, CORM-3

DEVELOPMENT OF ESTERASE-SENSITIVE PERSULFIDE PRODRUGS AND STUDIES OF CO-INDEPENDENT REACTIVITIES FROM RUTHENIUM-BASED CO-RELEASING MOLECULES

by

ZHENGNAN YUAN

A Dissertation Submitted in Partial Fulfillment of the Requirements for the Degree of

Doctor of Philosophy

in the College of Arts and Sciences

Georgia State University

2020

DEVELOPMENT OF ESTERASE-SENSITIVE PERSULFIDE PRODRUGS AND STUDIES OF CO-INDEPENDENT REACTIVITIES FROM RUTHENIUM-BASED CO-RELEASING MOLECULES

by

ZHENGNAN YUAN

Committee Chair: Binghe Wang

Committee: Kathryn Grant

Suazette Reid Mooring

Electronic Version Approved:

Office of Graduate Services

College of Arts and Sciences

Georgia State University

December 2020

DEDICATION

Dedicated to my parents, Hongxia An and Shunde Yuan, who love and support me unconditionally.

Dedicated to my late grandparents, Xiuzhen Li and Yansen An, who I miss so much.

ACKNOWLEDGEMENTS

First of all, I would like to express my sincere gratitude to my advisor, Prof. Binghe Wang. Without his guidance and support, I couldn't be where I am now. Working in the Wang lab make me become a confident and independent scientist. I appreciate everything Prof. Wang did to help me achieve my academic goals. I am so proud that I am one of his students.

I would like to thank my dissertation committee, Prof. Kathryn Grant and Prof. Suazette Reid Mooring. I appreciate your help along my dissertation journey.

I would like to thank Dr. Siming Wang for her help on MS studies.

I would like to thank Dr. Xinhui Lou, who is Prof. Wang's former Ph.D student. Without her recommendation, I couldn't get an interview opportunity.

I would like to thank the financial support from Brain & Behavior fellowship.

I would like to thank all of my research group members for their help and support in the last five years. Drs. Yueqin Zheng and Bingchen Yu, thank you for your hand by hand mentoring during my early lab training. Drs. Shawn Yang and Wen Lv, our research discussions are always fruitful and inspiring. Manjusha, Kim, Ravi, Ce, Shameer, Zach and other lab mates, thank you for your help. All of you make my lab time more enjoyable.

I would like to thank my friends, Ferdoushi, Matt, Dandan, Lingyun, Weiqing, Ananya and Paola, for their support and encouragement.

Last but not the least, I would like to thank my parents for their support. In the last five years, we have only seen each for one time due to the long distance between us. But our connections have never stopped. Thank you for understanding my career goal, I wish you both could be so proud of me.

TABLE OF CONTENTS

LIST OF TABLES

LIST OF FIGURES

LIST OF ABBREVIATIONS

2,4-Dinitrofluorobenzene (DNFB)

Carbon monoxide (CO)

Carboxyhemoglobin (COHb)

CO-releasing Molecules (CO-RMs)

Cysteine persulfide (CysSSH)

Dithiothreitol (DTT)

Glutathione persulfide (GSSH)

Hydrogen sulfide (H_2S)

N-acetyl cysteine (NAC)

N-isobutyl-4-nitrobenzamide (PNB)

Nitric oxide (NO)

p-aminobenzamide (PAB)

Porcine liver esterase (PLE)

Protein post-translational modification (PTM)

Reactive oxygen species (ROS)

1 DEVELOPMENT OF ESTERASE-SENSITIVE PERSULFIDE PRODRUGS

1.1 Introduction

(This chapter is mainly based on my publications: *Org. Lett.* **2018,** *20* (20), 6364-6367, *Chin. J. Nat. Med.* **2020,** *18* (4), 296-307.)

With well-established physiological effects in mammal, Hydrogen sulfide (H_2S) is often referred to as the third gasotransmitter alongside nitric oxide (NO) and carbon monoxide (CO), though some suggest that they be best termed as small signaling molecules. With the first pKa of 6.88 and second pKa of 19, H_2S largely exists in the mono-ionized form under physiological conditions (pH = 7.4, 37 ^oC). H_2S and its ionized forms are easily oxidized in aqueous solution. The oxidation of H_2S is complicated, producing various sulfur species including elemental sulfur, persulfide, polysulfide, sulfite, sulfate, thiosulfate among other possibilities. Among these sulfur species, persulfides are emerging as important regulators in sulfur-related cell signaling. Studies showed more potent activities of persulfides on inducing protein S-persulfidation and quenching H_2O_2 as compared with that from H_2S. For studying the biological significance of persulfide species, there are some important challenges. On one hand, persulfides and thiols exhibit similar chemical reactivities. Tools are needed for selective detection of persulfide, especially, products of S-persulfidation, which is believed to the mechanism for reactive sulfur species (RSS) to participate in cellular signaling processes. On the other hand, persulfides are not chemically stable under near physiological conditions. In order to study their activities in biological systems, a suitable persulfide delivery system is needed. Below we discussed current advances related to these two aspects.

1.1.1 S-persulfidation

Protein post-translational modification (PTM) is important in cellular signaling. In terms of sulfur-related PTM, a cysteine residue of a protein can undergo gluthathionylation,[1-4] S-

sulfenylation[5, 6] and S-persulfidation[7-10] under different biochemical and redox conditions. Up to now, more than 50 proteins have been reported to undergo S-persulfidation as part of PTM, which is one mechanism through which H_2S is involved in cellular signaling.[11, 12]

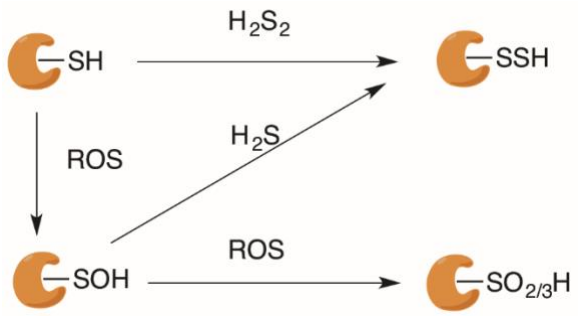

Figure 1.1 The proposed mechanism for protein persulfidation induced by H_2S, ROS and H_2S_2.

From a chemistry perspective, persulfide can form either from the oxidation of thiol species or reduction of polysulfide or other species at a higher oxidation state. Others and we have reported that H_2S_2 can independently induce S-persulfidation on GAPDH.[11, 13, 14] In the presence of ROS, a thiol group can be oxidized to sulfenic acid or further to sulfinic and sulfonic acids (**Figure 1.1**).[9] As a simple reducing agent, H_2S itself can directly react with oxidative species to play the role of a quencher. Small polysulfide molecules can also be reduced by H_2S to produce persulfide. More importantly, several studies demonstrated that H_2S can reduce sulfenic acid to persulfide as a mechanism of reducing oxidative stress since further oxidation to the stage of sulfinic or sulfonic acid would lead to practically irreversible changes (**Figure 1.1**).[15] In the cellular environment, the level of H_2S and persulfidated proteins are strongly correlated with the level of oxidative species such as H_2O_2.

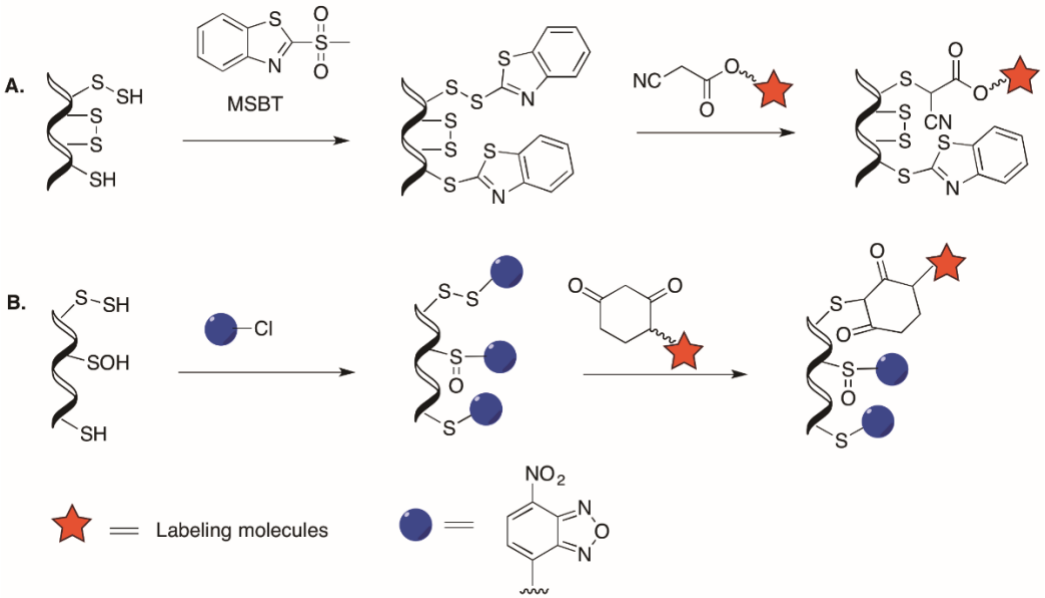

Figure 1.2 Tag-switch methods for persulfide labeling.

In studying protein persulfidation, it is important to be able to selectively capture or identify persulfidation site(s). Along this line, several methods have been developed. Methyl methanethiosulfonate (MMTS) was previously reported to specifically react with thiols rather than persulfides. However, several studies have shown that persulfides can also react with MMTS.[16, 17] Later it was found that this approach is not selective for persulfidation sites. Another strategy to detect persulfides first uses iodoacetic acid (IAA) to react with both of thiol and persulfide residues. Only the disulfide residues formed with IAA can be reduced by dithiothreitol (DTT) to yield the free thiol group, but not the product from thiol and IAA. This two-step process allows for the labeling of the thiol product from DTT reduction, and thus unequivocally identify the persulfidation site. In 2014, Xian and coworkers developed a two-steps tag-switch method for detection of protein S-persulfidation (**Figure 1.2**).[18] In the first step, a thiol-blocking reagent, methylsulfonyl benzothiazole (MSBT) can be used to block thiol and persulfide residues. Then a cleverly designed carbon-based nucleophile, methyl cyanoacetate (MCA) is

used to selectively tag the disulfide intermediate by removing the MSBT moiety. In solution studies, the yield of MCA and a derivative of cysteine disulfide intermediate was shown to be 98%. Using a model protein, bovine serum albumin (BSA), it was shown that the method was able to selectively detect persulfidation modifications among other possibilities such as sulfenic acid (BSA-SOH), thiol (BSA-SH) and glutathionylation modification (BSA-SSG). Further studies in cell lysates using Jurkat cells, elevated levels of persulfidation of Hsp70 and GAPDH were detected after treatment of the cells with H_2S for 30 min. Along a similar line, Filipovic and coworkers developed another tag-switch method for detection of protein persulfidation by using a different blocking reagent and nucleophilic tag molecule (**Figure 1.2**).[15] In their design, 4-chloro-7-nitrobenzofurazan (NBF-Cl) was used to react with sulfur-related nucleophilic species including thiol (-SH), sulfenic acid (-SOH) and persulfide (-SSH). In the next step, dimedone was used to selectively attack the disulfide bond formed between persulfide and NBF-Cl to achieve selective labeling.

1.1.2 Literature persulfide donors

It is very important to note that persulfidation cannot happen with hydrogen sulfide *per se*. It has to be converted to a species at a higher oxidation state, e.g. persulfide. It is believed that increased persulfidation in the presence of hydrogen sulfide is at least partially the result of increased "sulfur pool" and subsequent oxidation to a higher oxidation state, which allows for persulfidation to happen. Alternatively, cysteine thiol can be oxidized to sulfenic acid, which can be converted to persulfidation product by reaction with H_2S (**Figure 1.1**). Then there is the question of whether delivering sulfur species at the persulfide state would offer more efficient persulfidation in solution, *in vitro*, and *in vivo.* With such thinking in mind, there have been efforts in making prodrugs and donors of persulfides.

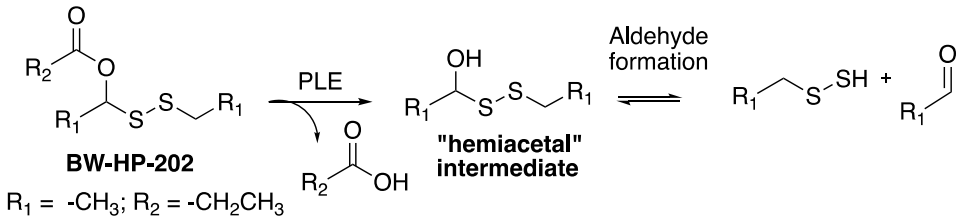

Figure 1.3 Esterase-sensitive persulfide prodrugs.

A series of esterase-sensitive persulfide prodrugs was developed in our lab (**Figure 1.3**) by taking advantages of an unstable "hydroxymethyl disulfide" intermediate.[16] After the removal of the ester masking group from the donor, the persulfide is released from the decomposition of the "hemiacetal" intermediate. By varying the steric hindrance on the masking ester group, we were able to tune the half-lives of the prodrugs from 12 to 145 s in the presence of 1 U PLE/mL. For analysis of the release yield, persulfide was directly trapped by an electrophile, dinitrofluorobenzene (DNFB), to give yields in the range of 82% to 92%. Models of heart myocardial infarction reperfusion (MI/R) injury are commonly used to assess the effectiveness of sulfur donors in reducing damage size as measured by infarct size per area-at-risk ratio. In assessing the effectiveness of the persulfide donors described, it was found that treatment with 50-100 μg kg^{-1} of the prodrug **BW-HP-202** was able to significantly decrease the infarct size per area-at-risk.

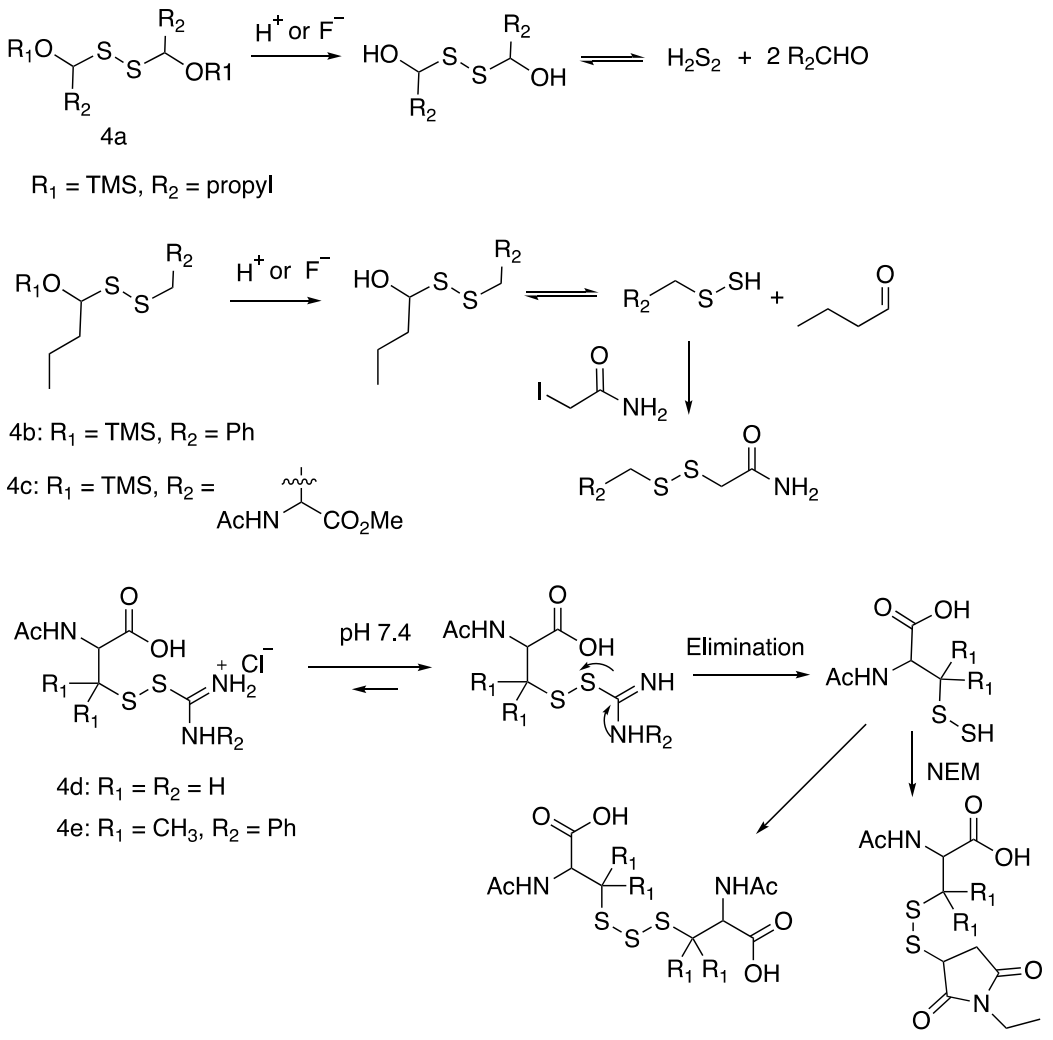

Figure 1.4 pH- and fluoride-sensitive persulfide prodrugs.

Xian and coworkers also utilized an unstable "hydroxy methyl" disulfide intermediate to release persulfides (**Figure 1.4**).[19] Specifically, TMS and TES protecting groups were used as acid- or fluoride-sensitive moieties. In DMF/PBS buffer (4:1), at pH 7.4, for prodrug **4a**, the total decomposition required 10 h, while at pH 2.5, it required 2.5 h to achieve total consumption of the prodrug. Persulfide trapping with iodoacetamide in pure methanol was used. In the presence of KF, the trapping yields for benzyl and protected cysteine persulfides from donor **4b** and **4c** were 94% and 38% respectively. Toscano presented a precursor of modified cysteine persulfide

based on S-substituted-thioisothioureas.[20] The terminal sulfhydryl moiety of the persulfide was protected in a S-alkylthioisothiourea form. Under physiological conditions, the precursor **4d** was designed to initiate deprotonation followed by an elimination reaction to produce persulfide and thiourea derivative (**Figure 1.4**). However, the persulfide seemed to prefer undergoing a trapping reaction with itself instead of the trapping reagent, *N*-ethylmaleimide (NEM). To overcome self-trapping, a gem-dimethyl moiety was installed next to the inner sulfur atom to prevent the self-perturbation of persulfide species. Then the persulfide trapping yield of prodrug **4e** improved to 96% with 20 mM NEM in pH 7.4 PBS buffer containing 10% D_2O.

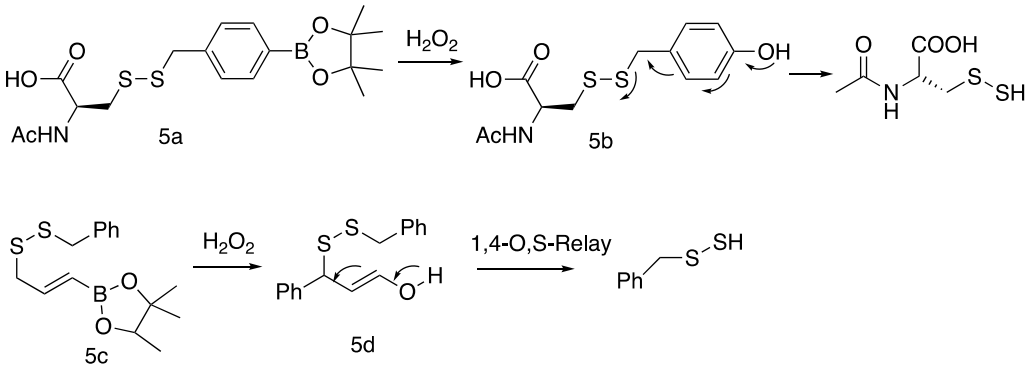

Figure 1.5 ROS-sensitive persulfide prodrugs.

Several ROS-sensitive persulfide prodrugs have also been reported. Matson and coworkers used an 1,6-elimination system to release *N*-acetyl cysteine (NAC) persulfide (**Figure 1.5**).[21] An aryl boronic ester was used as a latent hydroxyl group, generation of which is dependent on reaction with H_2O_2. Further, the formation of the hydroxyl group initiates self-immolation, leading to NAC persulfide and *p*-hydroxy-benzyl alcohol. The NAC persulfide was directly detected by LC-MS. 200 μM of the donor **5a** was shown to improve cell survival of H_2O_2-induced death from 30% to 100%. It should be noted that the control compound, which only contains aryl boronic ester group, was also able to increase the cell viability to around 70%.

Chakrapani and co-workers also reported a ROS-sensitive benzylpersulfide donor using the boronate approach. Upon removal of the vinyl boronate ester by H_2O_2, the unstable enolate intermediate **5d** can undergo a 1,4-O,S-relay to generate benzyl persulfide and byproduct cinnamaldehyde (**Figure 1.5**).[22] In the presence of 10 equiv of H_2O_2, the decomposition rate constant of donor **5c** was determined to be 5.3×10^{-2} min^{-1}. However, it was suggested that byproduct cinnamaldehyde could also react with benzyl persulfide, complicating the interpretation of the results somewhat. The donor (**5c**) was also examined on its protective effects toward DLD-1 cells under oxidative stress. In the presence of 50 μM of an oxidative stress inducer, menadione, 100 μM of **5c** increased the cell viability from 30% to 70%. The control compound, which only bears the aryl boronic ester group, did not show any protective effect.

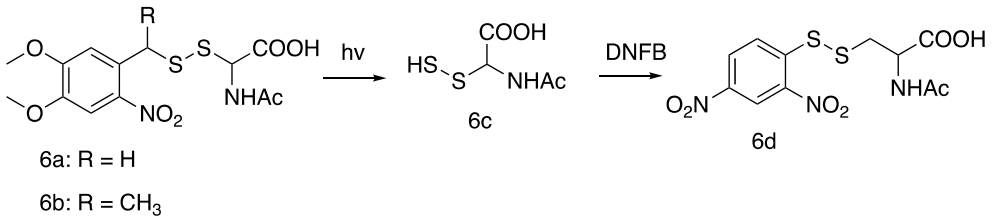

6a: R = H

6b: R = CH_3

6c

6d

Figure 1.6 Photo-sensitive persulfide prodrugs.

Singh and coworkers reported a strategy to develop photo-sensitive persulfide prodrugs by using a well-known ortho-nitrobenzyl (ONB) phototrigger.[23] As shown in **Figure 1.6**, the terminal sulfhydryl group on NAC persulfide was protected by ONB. Upon light irradiation ($\lambda \geq$ 365 nm), ONB group was removed from prodrugs **6a** and **6b** followed by the release of NAC persulfide. The decomposition of **6a** and **6b** was studied in ACN/PBS (3:7) by HPLC; and their quantum yields were determined to be 0.07 and 0.36 respectively. In order to quantify the release of NAC persulfide from the prodrugs, DNFB was used as a direct trapping agent. In the presence

of 5 mM DNFB, 57 and 59 μM of NAC persulfide were detected from prodrugs **6a** and **6b,** respectively, after photolysis. The prodrugs were further examined for their anti-oxidation ability. Under light irradiation for 30 min, incubation of 200 μM of **6a** with Hela cells increased cell viability from 50% to 70% after H_2O_2 treatment.

Overall, a good number persulfide prodrugs with triggered release have been reported in recent years. Most of them have been examined for their anti-oxidation effect at the cellular level, suggesting improved protective effects over that of the corresponding thiol.

1.1.3 Current challenges in developing persulfide prodrugs

Although, several persulfide donors have been reported with demonstrated biological activities, there are still some issues remaining to be resolved. First, for distinct biologically relevant persulfides (GSSH, CysSSH), no donor is available for studying their activities. GSSH was said to be the most abundant persulfide species in the physiological environment, and was shown to have strong H_2O_2-scavenging ability.[24] It might imply the importance of GSSH in cellular antioxidant defense. Currently, the generation of GSSH mostly depends on redox reactions involving H_2S with GSSG.[25, 26] However, the presence of H_2S in the mixture limits their applications for exploring functions of GSSH other than H_2S. Tools are needed for delivering pure GSSH to biological systems. Second, the stability of persulfide species has not been studied under physiological conditions. Understanding the stability and degradation profiles of persulfides would be important for answering the questions related to their mechanism of actions.

In this chapter, we discussed our efforts in developing a general prodrug strategy to store and deliver GSSH and various other persulfides for helping understand the above-referenced issues.

1.2 Results and discussions

1.2.1 Design of a GSSH prodrug

To prepare a donor of unprotected GSSH, one key issue is developing a synthetic route, which can tolerate the free amino and carboxylic group. Thus, we first built a reactive disulfide bond by treating GSH with 2,2'-dipyridyldisulfide,[27] which was further treated with thiol acid BW-HP-101 to afford GSSH donor **BW-GP-401**(**401**), a stable odorless white powder (**Figure 1.7, see Experimental part**). Using this route, we protected the outer sulfur of the persulfide group, and caged it as a thioester, which has an esterase-sensitive trigger using a "trimethyl lock" system.[28] After the removal of the protecting group by an esterase, the phenol hydroxyl group is expected to undergo lactonization to release GSSH (**Figure 1.7**). Several reasons were considered for choosing this system. Previously, we have used this strategy to release H_2S and H_2S_2 and the chemistry is well understood.[29, 30] Additional factors that control the release rates have been extensively studied.[29] Different masking groups on the phenol hydroxyl group should allow for tuning the release rates, and on-demand and selective prodrug activation.[29, 30] The prodrug moiety can also be used to improve stability and water solubility.[30] The byproduct lactone is a nontoxic and stable molecule that helps to minimize potenti issues in application in biological systems.[30]

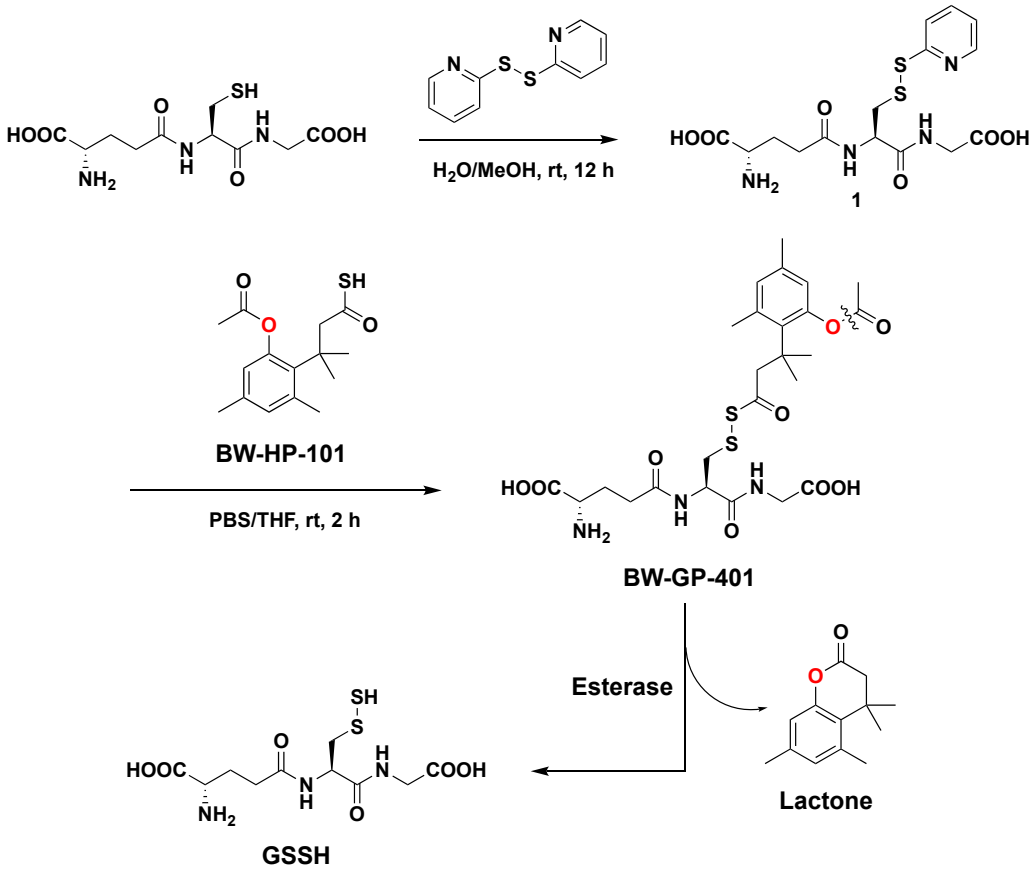

Figure 1.7 Synthesis and release mechanism of BW-GP-401.

1.2.2 Validation of GSSH release

We first examined the release of GSSH from **401**. Since GSSH is unstable for detection under physiological conditions, we studied the release kinetics by using HPLC to monitor lactone formation. Specifically, 100 μM **401** was incubated with 2 unit/mL porcine liver esterase (PLE) at 37 ºC. At different time points, the generation of the lactone was analyzed by HPLC. After 10 min, the donor peak became almost undetectable. As shown in **Figure 1.8B**, at the 30-min time point, the lactone peak corresponded to over 80% conversion. To verify that triggered-release only happens in the presence of PLE, we also incubated the GSSH donor in phosphate-buffered saline (PBS) without introducing PLE; no lactone was detected and the donor peak

remained about the same area over a period of 2 h, the maximal time of incubation period studied.

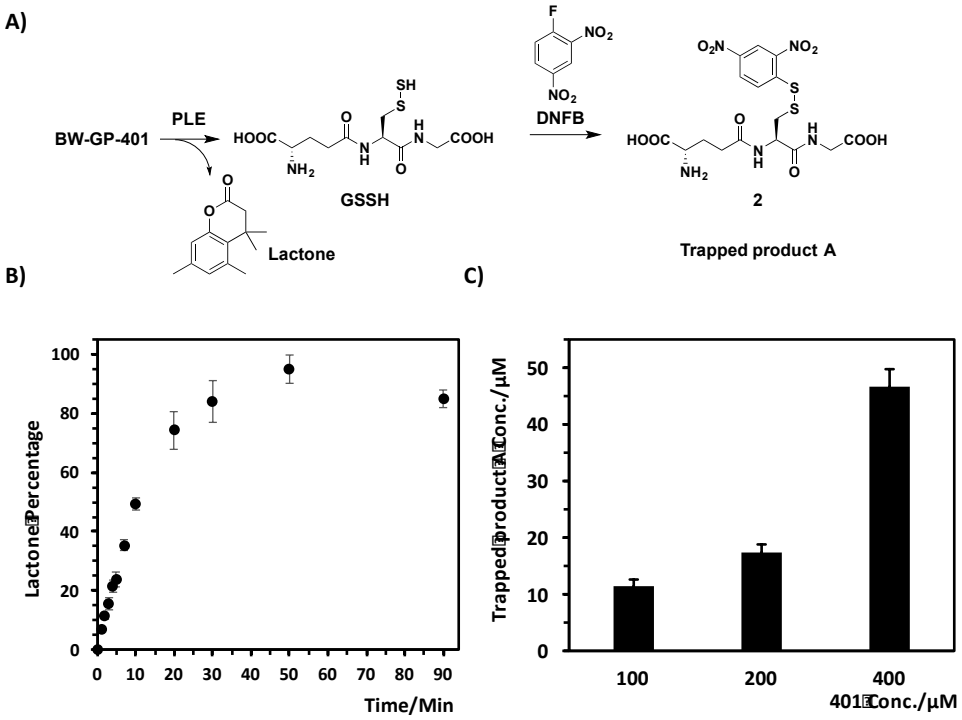

*Figure 1.8 A) Activation of **401** and subsequent GSSH trapping by DNFB; B) Released lactone was detected by HPLC. n = 3; C) Trapped product **A** was monitored by HPLC. n = 3.*

To further validate the release, we used a trapping reagent to directly capture GSSH from **401**. Unlike H_2S and H_2S_2,[31, 32] no specific probe has been developed to detect GSSH. Previously, our laboratory used 2,4-dinitrofluorobenzene (DNFB) to trap benzyl persulfide with a yield of over 80%.[16, 33] In this study, we also used DNFB to trap GSSH (**Figure 1.8A**). To fully consume **401** within a short period of time, 10 unit/mL PLE was added to the solutions of **401** at 100, 200, and 400 μM with 2 mM DNFB. The resulting mixture was allowed to be incubated for 30 min at 37 °C. The generation of the trapped product A was analyzed by HPLC (**Figure 1.8C**). For the purpose of quantitative analysis of the trapped product A, the standard compound was synthesized (see **Experimental part**). Different concentrations of **401** gave various amounts of

trapped product A, Specifically, about 12 µM, 18 µM and 45 µM GSSH (~10%) were detected by treating with 100 µM, 200 µM and 400 µM of 401 with 10 unit/mL PLE, respectively (**Figure 1.8C**). Since the trapping method has been successfully applied to benzyl persulfide with high yield,[16] the low trapping efficiency might be due to the unstable nature of GSSH under physiological conditions and/or further scrambling by other thiol species present. It has been well accepted that the general stability of persulfide species is poor.[34] Only a limited number of small molecule persulfide species has been obtained and partially characterized.[35-39] In the trapping process, there is a competition between trapping and decomposition of the persulfide species through disproportionation. To further identify the products from GSSH, we used mass spectrometry to analyze the incubation solution and found the increasing relative intensity of a peak attributed to GSSSG as the release reaction progressed (**Figure 1.9** and **1.10**).

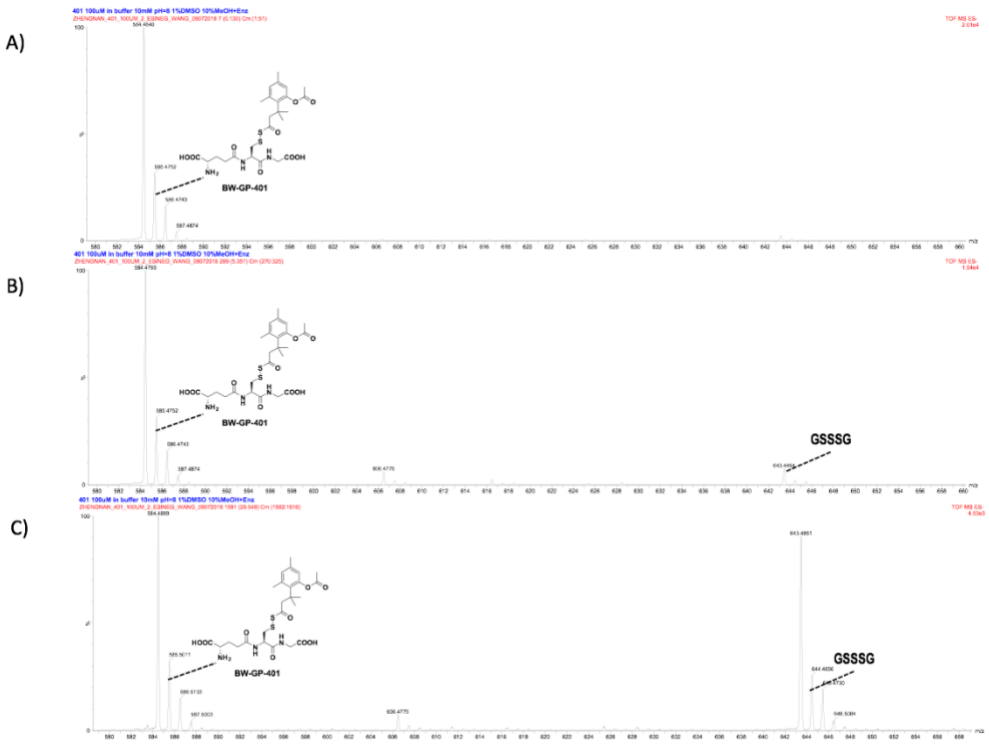

Figure 1.9 LRMS of the reaction mixture between A) 0 to 1 min; B) 5 to 6 min; C) 29 to 30 min.

Such results further suggest GSSH disproportionation as a contributing factor for the low yield in the trapping experiments. As an effort to minimize the bimolecular disproportionation reaction, we conducted additional release experiments using a lower level of **401** (5 µM) and PLE (1 unit/mL) and was able to achieve 34 ±3% yield of the trapped product with the remaining mass balance being predominately GSSSG.

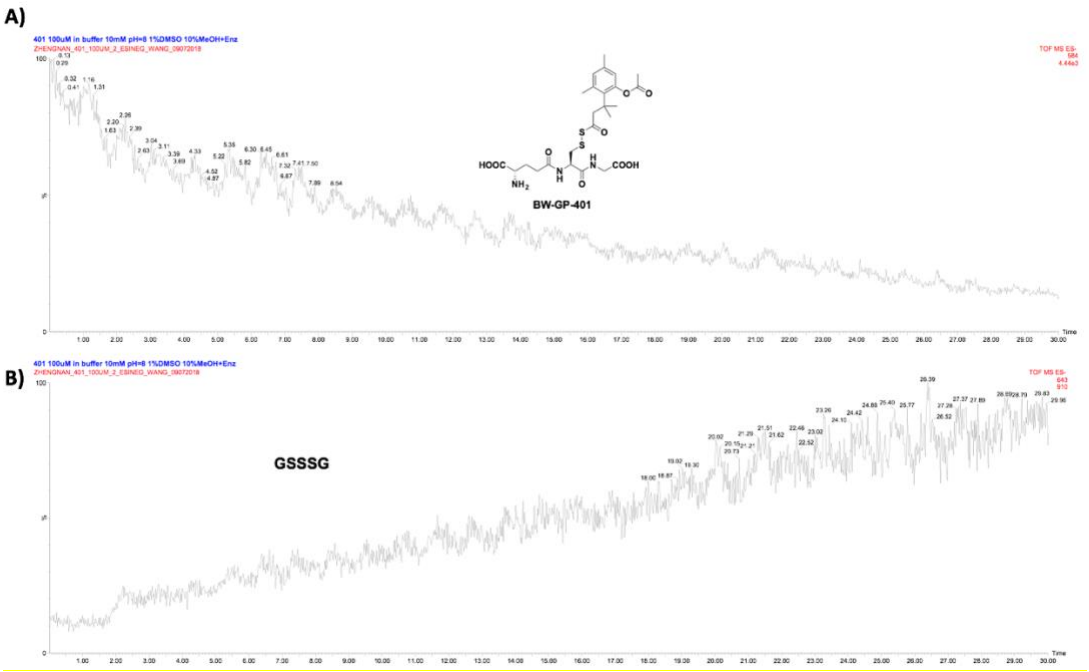

*Figure 1.10 Relative intensity of the peaks corresponding to A) **401** and B) GSSSG over a period of 30 min.*

H_2S was considered to be one of the products from persulfide through disproportionation (**Figure 1.11A**).[34, 39] Compound **401** provides a chance to study the H_2S release from pure GSSH. In this case, 200 µM of **401** was incubated in PBS containing 10 unit/mL PLE. The methylene blue (MB) method was used to probe H_2S generation. 50 µM of H_2S was detected from 200 µM of **401** between 2 and 10 min (**Figure 1.11B**). In the control group without PLE, no generation of H_2S was observed within 10 min (**Figure 1.11B** and **1.12**). In a biological environment, the level of cysteine or other free thiol groups is high.[24] GSSH is known to quickly

react with thiol and yield the disulfide byproduct and H_2S (**Figure 1.11A**).[34, 40] We then applied 2 mM NAC into the same system used above. At the 2-min point, the H_2S level reached a peak concentration of 115 μM, and then decreased to 28 μM at the 10-min point (**Figure 1.11B**). It should be noted that the peak concentration for a gasotransmitter generated from a prodrug is a different concept as compared to the maximal concentration for a non-volatile drug generated from a prodrug.[41, 42] We have demonstrated in the past that a peak concentration at 50% of the prodrug concentration was about the highest that one can achieve from a H_2S donor.[29] Thus, it is reasonable to assume that the generation of 115 μM of H_2S represents a near quantitative reaction. The G-SS-NAC disulfide byproduct was also quantified by mass spectrometry, and the yield was 38% (see **Experimental part**). There is a clear discrepancy between H_2S production and G-SS-NAC formation in quantity. This is easy to understand because of the scrambling effect of the existing thiol (excessive NAC) species, which can react with G-SS-NAC to give GSH and NAC disulfide.

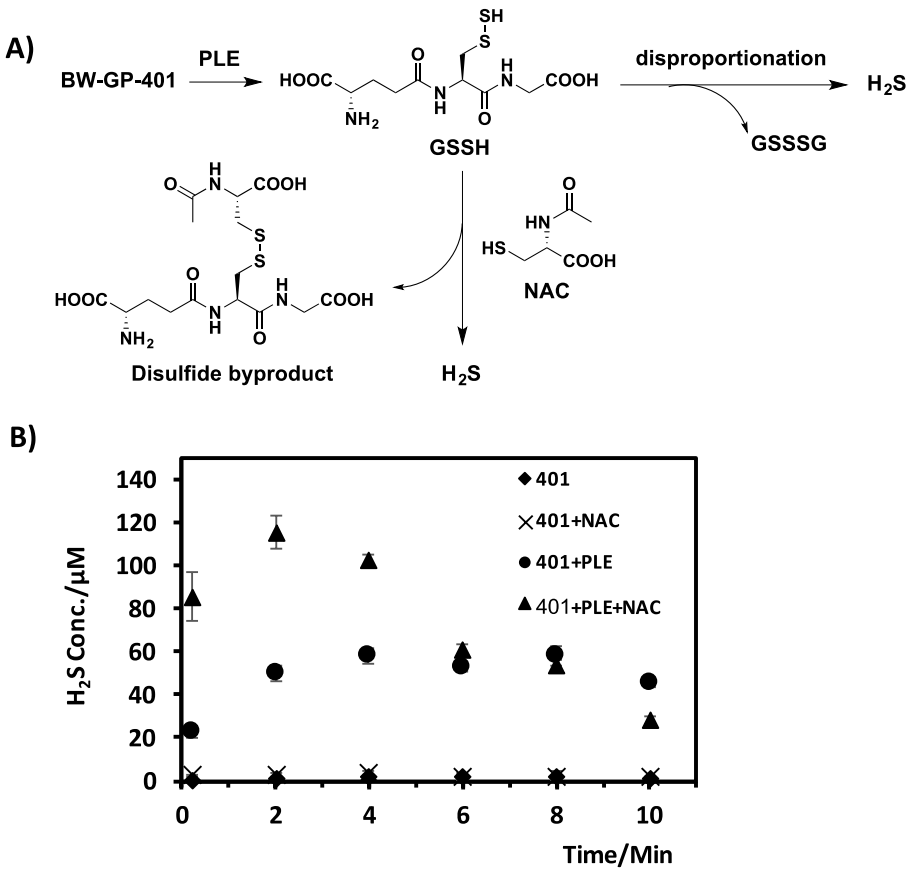

*Figure 1.11 A) H_2S was released from **401** with or without NAC; B) H_2S detection by the MB method. n = 3.*

In this case, we also quantified the GSH in the system, and the yield was about 77% (see **Experimental part**). All these explains the mass balance issue. However, in the absence of PLE, H_2S was not detectable at the 10-min point with exposure to a high concentration of NAC (**Figure 1.11A** and **1.12**). The results further demonstrate the need for an esterase to trigger the release of GSSH from **401**, supporting the instability of GSSH and the stability of the prodrug under physiological conditions. Further, the relative low trapping yield of GSSH and the high conversion yield in the reaction with NAC give further hint on why nature "chose" GSSH as a reagent for protein thiol modification.

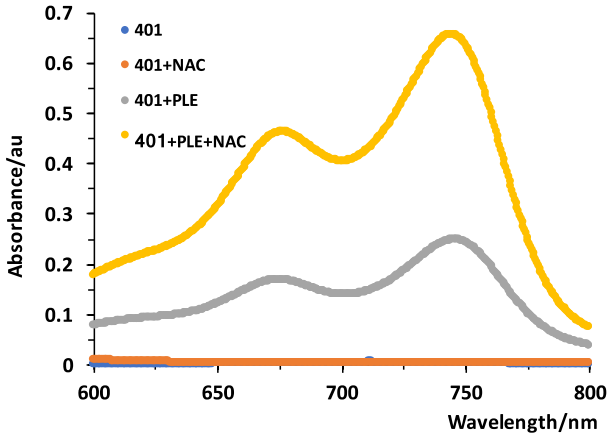

Figure 1.12 Detection of MB by UV spectrometry.

1.2.3 Biological activities of the GSSH prodrug

It has been reported that RSSH can regulate the activity of glyceraldehyde 3-phosphate dehydrogenase (GAPDH) through *S*-persulfdation.[43, 44] We previously applied our H_2S_2 donor on GAPDH and confirmed the correlation between elevated protein sulfhydration levels and decreased enzyme activity.[30] In the physiological environment, GSSH was said to be the most abundant small molecule persulfide and may also be involved in the regulation of GAPDH activity.[24, 43, 44] To explore this aspect, GAPDH was incubated with 100, 50 and 25 μM of **401**, respectively, for 30 mins in the presence of 10 unit/mL PLE. Then its catalytic activity was determined. Compared to the vehicle group, the catalytic ability decreased to 62 ±1%, 44 ±9% and 37 ±8% of the maximal activity, respectively (**Figure 1.13**). A control group treated with the lactone did not show any effect on GAPDH activity. To see if the decreased activity was caused by persulfdation, 2 mM dithiothreitol (DTT), which can reduce the persulfide group to a thiol residue, was added to each group. A significant increase in activity was observed after incubation for another 2 h at room temperature (**Figure 1.13**). According to the above results, GSSH can

also inhibit the activity of GAPDH and might acts as a redox regulator participating in regulating cellular metabolism.

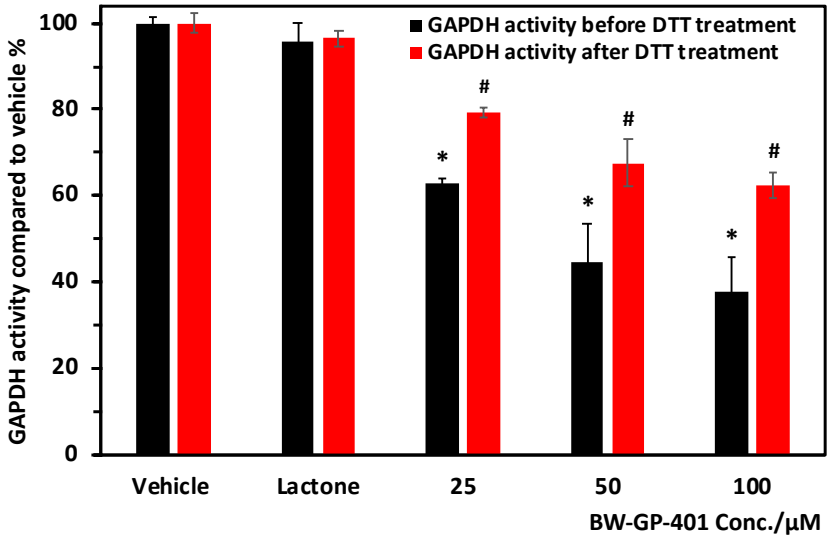

*Figure 1.13 Inhibition of GAPDH activity by 401. 2 μg/mL GAPDH was incubated with various concentration of **401** or 100 μM lactone for 0.5 h with 10 unit/mL PLE and 1% DMSO, after which the enzyme activity was measured. Each group was then incubated with 2 mM DTT at rt for 2 hours before the measurement of GAPDH activity. n = 3. *P < 0.01 for the comparison with the vehicle group. #P < 0.05 for the comparison with the group before DTT treatment.*

GSSH was found to be more potent in providing cytoprotective effects in highly oxidative cellular environment than GSH or H_2S.[24] In an effort to probe this point, we used **401** to rescue cells in highly oxidative environments. We first tested the cytotoxicity of **401** on H9c2 cells; no obvious toxicity was observed at 200 μM after 24 h of incubation (**Figure 1.14**). We next treated cells with 50, 100 and 150 μM **401** before exposure to H_2O_2 (**Figure 1.15**). Without treatment with **401,** after the incubation with 450 μM H_2O_2, cell viability was reduced by 60% compared with vehicle group. In the presence of **401**, this reduction in viability was less than 40% and was concentration dependent (**401**). Meanwhile, the byproduct lactone failed to rescue cells from H_2O_2. H9c2 cells were also treated with GSH and Na_2S before adding H_2O_2. However,

no obvious increase in viability was observed (**Figure 1.15**). The above results further support the fact that GSSH is more effective than GSH and H_2S in protecting cells from highly oxidative environment, which might indicate its unique property in defending cellular oxidative stress.

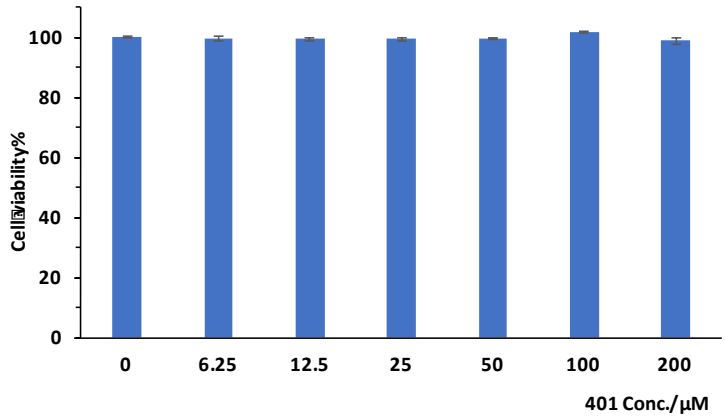

*Figure 1.14 Cytotoxicity of 401. H9c2 cells were treated with **401** at various concentrations. After 24 h incubation, cell viability was determined by Cell Counting Kit-8. Cell culture media has 1% DMSO.*

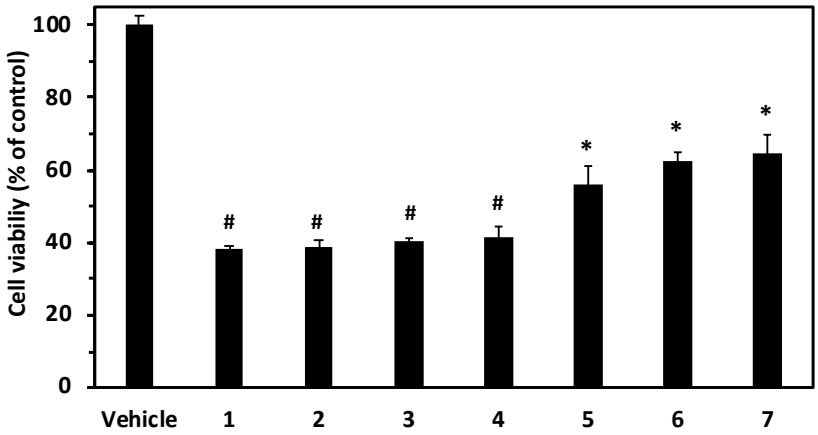

*Figure 1.15 Effects of different concentrations of 401 or various controls and relevant compounds on H9c2 cell line in the presence of H_2O_2. Prior to incubation with H_2O_2 (450 μM) for 3 h at 37 ºC (except for vehicle group), H9c2 cells were treated with 1) Blank control; 2) 150 μM Na_2S; 3) 150 μM lactone; 4) 150 μM GSH; 5) 50 μM 401; 6) 100 μM **401**; 7) 150 μM **401** for 1 hour at 37 ºC. Cell viability was measured by Cell Counting Kit-8 (CCK-8). n = 3. *P < 0.01 for the comparison with group 1. #P < 0.01 for the comparison with group 5.*

1.2.4 Design of a general persulfide delivery system

Based on studies of the esterase-sensitive GSSH prodrug, we envisioned this system being adapted to be a universal delivery system for various persulfide species. As such, four persulfide donors **BW-PP-501** to **504 (PP-501** to **504)** that release distinct persulfides were synthesized (**Figure 1.16, see experimental part**). Upon the hydrolysis of the ester bond by an esterase, the unmasked phenol group would go through lactonization to release the caged persulfide (**Figure 1.16**).

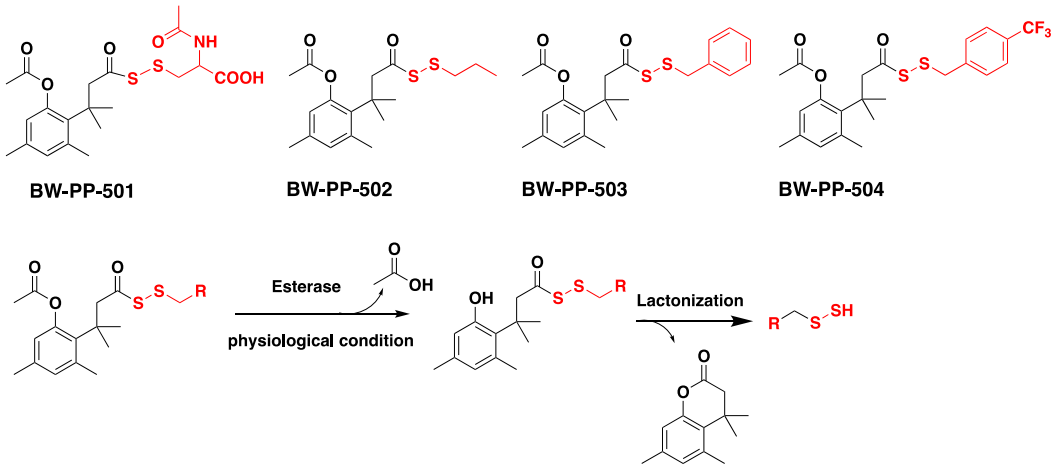

Figure 1.16 Persulfide prodrugs synthesized in this study and their release mechanism.

1.2.5 Validation of persulfide species release

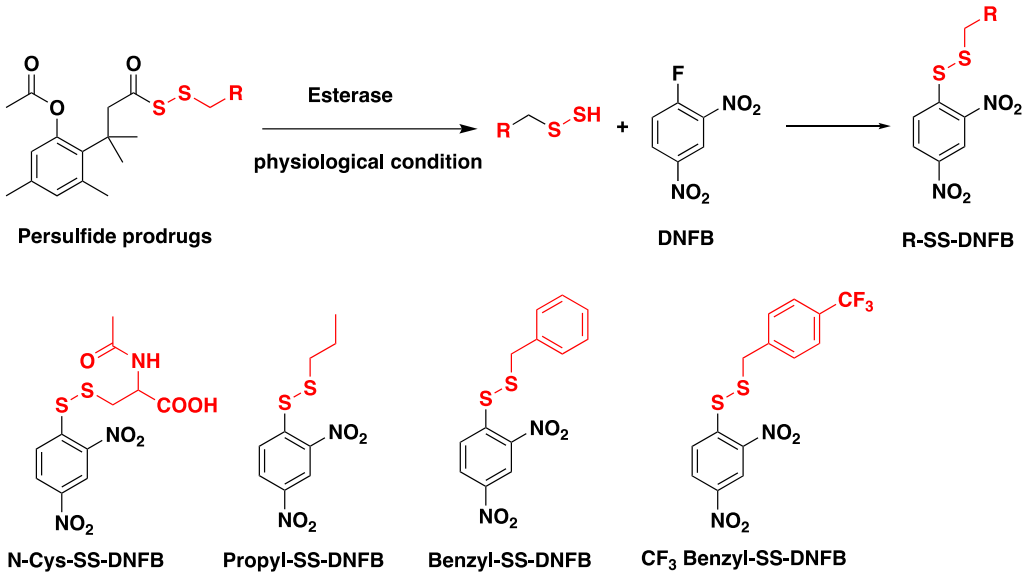

Figure 1.17 Detection of the released persulfides by trapping with DNFB and structures of R-SS-DNFB.

In this case, we also chose to used dinitrofluorobenzene (DNFB) to trap the released persulfides in a relatively stable disulfide (R-SS-DNFB) form for detection purpose (**Figure 1.17**). All trapped products R-SS-DNFB were synthesized as standards for quantifying the persulfide release yield from the respective prodrugs (see Experimental part). Specifically, 25 µM of a persulfide prodrug was incubated with 10 units/ml esterase from porcine liver (PLE) and 10 mM DNFB for 30 min in PBS buffer (pH = 7.4) at 37 °C. The trapped product R-SS-DNFB was then quantified by HPLC. Using this method, all 4 persulfide donors led to a relatively high yield of R-SS-DNFB formation, between 76 to 94 % (**Table 1.1, Figure 1.18-1.21**). Lactone formation was also observed by HPLC (**Figure 1.18-1.21**). This high yield of R-SS-DNFB formation indicates the efficient release of the persulfide from the prodrug. In contrast, no persulfide was released after 30 min of incubation in PBS without PLE, showing the esterase-sensitive nature of persulfide release.

Table 1.1 Trapping yield of various persulfides released from the prodrugs by DNFB (n = 3).

Prodrugs	**501**	**502**	**503**	**504**
Trapping yield (%)	84.2±1.9	94.0±1.3	77.5±2.0	76.0 ± 2.8

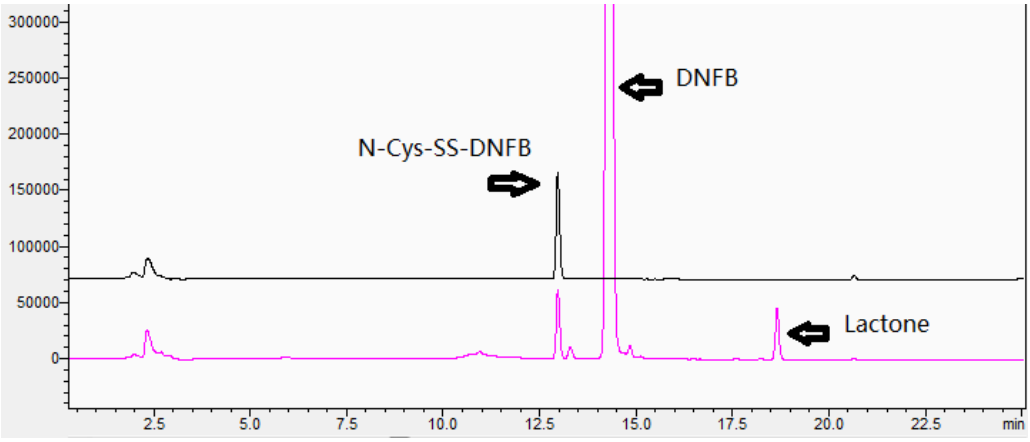

*Figure 1.18 N-CysSSH released from PP-501 was trapped by DNFB for detection purpose. HPLC chromatograms of synthesized N-Cys-SS-DNFB (black line) and the released N-CysSSH from 25 µM **PP-501** trapped by DNFB (pink line). 25 µM **PP-501** was incubated with 10 units/mL esterase from porcine liver (PLE) and 10 mM DNFB in phosphate-buffered saline (PBS, pH 7.4) for 30 min at 37 °C. The trapped product N-Cys-SS-DNFB was then quantified by HPLC (pink line). The synthesized N-Cys-SS-DNFB was used as reference standard for detection/quantification purpose.*

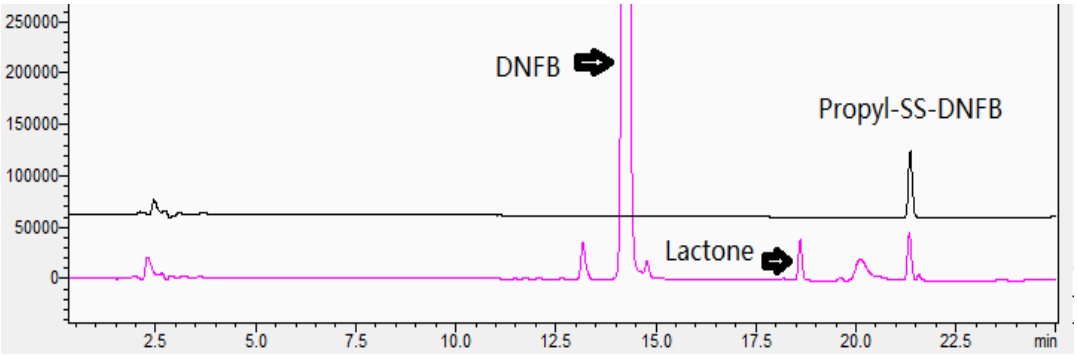

*Figure 1.19 Propyl persulfide released from PP-502 was trapped by DNFB for detection purpose. HPLC chromatograms of synthesized propyl-SS-DNFB (black line) and the released Propyl persulfide from 25 µM **PP-502** trapped by DNFB (pink line). 25 µM **PP-502** was incubated with 10 units/mL esterase from porcine liver (PLE) and 10 mM DNFB in phosphate-buffered saline (PBS, pH 7.4) for 30 min at 37 °C. The trapped product propyl-SS-DNFB was then quantified by HPLC (pink line). The synthesized propyl-SS-DNFB was used as reference standard for detection/quantification purpose.*

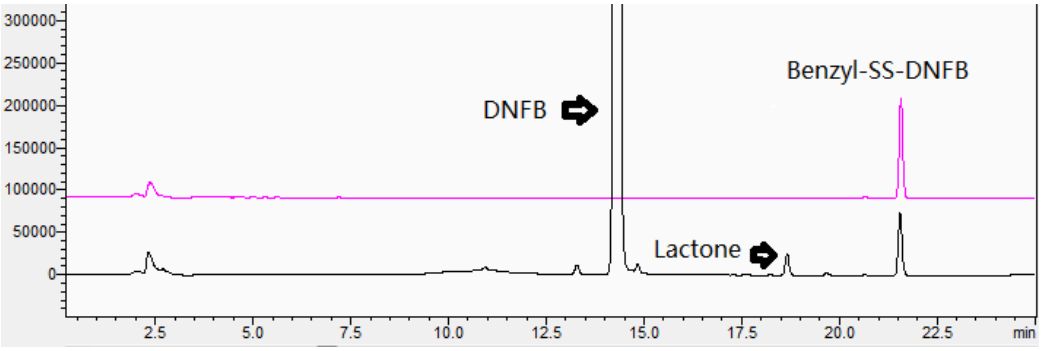

Figure 1.20 Benzyl persulfide released from PP-503 was trapped by DNFB for detection purpose. HPLC chromatograms of synthesized benzyl-SS-DNFB (black line) and the released benzyl persulfide from 25 µM ***PP-503*** *trapped by DNFB (pink line). 25 µM* ***PP-503*** *was incubated with 10 units/mL esterase from porcine liver (PLE) and 10 mM DNFB in phosphate-buffered saline (PBS, pH 7.4) for 30 min at 37 °C. The trapped product benzyl-SS-DNFB was then quantified by HPLC (pink line). The synthesized benzyl-SS-DNFB was used as reference standard for detection/quantification purpose.*

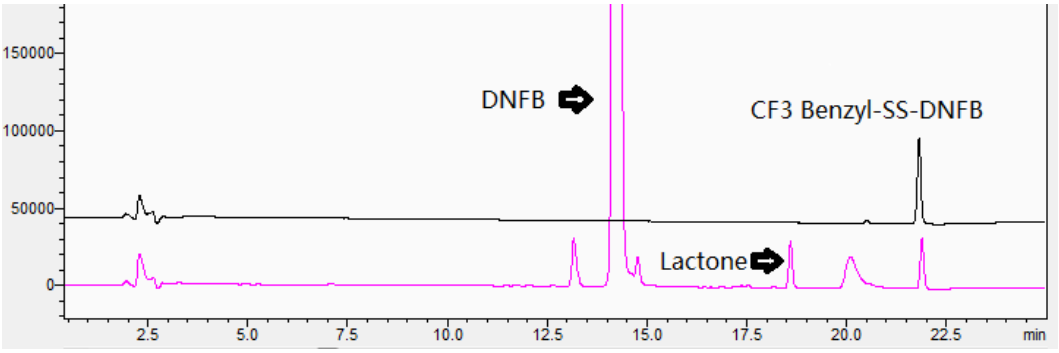

Figure 1.21 CF_3 Benzyl persulfide released from PP-504 was trapped by DNFB for detection purpose. HPLC chromatograms of synthesized CF_3 benzyl-SS-DNFB (black line) and the released CF_3 benzyl persulfide from 25 µM ***PP-504*** *trapped by DNFB (pink line). 25 µM* ***PP-504*** *was incubated with 10 units/mL esterase from porcine liver (PLE) and 10 mM DNFB in phosphate-buffered saline (PBS, pH 7.4) for 30 min at 37 °C. The trapped product CF_3 benzyl-SS-DNFB was then quantified by HPLC (pink line). The synthesized CF_3 benzyl-SS-DNFB was used as reference standard for detection/quantification purpose.*

1.2.6 Stability studies of the various persulfide species

This high-yield formation of R-SS-DNFB indicates: 1) this system can almost quantitatively generate pure persulfide species and 2) DNFB can effectively trap persulfide species as R-SS-DNFB for detection purpose. These two key points forms the foundation of the

following persulfide stability studies, which need 1) a donor system to efficiently deliver a pure persulfide and 2) a detection method to quantify the persulfide. With this persulfide prodrug system and quantification method in hand, we then studied the stability of various persulfides in PBS (pH = 7.4) at 37 °C. Briefly, 25 μM of a prodrug was incubated with 20 units/ml PLE in PBS at 37 °C. At different time points, aliquots of the reaction mixture were extracted and reacted with 10 mM DNFB for 30 min. The trapped product R-SS-DNFB was then quantified by HPLC. In the presence of a high concentration (20 units/ml) of PLE, 25 μM of persulfide prodrugs were fully consumed within 10 s of incubation at 37 °C, suggesting the release of the persulfide species was also completed under these conditions. As such, we started at 10 s-time point to monitor the concentration of persulfides in PBS solution. For **PP-501**, at 10 s, there was 13 μM *N*-acetyl-*L*-cysteine persulfide (*N*-CysSSH) remaining and within 1 min, the *N*-CysSSH concentration dropped below 5 μM due to degradation (**Table 1.2**). Other persulfide species released from **PP-502** to **504** also showed similar patterns under similar conditions (**Table 1.2**). As demonstrated here, persulfide species are very unstable in PBS at 37 °C, the concentration of persulfide released from 25 μM prodrugs would quickly drop below 5 μM within 60 s.

Table 1.2 The concentrations of the trapped product R-SS-DNFB from different persulfide prodrugs at different time points.

Time (s)	**Conc. of the trapped product (μM)**			
	PP-501	**PP-502**	**PP-503**	**PP-504**
10	13.2	14.6	11.3	10.8
20	8.9	10.1	5.4	7.4
30	5.6	8.1	4.1	6.1
40	4.9	7.3	4.0	5.6
50	3.8	6.2	3.0	5.3

60	3.1	4.7	2.6	4.5

After observing the quick degradation of persulfide species, we were motivated to study the degradation profile. We chose to use **PP-501** to probe the degradation profile of *N*-CysSSH under near phycological conditions. Specifically, 100 μM **PP-501** was incubated with 10 units/ml PLE in PBS at 37 °C for 30 min to fully complete the release and degradation of *N*-CysSSH. By using the methylene blue method, around 15 μM of H_2S was detected in the reaction solution. In contrast, almost no H_2S was formed in the absence of PLE. Hydrogen polysulfide (H_2S_n, $n \geq 2$) was also produced due to the degradation of *N*-CysSSH as revealed by a H_2S_n selective fluorescence probe DSP-3 (**Figure 1.22B**).[45] Compared to the positive control group (Na_2S_2), nearly 10 μM of H_2S_n was generated in the degraded reaction mixture based on increase of the fluorescent intensity from DSP-3. Other degradation products include disulfide, trisulfide, tetrasulfide and free thiol are identified by mass spectrometry in the reaction mixture (**Figure 1.22C, 1.23**). At this point, we have identified several sulfur species with different oxidation states in the degradation mixture of *N*-CysSSH. These observations show that, although the scrambling effect leads to a quick decomposition of *N*-CysSSH, sulfane sulfur species include H_2S_n, trisulfide and tetrasulfide still remain in the mixture, which might indicate the "overall oxidation state" of persulfide is maintained at certain degree.

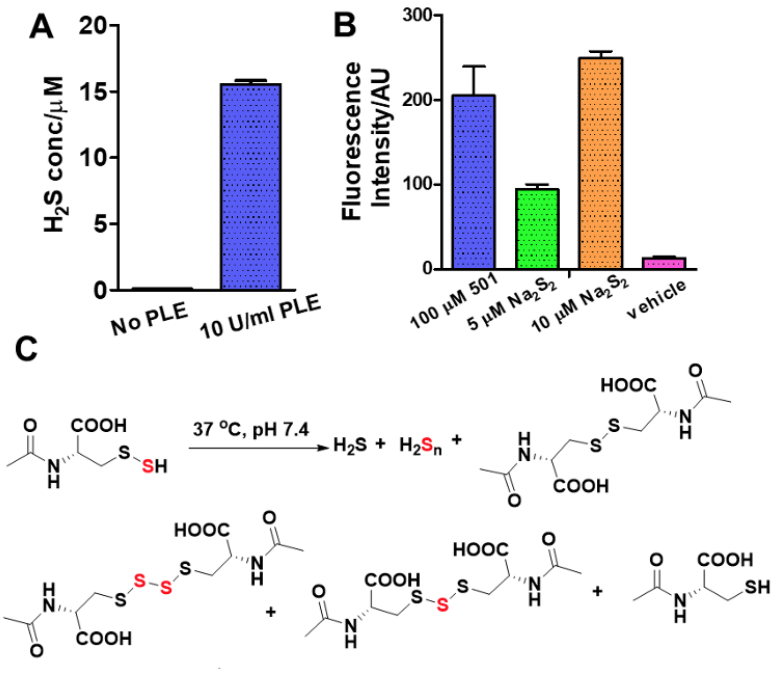

Figure 1.22 Degradation study of N-CysSSH released from PP-501. A). 100 μM ***PP-501*** *was incubated with 10 units/ml PLE or without PLE at 37 °C for 10 min in PBS, after that, the H_2S concentrations were quantified by methylene blue method. Values are means ± SD. n = 3; B). 100 μM* ***PP-501*** *was incubated with 10 units/ml PLE at 37 °C for 10 min in PBS, H_2S_n production was determined by DSP-3, Na_2S_2 was used as the positive control, background fluorescent intensity was recorded as vehicle group. Values are means ± SD. n = 3; C). Illustration of the degradation products of* N-*CysSSH.*

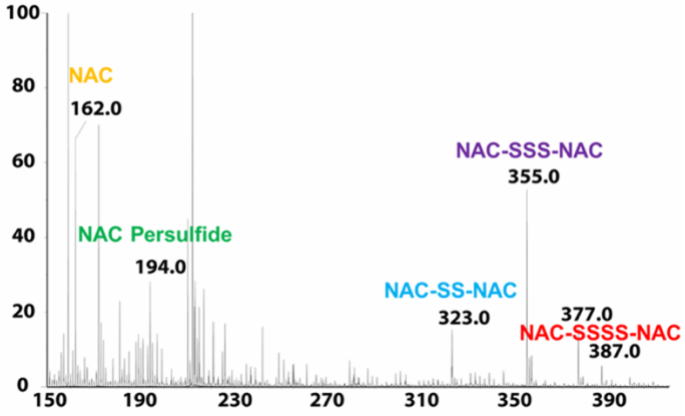

Figure 1.23 Degradation study of N-CysSSH released from PP-501 examined by MS. 100 μM ***PP-501*** *was incubated with 10 units/mL PLE at 37 °C for 10 min in 10 mM NH_4HCO_3 buffer. Then, the degradation product was examined by MS.*

1.2.7 Cytoprotective effects of persulfide prodrugs

Next, we were interested in testing the effects of these persulfide prodrugs in protecting cells from oxidative stress. To allow complete release of persulfide from the prodrugs, H9c2 cells were pretreated with 100 μM of various prodrugs for 1 hour with 1 unit/ml PLE at 37 ºC. Cells were then challenged with 500 μM H_2O_2 for 4 hours followed by determining cell viability. As shown in **Figure 1.24,** all persulfide donors (**PP-501** to **504**) pretreated group elevated the cell viability from 30 % to around 60 %, and Na_2S treated group didn't show significant protective effect. Additionally, we did not observe significant potency differences among the different persulfide donors. These results are consistent with our observations on cytoprotective studies of the GSSH prodrug, indicating a more potent antioxidative effect of persulfides compared to that from H_2S.

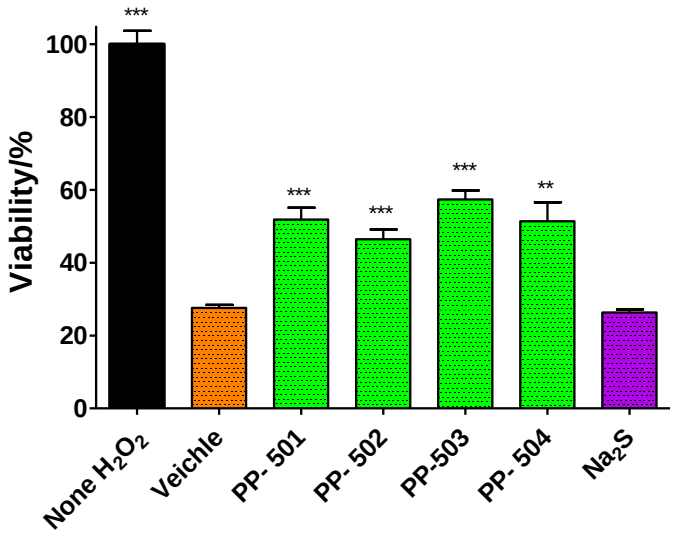

*Figure 1.24 Cytoprotective effect of various persulfide donors against H_2O_2 induced damage. H9c2 cells were pretreated with various compounds for 1 hour with 1 unit/ml PLE, then cells were challenged with 500 μM H_2O_2 for 4 hours. After that, the cell viability was determined. "None H_2O_2" group means cells were not challenged with H_2O_2. Values are means ± SD. n = 3, *P<0.05, **P<0.01, ***P<0.001 versus the vehicle group.*

1.3 Conclusion

In conclusion, we have developed an esterase-sensitive prodrug system to deliver various persulfide species under near physiological conditions. The release of persulfides were validated by the formation of byproduct lactone and direct trapping with DNFB. Using these persulfide prodrugs, we studied the stability and degradation of GSSH and *N*-CysSSH. In a biological context, we examined those persulfide prodrugs in the inhibition of GAPDH activity and cytoprotective effects against oxidative damage. Taken together, we provide the chemistry that helps storing and delivering persulfide species for studying their biological relevance. However, we should also note that the easy scrambling process involving persulfide means that the concentration and time-scale make a difference in the experimental outcome when designing biological studies.

1.4 Experimental part

1.4.1 General information

All reagents and solvents were of reagent grade and purchased from commercial suppliers (Sigma Aldrich, VWR International, Oakwood Chemicals and Fisher Chemicals). ^{1}H (400 MHz) and ^{13}C (100 MHz) NMR spectra were recorded on a Bruker-400 spectrometer. Mass spectrometric analyses were performed on a Q-TOF micro (Waters Micromass) mass spectrometer. HPLC analyses were performed on a Shimadzu Prominence UFLC (column: Waters C18 3.5 μM, 4.6×100 mm). UV-Vis absorption spectra were recorded on a Shimadzu PharmaSpec UV-1700 UV-Visible spectrophotometer. Purification was performed on a Shimadzu HPLC (column: Waters Semi-Prep Column, 20×250 mm). 96-well plates were read and recorded on a PerkinElmer 1420 multi-label counter. Porcine liver esterase (PLE) was purchased from Aldrich (E3019). Lactone was synthesized according to a literature procedure.[28]

BW-HP-101 was synthesized according to literature procedures.[29] The H_2S_n selective fluorescence probe, DSP-3, was synthesized according to literature procedures.[45]

1.4.2 Synthesis of the GSSH prodrug and trapped product A

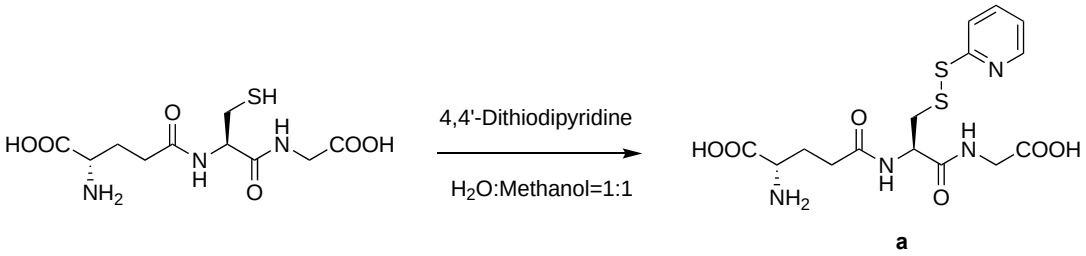

Figure 1.25 Synthesis of N^5-(1-((carboxymethyl)amino)-1-oxo-3-(pyridin-2-yldisulfanyl)propan-2-yl)glutamine (a).

Synthesis of N^5-(1-((carboxymethyl)amino)-1-oxo-3-(pyridin-2-yldisulfanyl)propan-2-yl)glutamine (a). To a solution of L-glutathione (463 mg, 1.11 mmol) in H_2O (8 mL) and methanol (8 mL) was added 4,4′-dithiodipyridine (490 mg, 2.22 mmol). The mixture was stirred at room temperature for 13 h. Then methanol was removed from the reaction mixture under reduced pressure. The residual solution was washed with dichloromethane (5 x 10 ml), and then evaporated under reduced pressure to give the crude product (368 mg), which is a light yellow solid. The crude product was used for next step without purification.[46]

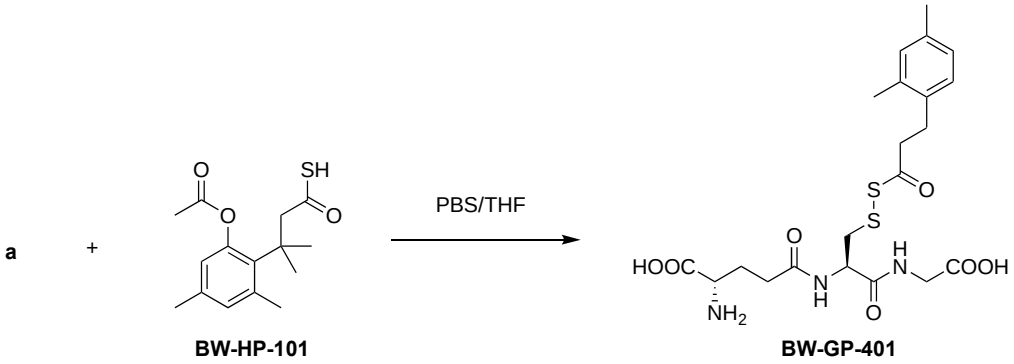

Figure 1.26 Synthesis of BW-GP-401.

*Synthesis of N^5-(3-((3-(2-acetoxy-4,6-dimethylphenyl)-3-methylbutanoyl)disulfanyl)-1-((carboxymethyl)amino)-1-oxopropan-2-yl)glutamine (**BW-GP-401**).* To a solution of **a** (368 mg) in PBS (3 ml) was added dropwise BW-HP-101 (110 mg, 0.39 mmol) in THF (1 ml). The mixture was stirred at room temperature for 2 h. Then THF was removed from mixture under reduced pressure. The aqueous residue was directly purified by RP-HPLC to yield a white solid (152 mg, 66%). ^{1}H NMR (CD_3OD): 6.84 (s, 1H), 6.62 (s, 1H), 4.46 (dd, *J* = 8.8, 5.0 Hz, 1H), 3.90 (s, 2H), 3.83 (t, *J* = 6.3 Hz, 1H), 3.29 (d, *J* = 1.5 Hz, 2H), 2.98 (ddd, *J* = 22.8, 13.9, 6.9 Hz, 2H), 2.62-2.43 (m, 5H) ,2.32 (s, 3H), 2.19 (d, *J* = 15.4 Hz, 3H), 2.15 (q, *J* = 6.8 Hz, 2H), 1.57 (s, 6H). ^{13}C NMR (CD_3OD): 197.4 174.4, 172.5, 172.4, 171.7, 150.9, 139.2, 137.7, 133.7, 133.9, 124.3, 56.1, 53.6, 49.6, 41.7, 41.0, 32.4, 32.1, 32.0, 27.0, 25.6, 21.9, 20.2. HRMS calculated for $C_{25}H_{36}N_3O_9S_2$ $[M+H]^+$: m/z 586.1893 found 586.1902.

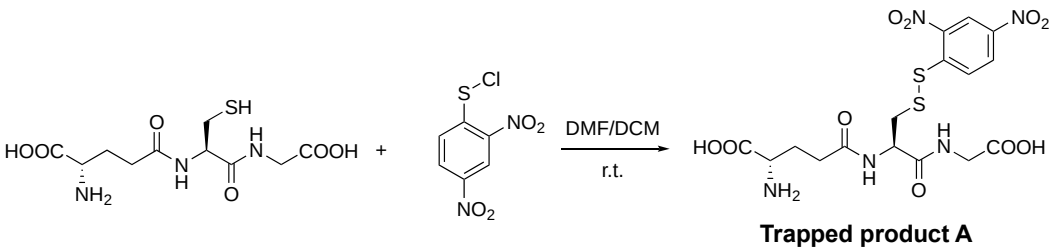

Figure 1.27 Synthesis of trapped product A.

Synthesis of N^5-(1-((carboxymethyl)amino)-3-((2,4-dinitrophenyl)disulfanyl)-1-oxopropan-2-yl)glutamine (trapped product A). To the solution of 2,4-dinitrobenzenesulfenyl chloride (38 mg, 0.161 mmol) in anhydrous DCM (1ml) was added dropwise L-glutathione (67 mg, 0.16 mmol) in DMF (10 ml). The mixture was allowed to stir at room temperature under the protection of nitrogen. After 1 h, the mixture was concentrated to 3 ml in DMF, and directly purified by RP-HPLC to give the product as white solid (35 mg, 43%). ^{1}H NMR (DMSO-d_6): 8.90 (d, J = 4.0 Hz, 1H), 8.89-8.86 (m, 1H), 8.69 (d, *J* = 8.4 Hz, 1H), 8.59 (dd, *J* = 9.0, 2.4 Hz,

1H), 8.50 (d, *J* = 9.0 Hz, 1H), 4.50 (td, *J* = 9.8, 4.1 Hz, 1H), 3.66 (d, *J* = 5.7 Hz, 1H), 3.22 (dd, *J* = 13.6 Hz, 2H), 3.06 (dd, *J* = 13.4, 10.3 Hz, 2H), 2.34 (d, *J* = 7.0 Hz, 2H), 2.09-1.65 (m, 2H). ^{13}C NMR (DMSO-d_6): 171.9, 170.7, 170.1, 170.1, 145.3, 144.7, 144.5, 128.9, 128.2, 121.4, 52.9, 51.7, 48.6, 41.1, 31.5, 26.7. HMRS Calculated for $C_{16}H_{20}N_5O_{10}S_2$ $[M+H]^+$: m/z 506.0652 found 506.0643

1.4.3 Esterase-triggered lactone formation from 401 as monitored by HPLC.

Stock solution preparation: 401 was dissolved in DMSO to afford a 10-mM stock solution. 5 mg of porcine esterase (18 unit/mg esterase from porcine liver, PLE, Aldrich, E3019) was dissolved in 0.9 ml PBS to give a 100-unit/mL esterase stock solution.

401 (final Conc. 100 μM) was added to PBS (5 ml) with 2 unit/ml PLE at 37 °C. At different time points, 200 μL reaction mixture was taken out and added to a centrifugation tube containing 600 μL acetonitrile (ACN). After 5 min at -78 °C, the mixture was (14.5 × 1000 rpm, 3 min) centrifuged, and the supernatant was used as the sample for HPLC. The samples were analyzed by HPLC (column: Waters C18 3.5 μM, 4.6×100 mm, injection loop volume: 20μL). ACN and H_2O (pH=4) were used as mobile phase.

1.4.4 Direct detection of GSSH by DNFB

Stock solution preparation: **401** was dissolved in DMSO to afford a 40-mM stock solution and a 500 μM stock solution. DNFB was dissolved in DMSO to afford a 200-mM solution.

Group 1: 2.5 μL of 40-mM **401** stock solution, 7.5 μL DMSO and 10 μL of DNFB stock solution were added to 1 mL 10 unit/ml PLE solution. The mixture was incubated at 37 °C for 30 min.

Group 2: 5 µL of 40-mM **401** stock solution, 5 µL DMSO and 10 µL DNFB stock solution were added to 1 mL 10 unit/ml PLE solution. The mixture was incubated at 37 °C for 30 min.

Group 3: 10 µL of 40-mM **401** stock solution and 10 µL DNFB stock solution were added to 1 mL 10 unit/ml PLE solution. The mixture was incubated at 37 °C for 30 min.

Group 4: 10 µL of 500-µM **401** stock solution and 10 µL DNFB stock solution were added to 1 mL 1 unit/ml PLE solution. The mixture was incubated at 37 °C for 30 min.

400 µL of reaction mixture was taken out and added to a centrifuged tube containing 400 µL ACN at -78 °C for 5 min. The mixture (14.5 ×1000 rpm, 3 min) was centrifuged, and the supernatant was used as the sample for HPLC. The samples were analyzed by HPLC (column: Waters C18 3.5 µM, 4.6×100 mm, injection loop volume: 20µL). ACN and H_2O (pH=4) were used as mobile phase.

1.4.5 Analysis of decomposed products from GSSH by LRMS

100 µM of **401** was incubated with 5 unit/ml PLE in a 10-mM ammonium bicarbonate buffer contains 10% methanol at room temperature. At different time points, the reaction mixture was directly injected and analyzed by mass spectrometer in ESI negative mode.

1.4.6 The MB method for detection of H_2S release from 401

At specific time points, 200 µM of reaction solution was added into a 1.5 mL tube containing 100 µL zinc acetate (1%, w/v). The mixture was centrifuged for 10 min (14.5 × 1000 rpm), followed by the removal of the supernatant. The precipitate was dissolved in 400 µL *N*,*N*-dimethyl-1,4-phenylenediaminesulfate (0.2% w/v in 20% H_2SO_4 solution) and 200 µL ferric chloride (1% w/v in 0.2% H_2SO_4 solution). After 4 min incubation, the absorbance (at 740 nm)

of the solution was measured. The concentration of H_2S was determined by a standard curve of $Na_2S \cdot 9H_2O$.

Group 1: 200 µM **401** was incubated in PBS.

Group 2: 200 µM **401** and 2 mM NAC were incubated in PBS.

Group 3: 200 µM **401** was incubated in PBS contains 10 unit/mL PLE.

Group 4: 200 µM **401** and 2 mM NAC were incubated in PBS contains 10 unit/mL PLE.

1.4.7 Quantification of the disulfide byproduct and GSH by LRMS

Group 1 (NAC trapping experiment): 200 µM **401** and 2 mM NAC were incubated in PBS contains 10 unit/mL PLE for 30 min at 37 °C. The resulting solution was diluted 10 times with a 10-mM ammonium bicarbonate buffer contains 10% methanol and 100 µM internal standard before the analysis.

Group 2 (The disulfide byproduct standard): To the solution of GSH (31 mg, 0.1 mmol) and NAC (163 mg, 1 mmol) in 4 ml H_2O was added I_2 (140 mg, 0.55 mmol). The mixture was allowed to stir at room temperature for 30 min. The resulting solution was analyzed by MS to make sure the GSH was fully reacted with NAC to give a 25-mM stock solution of the disulfide byproduct. The stock solution was diluted to 20 µM in a 10-mM ammonium bicarbonate buffer contains 10% methanol and 100 µM internal standard before the analysis.

Group 3 (GSH standard): 154 mg GSH was dissolved in 5 ml H_2O to give a 100-mM stock solution. The stock solution was diluted to 20 µM in a 10-mM ammonium bicarbonate buffer contains 10% methanol and 100 µM internal standard before the analysis.

Internal standard: 100 µM of leu-enkephalin (Leu-Enk) was used as internal standard.

The analysis was performed in ESI negative mode.

1.4.8 GAPDH activity measurement after different treatment

GAPDH (Sigma, G2267-1KU) was dissolved in PBS to afford a 2 mg/mL stock solution. The solution was treated with 1 mM dithiothreitol (DTT) at 25 °C for 1 h. Then DTT was removed using Amicon ultra 10K tube ×3 (UFC501096) and bio-spin column (Thermo, 7K MWCO; 89882). PLE was dissolved in a GAPDH assay buffer 20 mM tris-HCl (pH 7.8) with 100 mM NaCl, BSA (0.1 mg/mL), and 2 mM NAD^+ (nicotinamide adenine dinucleotide) to afford a 10 unit/mL solution. Glyceraldehyde 3-phosphate was dissolved in the GAPDH assay buffer to give a 6-mM solution. Lactone and **401** were dissolved in DMSO to afford a 10-mM stock solution, respectively.

Group 1: 2 μL of GAPDH stock solution was added to PLE solution to make 2 μg/ml GAPDH solution. 10 μL of DMSO was added to the mixture, and the mixture was further incubated at 37 °C for 30 min.

Group 2: 2 μL of GAPDH stock solution was added to PLE solution to make 2 μg/ml GAPDH solution. 10 μL of lactone stock solution was added to the mixture, and the mixture was further incubated at 37 °C for 30 min.

Group 3: 2 μL of GAPDH stock solution was added to PLE solution to make 2 μg/ml GAPDH solution. 10 μL of **401** stock solution was added to the mixture, and the mixture was further incubated at 37 °C for 30 min.

Group 4: 2 μL of GAPDH stock solution was added to PLE solution to make 2 μg/ml GAPDH solution. 5 μL of **401** stock solution and 5 μL DMSO was added to the mixture, and the mixture was further incubated at 37 °C for 30 min.

Group 5: 2 µL of GAPDH stock solution was added to PLE solution to make 2 µg/ml GAPDH solution. 2.5 µL of **401** stock solution and 7.5 µL DMSO was added to the mixture, and the mixture was further incubated at 37 °C for 30 min.

Each group was divided into two parts after the above treatments. For the first part, GAPDH activity was determined. For the second part, the sample was incubated with 2 mM DTT at rt for 2 h and then GAPDH activity was determined.

For GAPDH activity measurement, 100 µL aliquot from each group was mixed with 100 µL of 6 mM glyceraldehyde 3-phosphate solution. The formation of NADH was spectrophotometrically monitored every two min at 340 nm at 37 °C.

1.4.9 Cytoprotective studies of BW-GP-401

Cytotoxicity of BW-GP-401: Cell viability was assessed by using Cell Counting Kit-8 (CCK-8, Dojindo, Japan). H9c2 cells were cultured in DMEM medium. The medium was supplemented with 10% fetal bovine serum and 1% penicillin/streptomycin. For cytotoxicity assays, The H9c2 cells were seeded in a 96-well plate one day before the experiment. Various concentrations of 401 were added to the cells. After incubation for 24 h at 37 °C in humidified atmosphere with 5 % CO_2, 10 µL of CCK-8 solution was added to each well, and the plate was incubated for an additional 2 h at 37 °C. The 96-well plate was read by a microarray reader for optical density at 450 nm; and the results were expressed as a percentage of the absorption of the untreated control.

Measurement of H9c2 cell viability in H_2O_2-induced cell damage with various pre-treatments: H9c2 cells were treated with various concentrations (50 µM, 100 µM and 150 µM) of **401** with addition of 2 unit/mL of PLE for 1 h at 37 °C. Then, the cells were exposed to H_2O_2 (450 µM) for another 3 h at 37 °C. The viability was evaluated by Cell Counting Kit-8 (CCK-8).

For the control groups, no compound was added before the exposure of cells to H_2O_2. 150 µM of lactone, GSH and Na_2S were also used in the same manner as the **401** group.

1.4.10 Synthesis of persulfide prodrugs BW-PP-501 to 504.

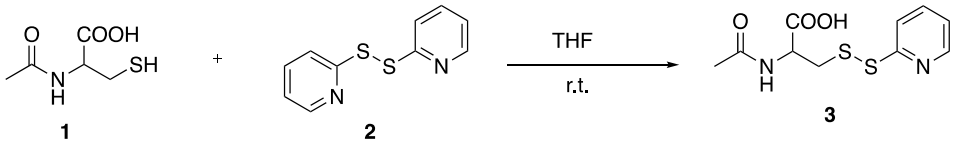

Figure 1.28 Synthesis of N-acetyl-S-(pyridin-2-ylthio)-L-cysteine (3).

Synthesis of N-acetyl-S-(pyridin-2-ylthio)-L-cysteine (3): To a stirred solution of 4,4′-dithiodipyridine (2, 148 mg, 0.67 mmol) in THF (5 mL) was added *N*-acetyl-*L*-cysteine (1, 100 mg, 0.61 mmol) in THF (5 mL) at room temperature. The reaction mixture was stirred for 5 h at room temperature. The solvent was evaporated under reduced pressure. The residue was purified by silica gel column chromatography to yield the pure product (3, 100 mg, 60 %). ^{1}H NMR (CD_3OD): δ 8.37 (d, *J* = 4.8 Hz, 1H), 7.77-7.76 (m, 2H), 7.21-7.17 (m, 1H), 4.66-4.63 (m, 1H), 3.32-3.27 (m, 2H), 3.14-3.09 (m, 1H), 1.94 (s, 3H). ^{13}C NMR (CD_3OD): δ 173.3, 160.7, 150.4, 139.1, 122.5, 121.4, 53.2, 41.5, 22.4; HRMS calcd for $C_{10}H_{12}N_2O_3S_2Na$ $[M+Na]^+$ 295.0184, found 295.0185.

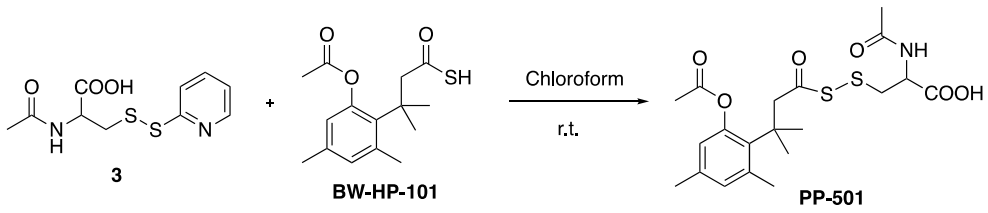

*Figure 1.29 Synthesis of **BW-PP-501**.*

*Synthesis of S-((3-(2-acetoxy-4,6-dimethylphenyl)-3-methylbutanoyl)thio)-N-acetylcysteine (**PP-501**):* **BW-HP-101** was synthesized according to published procedure. [1] To a solution of **3** (80 mg, 0.29 mmol) in chloroform (3 mL) was added dropwise **BW-HP-101**(81 mg, 0.29 mmol) in chloroform (1 mL). The mixture was stirred at room temperature for 2 h. The solvent was evaporated under reduce pressure. The residue was purified by silica gel column chromatography to yield the pure product (**PP-501**, 88 mg, 69 %). ^{1}H NMR ($CDCl_3$): δ = 7.46 (d, *J* = 6.8 Hz, 1H), 6.81 (s, 1H), 6.59 (s, 1H), 4.42-4.41 (m, 1H), 3.37 (dd, *J* = 14.2, 5.7 Hz, 1H), 3.30 (ABq, *J* = 16.0 Hz, 1H), 3.14 (ABq, *J* = 16.0 Hz, 1H), 2.83 (dd, J = 14.3, 4.6 Hz, 1H), 2.53 (s, 3H), 2.32 (s, 3H), 2.21 (s, 3H), 2.02 (s, 3H), 1.59 (s, 3H), 1.55 (s, 3H). ^{13}C NMR ($CDCl_3$): δ = 198.2, 172.6, 171.7, 170.1, 149.5, 138.0, 136.9, 132.7, 132.3, 123.3, 55.3, 52.1, 41.7, 40.2, 31.8, 31.6, 25.5, 22.6, 22.0, 20.3; HRMS calcd for $C_{20}H_{27}NO_6S_2Na$ $[M+Na]^+$ 464.1178, found 464.1194

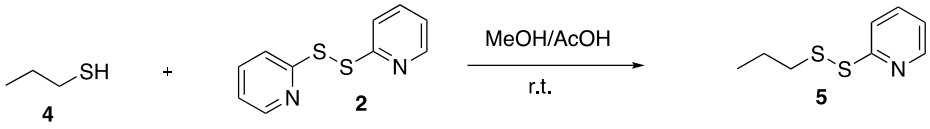

*Figure 1.30 Synthesis of 2-(propyldisulfanyl) pyridine (**5**).*

*Synthesis of 2-(propyldisulfanyl) pyridine (**5**):* To a stirred solution of 4,4′-dithiodipyridine (**2,** 159 mg, 0.72 mmol) and 25 µL acetic acid (AcOH) in MeOH (9 mL), was added propanethiol (**4**, 50 mg, 0.65 mmol) in MeOH (2 mL) at room temperature. The reaction mixture was stirred for 5 h at room temperature. The solvent was evaporated under reduced pressure. The residue was purified by silica gel column chromatography to yield the pure product (**5**, 90 mg, 81 %). ^{1}H NMR ($CDCl_3$): δ 8.39 (s, 1H), 7.71-7.58 (m, 2H), 7.01 (m, 1H), 2.75-2.70 (m, 2H), 1.70-1.66 (m 2H), 0.98-0.92 (m, 3H). ^{13}C NMR ($CDCl_3$): δ 160.6, 149.4, 136.9, 120.4, 119.4, 40.8, 22.2, 13.0; HRMS calcd for $C_8H_{12}NS_2Na$ $[M+H]^+$ 186.0411, found 186.0408.

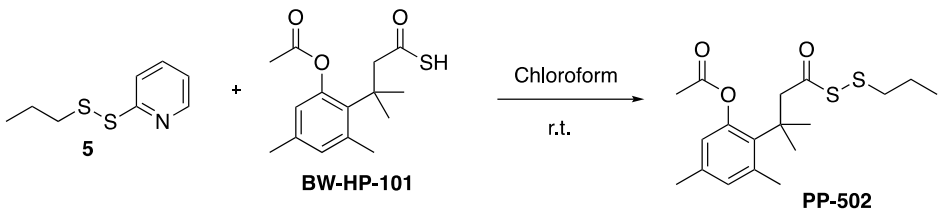

*Figure 1.31 Synthesis of **BW-PP-502**.*

*Synthesis of 3,5-dimethyl-2-(2-methyl-4-oxo-4-(propyldisulfanyl)butan-2-yl)phenyl acetate (**PP-502**):* To a solution of **5** (80 mg, 0.43 mmol) in chloroform (3 mL) was added dropwise **BW-HP-101** (121 mg, 0.43 mmol) in chloroform (1 mL). The mixture was stirred at room temperature for 2 h. The solvent was evaporated under reduce pressure. The residue was purified by silica gel column chromatography to yield the pure product (**PP-502**, 93 mg, 61 %).^{1}H NMR ($CDCl_3$): δ = 6.80 (s, 1H), 6.61 (s, 1H), 3.18 (s, 2H), 2.55-2.51 (m, 5H), 2.32 (s, 3H), 2.22 (s, 3H), 1.58 (s, 6H), 1.50 (dd, *J* = 14.8, 7.6 Hz, 2H), 0.95 (t, *J* = 7.6 Hz, 3H). ^{13}C NMR ($CDCl_3$): δ = 196.0, 169.9, 149.6, 138.0, 136.6, 132.7, 132.6, 123.2, 54.8, 40.7, 40.1, 31.6, 25.5, 22.3, 22.0, 20.3, 13.1; HRMS calcd for $C_{18}H_{26}O_3S_2Na$ $[M+Na]^+$ 377.1221, found 377.1213.

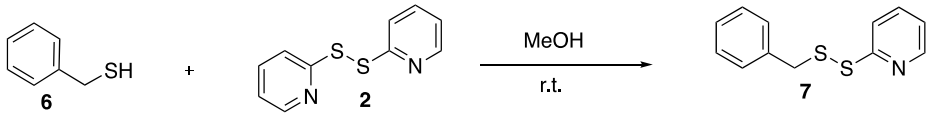

*Figure 1.32 Synthesis of 2-(benzyldisulfanyl) pyridine (**7**).*

*Synthesis of 2-(benzyldisulfanyl) pyridine (**7**):* To a stirred solution of 4,4′-dithiodipyridine (**2,** 155 mg, 0.70 mmol) in MeOH (10 mL) was added benzyl mercaptan (**4**, 80 mg, 0.59 mmol) in MeOH (5 mL) at room temperature. The reaction mixture was stirred for 5 h at room temperature. The solvent was evaporated under reduced pressure. The residue was purified by silica gel column chromatography to yield the pure product (**7**, 119 mg, 88 %). ^{1}H NMR ($CDCl_3$): δ 8.45 (m, 1H), 7.53 (m, 2H), 7.31-7.23 (m, 5H), 7.06-7.03 (m, 1H), 4.04 (s, 2H).

^{13}C NMR ($CDCl_3$): δ 160.1, 149.5, 136.8, 136.6, 129.4, 128.6, 127.7, 120.5, 119.5, 43.7; HRMS calcd for $C_{12}H_{11}NS_2Na$ $[M+Na]^+$ 256.0231, found 256.0228.

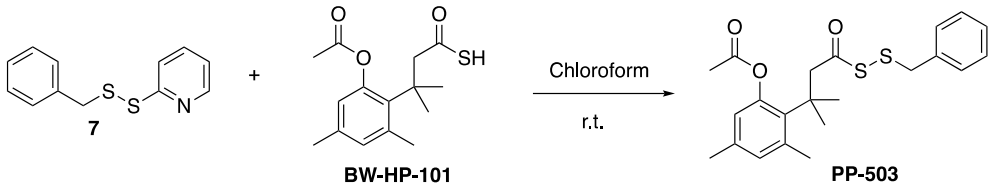

*Figure 1.33 Synthesis of **BW-PP-503**.*

*Synthesis of 2-(4-(benzyldisulfanyl)-2-methyl-4-oxobutan-2-yl)-3,5-dimethylphenyl acetate (**PP-503**):* To a solution of **7** (85 mg, 0.36 mmol) in chloroform (3 mL) was added dropwise **BW-HP-101** (100 mg, 0.36 mmol) in chloroform (1 mL). The mixture was stirred at room temperature for 2 h. The solvent was evaporated under reduce pressure. The residue was purified by silica gel column chromatography to yield the pure product (**HP-503**, 90 mg, 62 %). ^{1}H NMR ($CDCl_3$): δ = 7.30-7.25 (m, 5H), 6.82 (s, 1H), 6.62 (s, 1H), 3.80 (s, 2H), 3.16 (s, 2H), 2.53 (s, 3H), 2.31 (s, 4H), 2.23 (s, 3H), 1.55 (s, 6H). ^{13}C NMR ($CDCl_3$): δ = 195.4, 169.7, 149.3, 137.8, 136.5, 136.2, 132.7, 132.5, 129.3, 128.4, 127.6, 123.1, 54.8, 42.7, 39.8, 31.3, 25.4, 21.9, 20.2; HRMS calcd for $C_{22}H_{26}O_3S_2Na$ $[M+Na]^+$ 425.1221, found 425.1208.

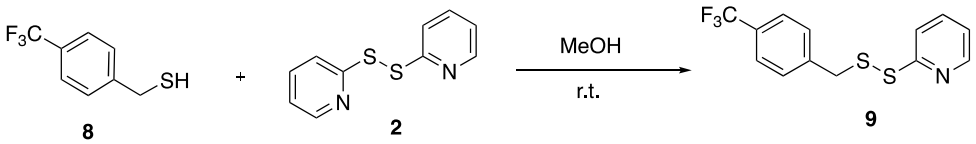

*Figure 1.34 Synthesis of 2-((4-(trifluoromethyl)benzyl)disulfanyl) pyridine (**9**).*

*Synthesis of 2-((4-(trifluoromethyl)benzyl)disulfanyl) pyridine (**9**):* To a stirred solution of 4,4′-dithiodipyridine (**2,** 137 mg, 0.62 mmol) in MeOH (10 mL) was added 4-trifluoromethylbenzyl mercaptan (**8**, 100 mg, 0.52 mmol) in MeOH (5 mL) at room temperature. The reaction mixture was stirred for 5 h at room temperature. The solvent was evaporated under

reduced pressure. The residue was purified by silica gel column chromatography to yield the pure product (**9**, 120 mg, 76 %). ^{1}H NMR ($CDCl_3$): δ 8.41-8.39 (m, 1H), 7.46-7.36 (m, 6H), 7.03-7.00 (m, 1H), 4.03 (s, 2H). ^{13}C NMR ($CDCl_3$): δ 159.4, 149.6, 140.8, 136.8, 129.8, 125.5 (q, *J* = 4 Hz), 122.7, 120.8, 119.8, 43.0; HRMS calcd for $C_{13}H_{10}NS_2F_3Na$ $[M+Na]^+$ 324.0097, found 324.0097.

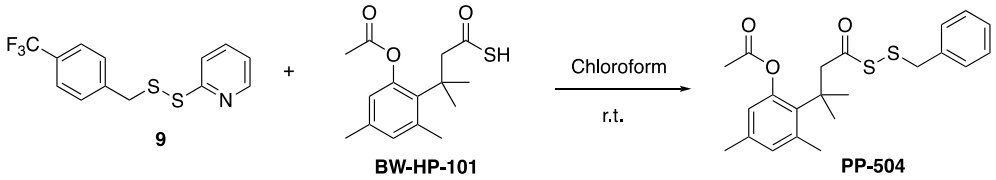

*Figure 1.35 Synthesis of **BW-PP-504**.*

*Synthesis of 3,5-dimethyl-2-(2-methyl-4-oxo-4-((4-(trifluoromethyl)benzyl)disulfanyl)butan-2-yl)phenyl acetate (**PP-504**):* To a solution of **9** (60 mg, 0.20 mmol) in chloroform (3 mL) was added dropwise **BW-HP-101** (66 mg, 0.23 mmol) in chloroform (1 mL). The mixture was stirred at room temperature for 2 h. The solvent was evaporated under reduce pressure. The residue was purified by silica gel column chromatography to yield the pure product (**PP-504**, 50 mg, 53 %).^{1}H NMR ($CDCl_3$): δ = 7.53 (d, *J* = 8.0 Hz, 2H), 7.31 (d, *J* = 8.0 Hz, 2H), 6.80 (s, 1H), 6.60 (s, 1H), 3.79 (s, 2H), 3.13 (s, 2H), 2.50 (s, 3H), 2.29 (s, 3H), 2.21 (s, 3H), 1.52 (s, 6H). ^{13}C NMR ($CDCl_3$): δ = 194.8, 169.7, 149.3, 140.4, 137.8, 136.6, 132.5, 129.6, 125.3, 123.1, 54.9, 41.8, 39.9, 31.3, 25.3, 21.8, 20.2; HRMS calcd for $C_{23}H_{25}F_3O_3S_2Na$ $[M+ Na]^+$ 493.1095, found 493.1083.

1.4.11 Synthesis of the persulfide trapped products

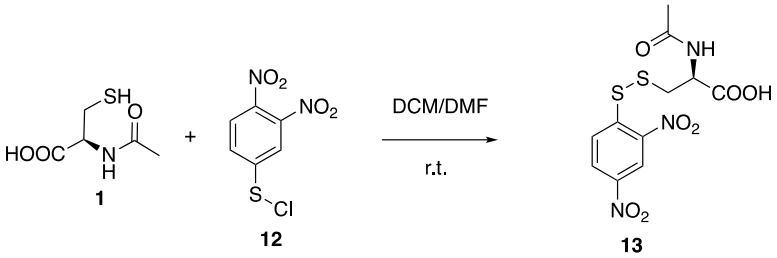

*Figure 1.36 Synthesis of N-acetyl-S-((2,4-dinitrophenyl)thio)-L-cysteine (**13**).*

*Synthesis of N-acetyl-S-((2,4-dinitrophenyl)thio)-L-cysteine (**13**):* To a stirred solution of 2,4-dinitrobenzenesulfenyl chloride (**12,** 115 mg, 0.49 mmol) in DCM (4 mL) was added *N*-acetyl-*L*-cysteine (**1**, 80 mg, 0.49 mmol) in DMF (1 mL) at room temperature. The reaction mixture was stirred for 6 h at room temperature. The solvent was evaporated under reduced pressure. The residue was purified by silica gel column chromatography to yield the pure product (**13**, 102 mg, 57 %). ^{1}H NMR (MeOD): δ 8.97 (s, 1H), 8.55-8.52 (m, 2H), 4.62-4.59 (m, 1H), 3.35-3.34 (m,1H), 3.21-3.16 (m, 1H), 2.02 (s, 3H). ^{13}C NMR (MeOD): δ 173.4, 147.1, 146.5, 130.1, 128.7, 122.3, 41.8, 22.7; HRMS calcd for $C_{11}H_{11}N_3O_7S_2Na$ $[M+Na]^+$ 383.9931, found 383.9936.

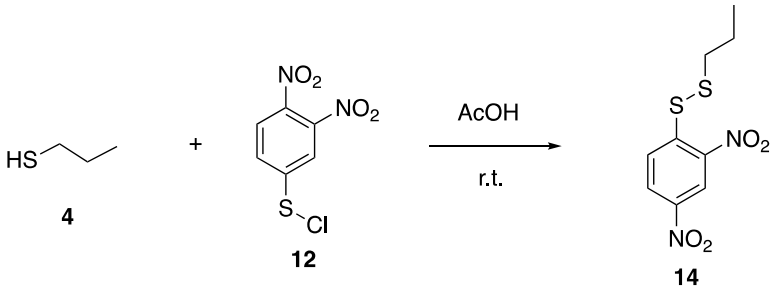

*Figure 1.37 Synthesis of 1-(2,4-dinitrophenyl)-2-propyldisulfane (**14**).*

*Synthesis of 1-(2,4-dinitrophenyl)-2-propyldisulfane (**14**):* To a stirred solution of 2,4-dinitrobenzenesulfenyl chloride (**12,** 100 mg, 0.42 mmol) in AcOH (4 mL) was added

propanethiol (**4**, 32 mg, 0.42 mmol) in AcOH (1 mL) at room temperature. The reaction mixture was stirred for 6 h at room temperature. The solvent was evaporated under reduced pressure. The residue was purified by silica gel column chromatography to yield the pure product (**14**, 97 mg, 84 %). ^{1}H NMR ($CDCl_3$): δ 9.09 (d, *J* = 2.4 Hz, 1H), 8.54-8.45 (m, 2H), 2.76 (t, *J* = 7.2 Hz, 2H), 1.74-1.69 (m, 2H), 1.02 (t, *J* = 7.2 Hz, 3H). ^{13}C NMR ($CDCl_3$): δ 146.9, 145.5, 145.1, 128.8, 127.4, 121.7, 40.6, 22.5, 13.2; HRMS calcd for $C_9H_{10}N_2O_4S_2Na$ $[M+Na]^+$ 296.9980, found 296.9978.

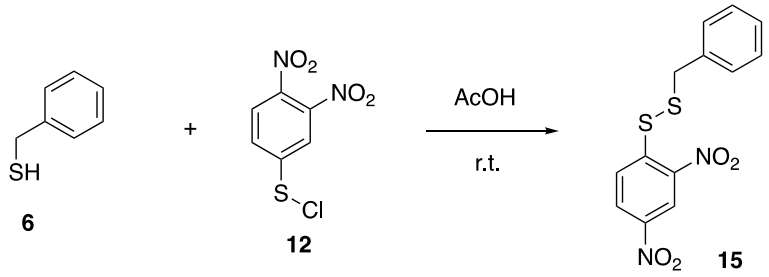

*Figure 1.38 Synthesis of 1-benzyl-2-(2,4-dinitrophenyl) disulfane (**15**).*

*Synthesis of 1-benzyl-2-(2,4-dinitrophenyl) disulfane (**15**):* To a stirred solution of 2,4-dinitrobenzenesulfenyl chloride (**12,** 137 mg, 0.58 mmol) in AcOH (3 mL) was added 4-benzyl mercaptan (**6**, 72 mg, 0.58 mmol) in AcOH (2 mL) at room temperature. The reaction mixture was stirred for 6 h at room temperature. The solvent was evaporated under reduced pressure. The residue was purified by silica gel column chromatography to yield the pure product (**15**, 102 mg, 55 %). ^{1}H NMR ($CDCl_3$): δ 8.98 (s, 1H), 8.14-8.03 (m, 2H), 7.24-7.16 (m, 4H), 4.00 (s, 2H). ^{13}C NMR ($CDCl_3$): δ 146.1, 145.2, 144.9, 135.5, 129.2, 128.8, 128.0, 126.5, 121.1, 43.5; HRMS calcd for $C_{13}H_{10}N_2O_4S_2$ $[M+Na]^+$ 344.9980, found 344.9987.

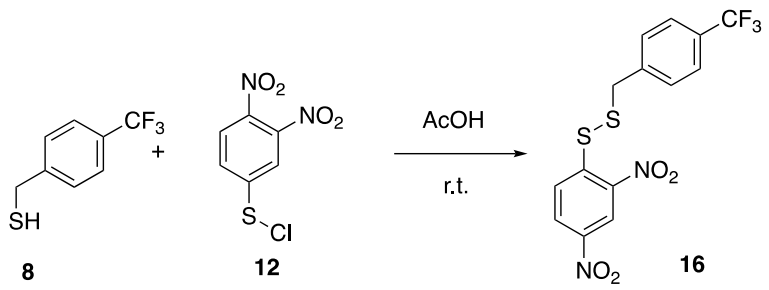

*Figure 1.39 Synthesis of 1-(2,4-dinitrophenyl)-2-(4-(trifluoromethyl)benzyl) disulfane (**16**).*

*Synthesis of 1-(2,4-dinitrophenyl)-2-(4-(trifluoromethyl)benzyl) disulfane (**16**):* To a stirred solution of 2,4-dinitrobenzenesulfenyl chloride (**12,** 137 mg, 0.58 mmol) in AcOH (3 mL) was added 4-trifluoromethylbenzyl mercaptan (**8**, 112 mg, 0.58 mmol) in AcOH (2 mL) at room temperature. The reaction mixture was stirred for 6 h at room temperature. The solvent was evaporated under reduced pressure. The residue was purified by silica gel column chromatography to yield the pure product (**16**, 120 mg, 53 %). ^{1}H NMR ($CDCl_3$): δ 8.98 (d, *J* = 2.0 Hz, 1H), 8.19-8.05 (m, 2H), 7.44-7.33 (m, 4H), 4.03 (s, 2H). ^{13}C NMR (CDCl3): δ 145.5, 145.4, 145.2, 139.7, 129.7, 128.8, 126.8, 125.7 (q, *J* = 4 Hz), 42.7; HRMS calcd for $C_{14}H_9F_3N_2O_4S_2Na$ $[M+Na]^+$ 412.9854, found 412.9866.

1.4.12 Quantification of persulfide release from 501 to 504

Stock solution preparation: Various persulfide prodrugs were dissolved in DMSO to afford 10-mM stock solutions. DNFB was dissolved in DMSO to afford a 400 mM stock solution.

For each prodrug, 2.5 μL of 10 mM prodrug stock solution and 25 μL of 400 mM DNFB stock solution were added to 972.5 μL PBS containing 10 units/mL PLE solution. The final concentrations for prodrug and DNFB were 25 μM and 10 mM respectively. The mixture was incubated at 37 °C for 30 min. 300 μL reaction mixture was taken out and added into a vial

containing 600 μL acetonitrile (ACN). The mixture was incubated in an acetone dry ice bath (-78 °C) for 5 min and centrifuged for 10 min (14.5 × 1000 rpm). The supernatant was subjected for HPLC analysis (column: Waters C18 3.5 μM, 4.6×100 mm). The mobile phase was acetonitrile (ACN)/H_2O (pH=4.0). Eluent conditions (% of ACN): 10% to 85%, 0 to 15 min; 85%, 15 to 20 min; 85% to 10%, 20 to 25 min.

The formation of R-SS-DNFB was calculated based on the corresponding R-SS-DNFB standard curve.

1.4.13 Persulfide stability studies

Stock solution preparation: Various persulfide prodrugs were dissolved in DMSO to afford 10 mM stock solutions. DNFB was dissolved in DMSO to afford a 130-mM stock solution.

To a 20 mL vial was added 4 mL of PBS containing 20 units/mL PLE and 10 μL 10 mM prodrug stock solution. At different time points (10s, 20s, 30s, 40s, 50s, 60s), 300 μL reaction mixture was taken out and added to a 1.5 mL tube containing 25 μL of 130 mM DNFB stock solution (the final DNFB concentration is 10 mM). The mixture was further incubated at 37 °C for 30 min. Then 575 μL ACN was added to the reaction mixture. Then the mixture was centrifuged for 4 min (14.5 × 1000 rpm). The supernatant was analyzed by HPLC. The mobile phase was acetonitrile (ACN)/H_2O (pH=4.0) with ratios defined in the table below.

Table 1.3 The HPLC eluent conditions for monitoring the persulfide concentration.

Persulfide prodrugs	Eluent conditions (% of ACN)
PP-501	30% to 90%, 0 to 30 min; 90% to 95%, 30 to 35 min; 95%, 35 to 50 min; 95% to 30%, 50 to 60 min

PP-502	30%, 0 to 5 min; 30% to 70%, 5 to 30 min; 70% to 95%, 30 to 35 min; 95%, 35 to 50 min; 95% to 30%, 50 to 60 min
PP-503	30%, 0 to 5 min; 30% to 70%, 5 to 30 min; 70% to 95%, 30 to 35 min; 95%, 35 to 50 min; 95% to 30%, 50 to 60 min
PP-504	30%, 0 to 5 min; 30% to 70%, 5 to 30 min; 70% to 95%, 30 to 35 min; 95%, 35 to 50 min; 95% to 30%, 50 to 60 min

1.4.14 N-CysSSH degradation studies

H2S detection from persulfide degradation: H_2S generation due to ***N***-CysSSH degradation was detected by the methylene blue method. **PP-501** was dissolved in DMSO to afford 5 mM stock solution. To 1 mL PBS with 10 units/mL PLE or without PLE was added 20 µL 5 mM HP-501 stock (the final **PP-501** concentration was 100 µM). The mixture was then incubated at 37 °C for 10 min. 200 µL of reaction solution was taken into a 1.5 mL tube containing 200 µL zinc acetate (1% in H_2O, w/v). Then the tube was centrifuged for 10 min (14.5 × 1000 rpm). The supernatant was removed. Then 100 µL N,N-dimethyl-1,4-phenylenediaminesulfate (0.2% w/v in 20% H_2SO_4 solution) and 100 µL ferric chloride (1% w/v in 0.2% H_2SO_4 solution) were added to the tube. After 6 min, the absorbance (at 740 nm) of the

resulting solution was measured. H_2S concentration was calculated based on a calibration curve of $Na_2S \cdot 9H_2O$.

H_2S_n detection from persulfide degradation: H_2S_n generation due to *N*-CysSSH degradation was detected by a fluorescent probe, DSP-3.[2] **PP-501** was dissolved in DMSO to afford a 5 mM stock solution. Na_2S_2 was dissolved in PBS to afford 5-mM stock solution. DSP-3 was dissolved in CAN to prepare a 0.5-mM stock solution. Cetrimonium bromide (CTAB) was dissolved in ethanol to prepare a 5-mM stock solution.

To 5 mL PBS with 10 units/mL PLE was added 100 μL 5 mM **PP-501** stock (the final **PP-501** concentration was 100 μM). The mixture was incubated at 37 °C for 10 min to allow for the release and degradation of *N*-CysSSH. Then 25 μL of 5-mM CTAB stock and 200 μL 0.5-mM DSP-3 stock were added to the mixture. The mixture was incubated at room temperature for 5 min. Then fluorescence intensity at 515 nm was recorded with excitation at 490 nm. PBS containing 10 units/mL PLE but without **PP-501** was used to record background fluorescence intensity. Na_2S_2 was used as positive control.

***N*-CysSSH degradation products studied by MS: PP-501** was dissolved in DMSO to afford a 5-mM stock solution. To 5 mL of 10 mM NH_4HCO_3 solution containing 10 units/ml PLE was added 100 μL the 5-mM **PP-501** stock solution. The final concentration for **PP-501** was 100 μM. The mixture was incubated at 37 °C for 10 min. After that, the mixture was subjected to MS analysis using the negative mode. A 10-mM NH_4HCO_3 solution containing 10 units/ml PLE but without **PP-501** was used for MS background analysis.

1.4.15 Kinetics studies of PP-501 by monitoring lactone formation

PP-501 (finial Conc. 200 μM) was added to PBS (5 mL) with 1 unit/mL esterase at 37 °C. 300 μL reaction mixture was taken out at different time point and added into a vial

containing 600 μL ACN. The mixture was incubated in an acetone dry ice bath (-78 ℃) for 5 min and centrifuged for 10 min (14.5 × 1000 rp). The supernatant (injection volume of 20 μL) was subjected for HPLC analysis (column: Waters C18 3.5 μM, 4.6×100 mm). The mobile phase was acetonitrile (ACN)/H_2O (pH=4.0). The gradient elution method is described below:

0 to 20 min: 45% to 65% ACN; 20 to 25 min, 65 to 95% ACN; 25 to 50 min, 95% ACN; 50 to 60 min, 95% to 45% CAN. Flow rate: 0.8 mL/min.

The retention time of lactone is 14.9 ± 0.2 min.

1.4.16 Cytoprotective studies of persulfide prodrugs

H9c2 cells were treated with 100 μM of various prodrugs with addition of 1 unit/mL of PLE for 1 h at 37 °C in humidified atmosphere with 5 % CO_2. Then, the cells were exposed to H_2O_2 (500 μM) for another 4 h at 37 °C. After that, the viability was evaluated by Cell Counting Kit-8 (CCK-8).

2 STUDIES OF CO- INDEPENDENT REACTIVITIES FROM RUTHENIUM-BASED CO-RELEASING MOLECULES

2.1 Introduction

(This chapter is mainly based on my publications: *Chem. Commun.* 2020**,** *56* (14), 2190-2193, *Anal. Chem.* 2020, under revision)

As an endogenously produced gaseous molecule, carbon monoxide (CO) has been well demonstrated by many studies to possess signaling roles in mammals.[47] More importantly, the therapeutic effects of CO have been validated extensively in various disease models, including

colitis, inflammatory sepsis, drug-induced organ toxicity and others.[48-52] Earlier studies including some human clinical trials employed inhalation form of CO.[48, 53] However, limitations such as the need for a special inhalation device, risk to patients and healthcare workers, and difficulties in controlling dosage[48, 54] led many to search for delivery forms that are more compatible for wide-spread use.[48, 50, 55-57] Along this line, Motterlini and Mann pioneered the use of metal-immobilized carbonyls as CO-releasing molecules (CO-RMs)[48, 58-61] with many others also reporting very interesting CORMs.[62-65] Among all the metal-based CORMs, two ruthenium-based, CORM-2 and CORM-3, are probably the most widely used as CO donors for a large number of studies. A quick PubMed search of "CORM-2 OR CORM-3" led to about 500 hits, demonstrating the broad impact of these two CO-RMs. Later efforts in developing CO donors include photo-sensitive organic CO-RMs[56, 66-72] and organic CO prodrugs (Figure **1**).[73-76]

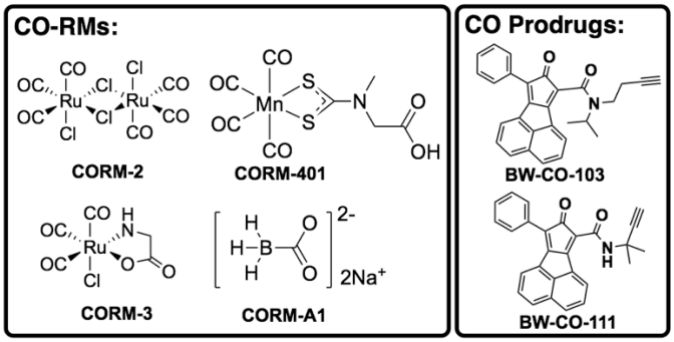

Figure 2.1 Structures of representative CO donors.

Both for mechanistic studies and pharmaceutical development, there is a need for a thorough understanding of the pharmacokinetic profiles of each delivery form and their correlation with pharmacodynamics in a given indication. Therefore, tools for real-time and highly accurate measurement of CO levels in circulation and at the cellular and tissue levels are in great need. Currently, oximeters are the most commonly used tools for determining carboxy hemoglobin (COHb) levels as a surrogate indicator of CO exposures in the systemic

circulation.[77] There have been continuous efforts in developing molecular fluorescent probes and sensors for CO for cellular and tissue-based CO measurements and imaging work. After Chang's palladium-based fluorescent probe for CO (COP-1),[78] there have been extensive efforts along a similar line, leading to several analogous CO probes (**Figure 2.2**).[79-82] He and coworkers also reported a genetically encoded fluorescent protein as CO sensor based on the binding affinity of CO to the iron center on a heme cofactor.[83] These probes all rely on the affinity of CO for a transition metal. Recently, there are exciting reports of metal-free fluorescent CO probes, which suggest the ability of CO to reduce a nitro group on an aromatic core, leading to fluorescent turn-on (**Figure 2.2**).[84-86] Such feasibility was demonstrated with two ruthenium-based CO-RMs, **CORM-2** and **CORM-3**, as the source of CO.[58, 61] We were interested in borrowing from this exciting strategy for designing CO probes for pharmacokinetic studies. As a first step, we confirmed the reported results using COFP, and thus the reproducibility of the literature results. However, upon further examination of these probes using different delivery forms of CO, it was found that the fluorescent probe only worked when the CO donors were ruthenium-based. As such, we examined the general utility of the published nitro reduction-based CO probes, and we concluded that these CO probes only sense ruthenium-based CO donors, **CORM-2** and **CORM-3**, not CO in general. Additionally, we found that **CORM-3** is capable of reducing an aryl nitro group to an amino group under near-physiological conditions, and such effects cannot be achieved by iCORM or CO from other sources including CO gas. Taken together, these results also firmly presented a CO-independent reactivity of ruthenium-based CO-RMs, **CORM-2,3**.

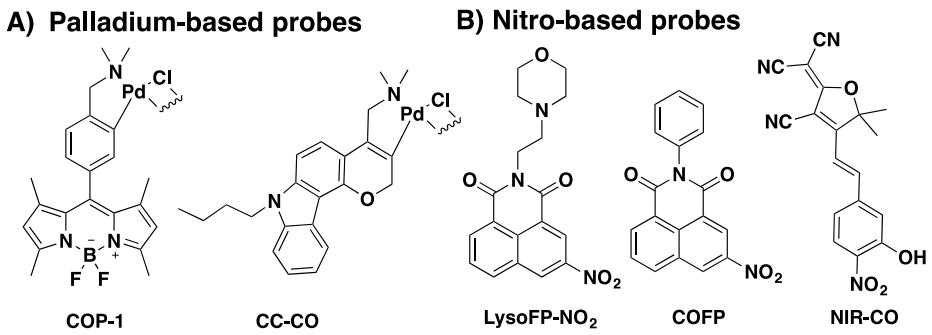

Figure 2.2 Structures of representative fluorescent CO probes for CO detection and in vitro imaging.

As shown in Figure **2.1**, **CORM-2** and **CORM-3** are both ruthenium-carbonyl complexes and have been reported to transfer CO spontaneously under physiological conditions.[48, 60] In a typical study using a metal-based CO-RM, the depleted CO-RM after release CO (iCO-RM) is used as the negative control. An ideal CO donor should not have CO-independent effects. If it does, then the iCO-RM control should duplicate such CO-independent effects in order to assess the true effect of CO. However, several recent studies indicated that some of the reported biological effects of metal-based CORMs such as **CORM-2** and **CORM-3** cannot be attributed to the ability for them to donate CO.[65, 87-100] Additional studies reported some unique chemical reactivities of ruthenium-based CO-RMs. For example, Poole and coworkers used NMR to determine the K_d between CORM-3 and biological thiol species (cysteine and glutathione) to be about 5 μM.[87] Heinemann and coworkers reported the CO-independent functions on K^+ channels by **CORM-2**.[98] Nielsen described that the widely studied effect of **CORM-2** against snake venom was through a CO-independent mechanism.[90] Stahl and colleagues described the ability for **CORM-2** to consume molecular oxygen in solution.[92] These results, coupled with our finding based on the reactivity of **CORM-2,3** on nitro-based CO probe, show a number of effects from ruthenium-based CO-RMs are CO-independent.

Given the wide-spread use, the large number of reports using **CORM-2,3** as CO donors, and the telltale signs of their chemical reactivity under physiological conditions, we decided to further systemically study the CO-independent reactivity of these two ruthenium-based CORMs with reagents commonly used in cellular assays such as resazurin, tetrazolium salts, nitrite and azide-based H_2S probes. It was found that both **CORM-2** and **CORM-3** have CO-independent reactivities toward these bioassay reagents. The implications of these findings are far-reaching. However, how such findings would affect the interpretations of results from each specific study, which has used **CORM-2** or **CORM-3**, is beyond the scope of this study, and is best left to experts who are most familiar with the interpretation of the biological problems examined in each study.

2.2 Results and discussions

2.2.1 Responses of COFP upon treatment with various CO sources

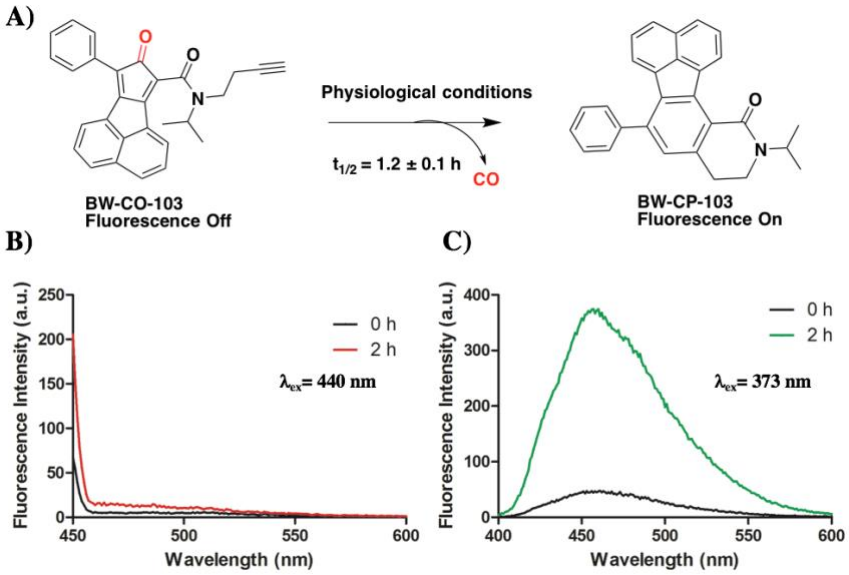

*Figure 2.3 Responses of **COFP** upon treatment with **CO-103**. A) CO release from **CO-103**; B) Fluorescence spectra of **COFP** (10 μM) upon treatment with **CO-103** (100 μM) over 2 h in DMSO/PBS (pH = 7.4) 5:1 at 37 ℃ (λ_{ex}= 440 nm, slit widths: W_{ex} = W_{em} = 10 nm); C) Fluorescence spectra of **CP-103** formation after the incubation with **COFP** in DMSO/PBS (pH = 7.4) 5:1 at 37 ℃ (λ_{ex} = 373 nm, slit widths: W_{ex} = W_{em} = 5 nm).*

Following the exciting work of Dhara *et al.*, we were interested in examining how well **COFP** would allow us to determine the quantity of CO release from different delivery forms. We first chose **BW-CO-103** (**CO-103**), which belongs to the class of metal-free organic CO prodrugs widely validated in multiple pharmacological animal models including colitis, liver injury, systemic inflammation, and kidney ischemia reperfusion injury.[73, 74, 101] An added advantage of using **CO-103** for the initial study is the prodrug's ability to concomitantly produce a fluorescent product, **CP-103**, together with CO release (**Figure 2.3A**).[73] This would give a way to cross-validate the results from the fluorescent probe in a quantitative fashion in solution, in cell culture, and possibly in animal models. With these design ideas in mind, we first explored the ability for the 1,8-naphthalimide-based probe **COFP** to sense the CO produced from **CO-103**. Much to our dismay, no fluorescent turn-on was observed at around 522 nm, which is expected within 2 h from the fluorescent turn-on CO probe (**Figure 2.3B**). In contrast, we observed a significant fluorescent intensity increase due to the production of **CP-103** after 2 h of incubation, suggesting CO production (**Figure 2.3C**).

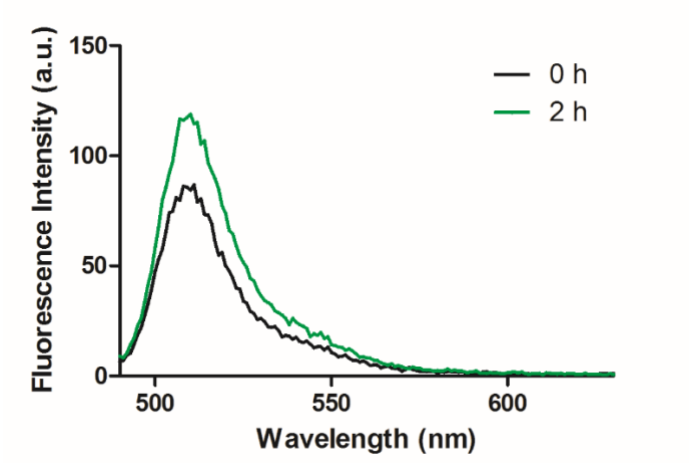

Figure 2.4 Fluorescence spectra of COP-1 (1 μM) upon treatment with ***CO-103*** *(100 μM) over 2 h in DMSO/PBS (pH = 7.4) 5:1 at 37 ℃ (λ_{ex} = 475 nm, slit widths: W_{ex} = 5 nm, W_{em} = 3 nm).*

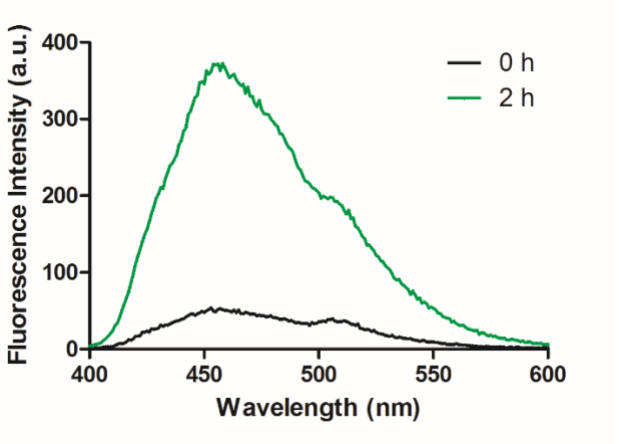

Figure 2.5 Fluorescence spectra of ***CP-103*** *formation during incubation with* ***COP-1*** *(1 μM) in DMSO/PBS (pH = 7.4) 5:1 at 37 ℃ (λ_{ex} = 373 nm, slit widths: W_{ex} = W_{em} = 5 nm).*

To further examine the generation of CO from **CO-103**, 1 μM COP-1 was incubated with **CO-103** under the same conditions. A fluorescent signal increase at 507 nm was observed from **COP-1** after 2 h (**Figure 2.4**) along with formation of **CP-103** (**Figure 2.5**). Such results also confirmed CO production. As additional positive controls, we also examined the probe's ability to detect CO released from **CORM-2** and **CORM-3** as reported in the literature (**Figure 2.6**).[84] As expected, it was reassuring that we were able to completely reproduce the solution studies of COFP as reported in the literature.

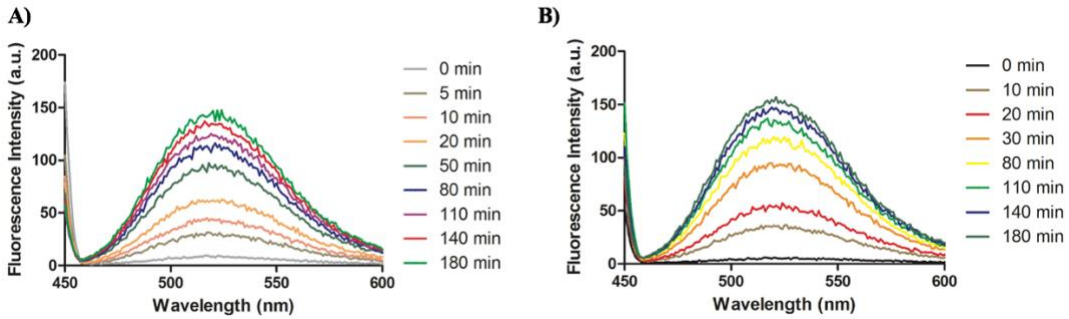

*Figure 2.6 Fluorescent spectra of **COFP** (10 μM) upon incubation with A) **CORM-2** (100 μM) and B) **CORM-3** (100 μM) in PBS (pH = 7.4, 4% DMSO) at 37 ℃. (λ_{ex}= 440 nm, slit widths: W_{ex} = W_{em} = 10 nm)*

As additional controls, we also bubbled CO gas through the probe solution and did not see any fluorescent changes (**Figure 2.7A**). We further examined the existence of CO in solution using Chang's probe, **COP-1**,[78] and observed strong fluorescent intensity changes at 507 nm (**Figure 2.7B**). Then, it became clear that **COFP** did not sense CO delivered in the form of CO gas or from **CO-103**.

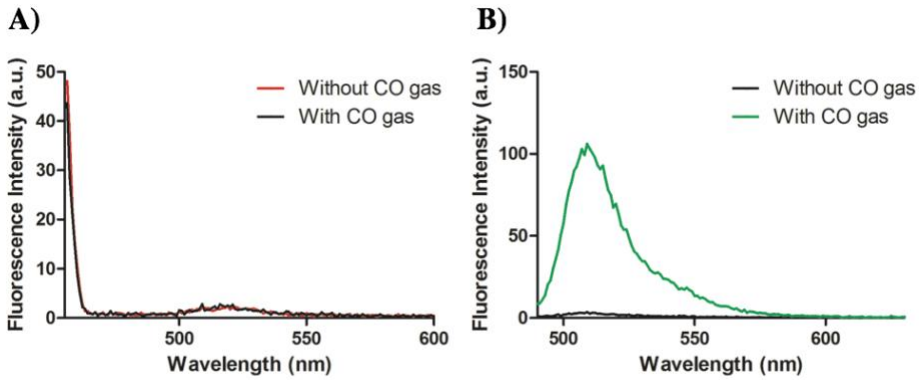

Figure 2.7 Fluorescence spectra of A) COFP (10 μM) and B) COP-1 (1 μM) upon treatment with CO gas in PBS (2% DMSO) at 37 ℃ for 1 h. (COFP: λ_{ex}= 440 nm, slit widths: W_{ex} = 15 nm, W_{em} = 10 nm; COP-1: λ_{ex} = 475 nm, slit widths: W_{ex} = 5 nm, W_{em} = 3 nm).

At this time, it is important to analyze CO's chemistry in the context of CO sensing and CO's reactivity *in vivo*. CO is a Lewis base with strong affinity for transition metals.[102-104] However, it is a consensus in the CO field that in the body, CO undergoes minimal metabolism, despite the presence of a large number of organic molecules with reducing ability and enzymes capable of catalyzing redox reactions.[105, 106] Administered CO largely eliminates through exhalation. There is a large body of literature along this line from studying the physiology and pharmacokinetic properties of CO and in the smokers' population.[107-109] All such reports suggest that CO is very inert. A further search of the chemistry literature indicates that CO is also inert

toward an arylnitro group under normal physiological conditions, as one would expect. However, there are ample precedents that CO is effective in reducing an arylnitro group in the presence of catalytic amounts of transition metal complexes such as that of Au, Ru, Se, and Rh among others.[110-114] Coincidentally, **CORM-2** and **CORM-3** were the only ones examined as CO sources in the reported work.[84-86] These nitro reduction-based CO probes were not tested on CO gas or other metal-free CO donors.

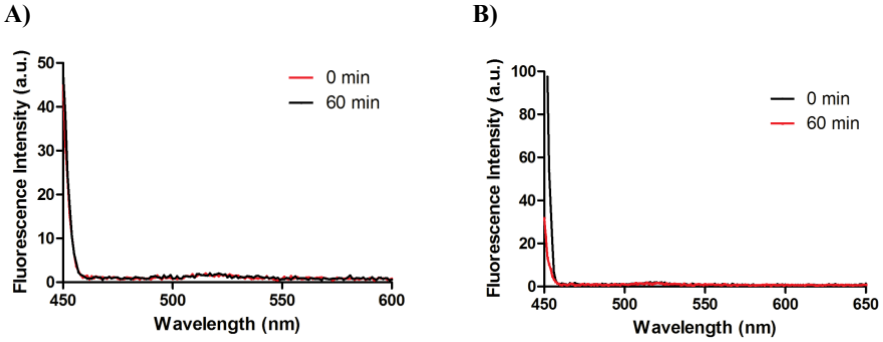

Figure 2.8 Fluorescent spectra of COFP (10 μM) upon incubation with A) CORM-A1 (100 μM) and B) CORM-401 (100 μM) over 60 min in PBS (pH = 7.4, 4% DMSO) at 37 ℃. (λ_{ex}= 440 nm, slit widths: W_{ex} = W_{em} = 10 nm)

In order to further examine the scope of the probe's ability to detect CO from other CO-RMs, we also conducted studies using a boron-based CO donor **CORM-A1** and a manganese-based **CORM-401** with reported release half-life being 21 min and less than 4 min respectively.[59, 115] Specifically, we incubated 10 μM **COFP** with 100 μM **CORM-A1** and **CORM-401** in PBS at 37 °C. However, we did not observe any fluorescent intensity changes from these CO-RMs within 60 min (**Figure 2.8**). As positive controls, **CORM-A1** and **CORM-401** were also incubated with COP-1 under the same conditions; and fluorescent signal increases at 507 nm from COP-1 were observed after 60 min (**Figure 2.9**).

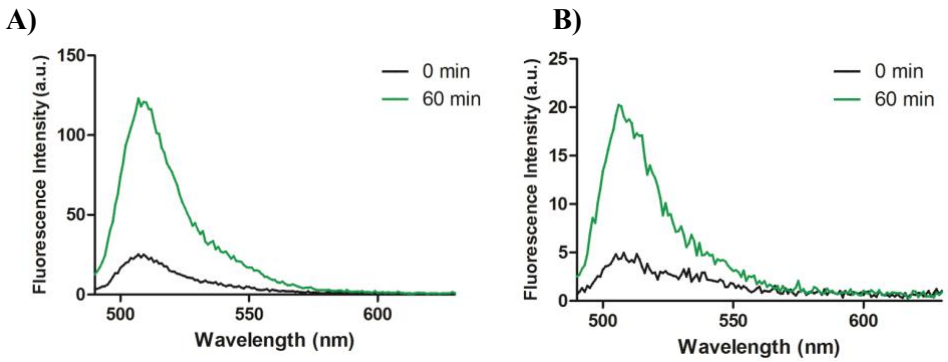

Figure 2.9 Fluorescent spectra of ***COP-1*** *(1 μM) upon incubation with A)* ***CORM-A1*** *(100 μM) and B)* ***CORM-401*** *(100 μM) over 60 min in PBS (pH = 7.4, 4% DMSO) at 37 ℃. (λ_{ex} = 475 nm, slit widths: W_{ex} = 5 nm, W_{em} = 3 nm).*

2.2.2 Responses of LysoFP-NO_2 and NIR-CO upon treatment with CO gas

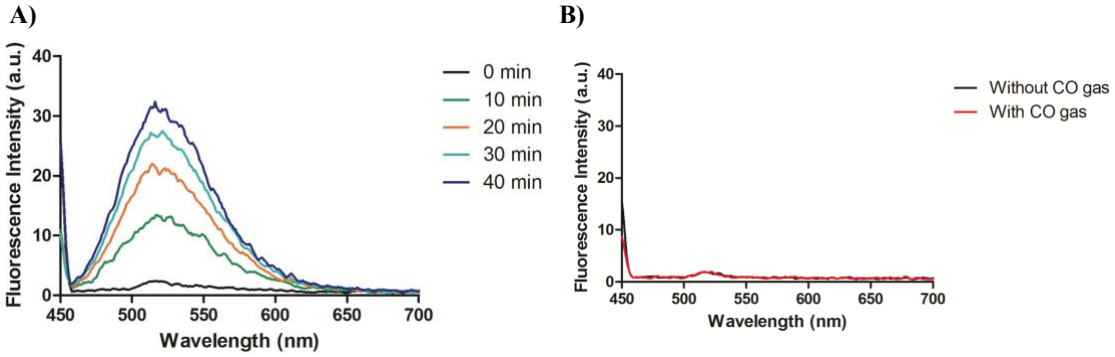

Figure 2.10 Fluorescent spectra of LysoFP-NO_2 (10 μM) upon incubation with A) CORM-3 (100 μM) and B) CO gas in PBS (pH = 7.4, 4% DMSO) at 37 ℃. (λ_{ex}= 440 nm, slit widths: W_{ex} = W_{em} = 10 nm)

As further assessment, we also studied the other two published nitro-based CO probes, **LysoFP-NO_2**[85] and **NIR-CO**[86] (**Figure 2.2**), for their response toward CO from ruthenium-based CO-RMs and pure CO gas. As shown in **Figure 2.10**, CO gas did not turn on **LysoFP-NO_2** after 1 h incubation at 37 °C. However, consistent with the original report, we did observe fluorescent signal increase from LysoFP-NO_2 upon the incubation with **CORM-3** (**Figure 2.10**). Indeed, the results are consistent with what the authors of the **LysoFP-NO_2** probe claim i.e. **LysoFP-NO_2** is a **CORM-3** probe. Next, **NIR-CO** was assessed by using various concentrations of **CORM-2**

following the reported procedure.[86] After incubation for 15 min at room temperature, it was found the absorption peak of **NIR-CO** at 400 nm decreased in a concentration-dependent fashion while the absorption peak at around 625 nm increased concomitantly, indicating the formation of the reduced amino product (**Figure 2.11**). In contrast, no spectroscopic change was observed for **NIR-CO** after treatment with pure CO gas (**Figure 2.11**). Such results indicate that **NIR-CO** does not sense CO delivered in the gas form and is not a general CO probe. Since the biology experiments are beyond the scope of the chemistry question on hand, we did not assess the ability for NIR-CO to sense CO in cell culture and in zebrafish as reported in the original study.

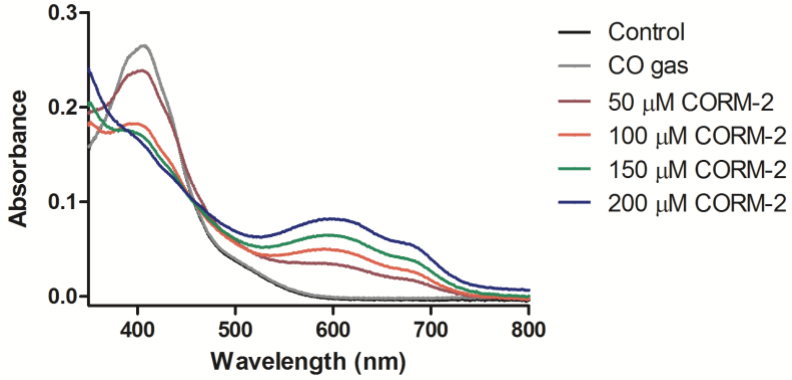

*Figure 2.11 Absorption spectra of NIR-CO (10 μM) upon the treatment with CO gas and various concentrations of **CORM-2** in HEPES buffer (5 mM, pH = 7.4, 30% DMSO) at r.t. for 15 min.*

2.2.3 Reduction of an arylnitro group by CORM-3

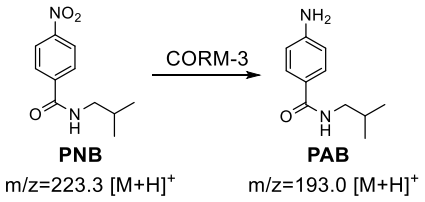

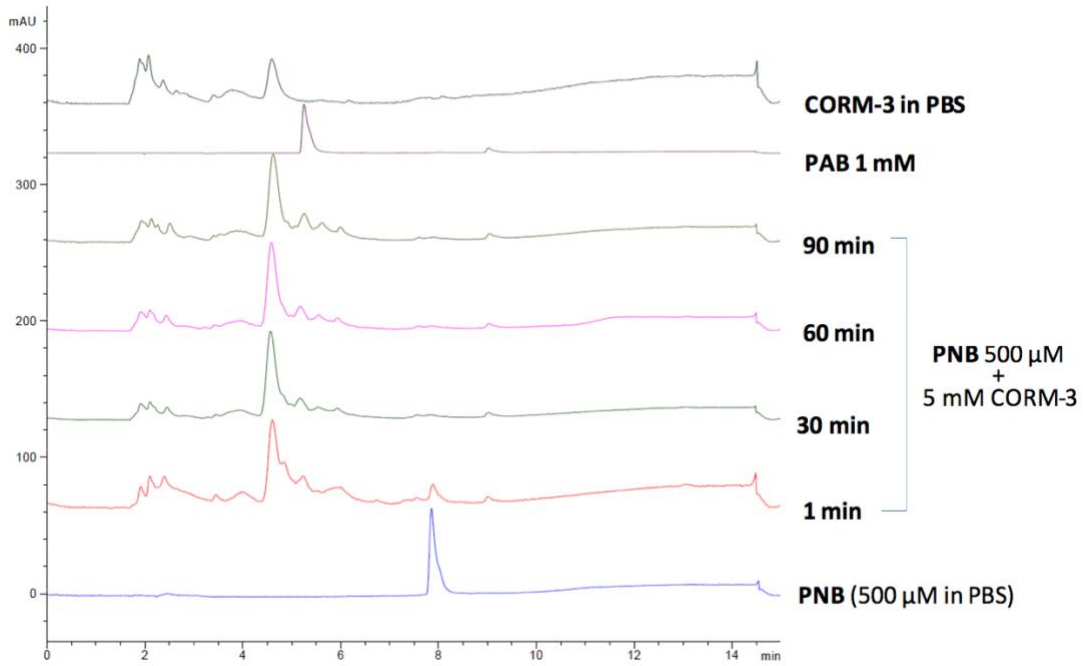

Figure 2.12 HPLC of the PNB/CORM-3 reaction.

To further investigate the ability for ruthenium-based CO-RMs to reduce an arylnitro group, we also studied a *p*-nitrobenzamide compound, PNB (**Figure 2.12**)**,** as a substrate. The HPLC results showed that PNB was completely consumed within 30 min after CORM-3 addition (**Figure 2.12**), accompanied by the formation of a new peak corresponding to the reduced product, *p*-aminobenzamide (PAB). We also performed LC-MS experiments as a secondary verification of the formation of PAB (**Figure 2.13**). After confirmation of CORM-3's ability to reduce PNB to PAB, CO gas was used to conduct the same experiments. It was found that bubbling CO gas into a PNB solution for 2 h at 37 °C did not lead to either changes to the PNB peak nor formation of PAB as studied using HPLC and LC-MS. Such results again indicate that CO alone does not reduce an arylnitro group in the absence of a metal complex such as CORM-3 (**Figure 2.13**). As such, it is reasonable for us to conclude that CO alone does not reduce an arylnitro group to turn on the fluorescence of the probes in question. Likely, the ruthenium core

in CORM-2 or CORM-3 played a catalytic role in enabling the reduction of the nitro group by CO.

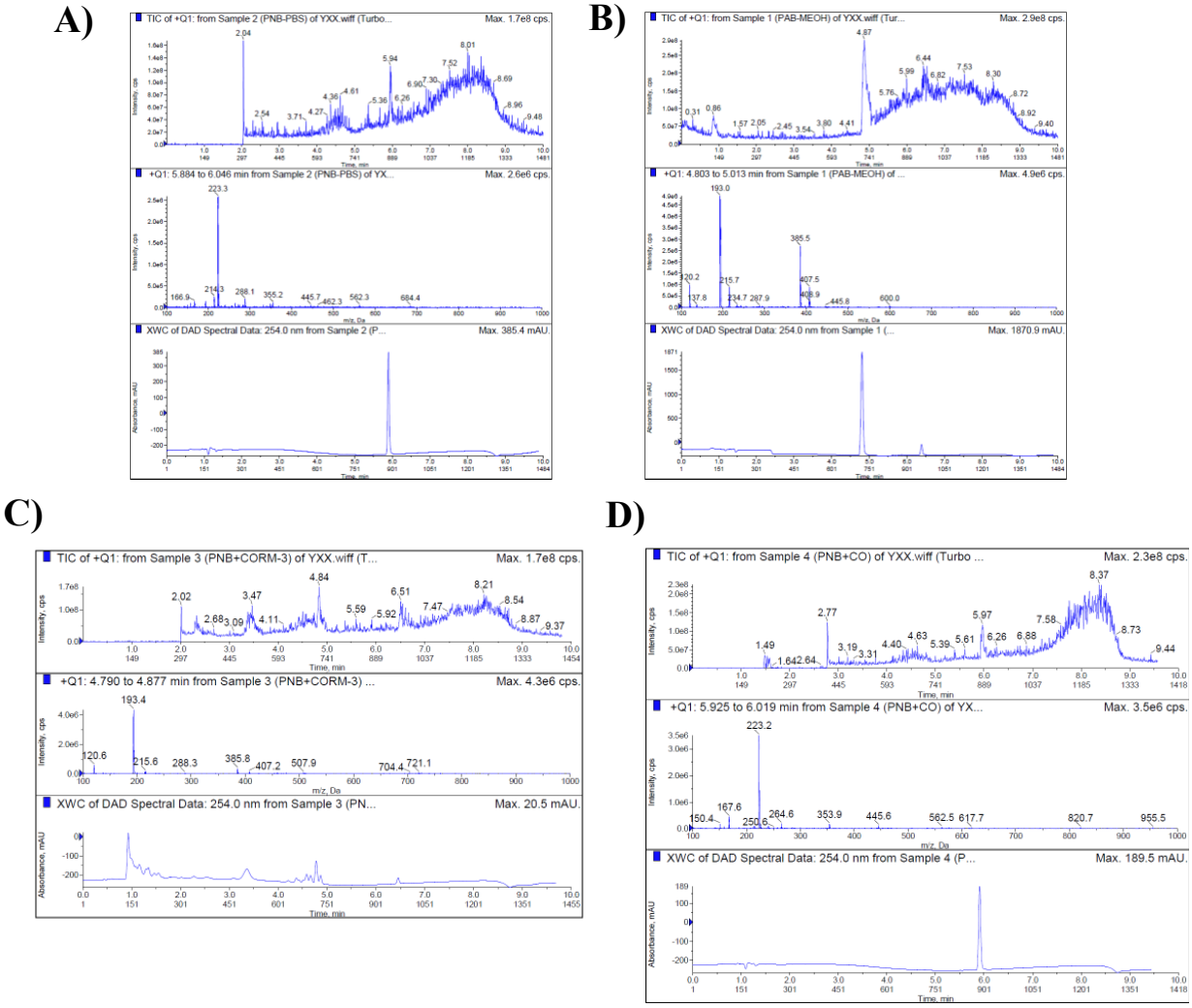

*Figure 2.13 LC/MS analysis of the HPLC sample: (**A**) Before addition of CORM-3, PNB peak at 5.9 min with m/z=223.3 $[M+H]^+$; (**B**) **PAB** reference peak at 4.8 min with m/z=193.0 $[M+H]^+$; (**C**) Reaction mixture with CORM-3 showed **PAB** peak at 4.8 min with m/z=193.4 $[M+H]^+$; (**D**) Bubbling PNB with CO showed only **PNB** peak at 5.9 min with m/z=223.2 $[M+H]^+$*

2.2.4 Reactivities of inactive CORMs toward COFP

Then we looked into whether the ruthenium core without CO would turn on **COFP** by itself. **Complex D** was obtained without carbonyl groups attached to the ruthenium core (**Figure**

2.14B).[116] Upon incubation of **Complex D** with **COFP** in PBS at 37 °C, no fluorescent increase was observed within 1 h (**Figure 2.15**). Such results suggest that the ruthenium core alone cannot reduce the aryl nitro group. Then, it is reasonable to assume that the reducing ability of **CORM-2** and **CORM-3** might come from the ruthenium-carbonyl complex.

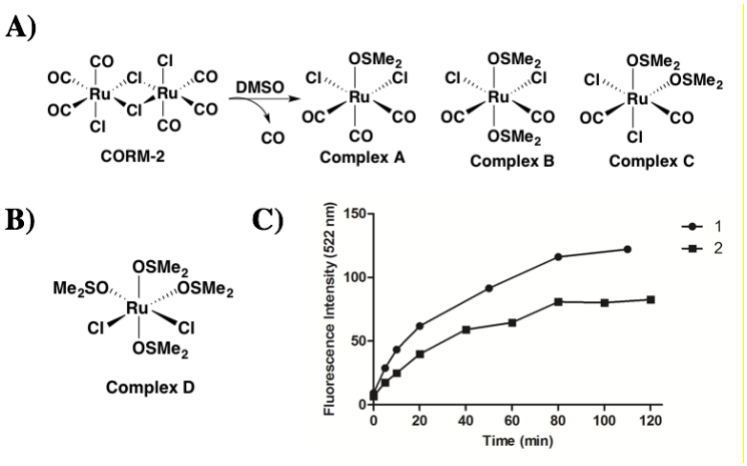

Figure 2.14 ***The reactivities of CORM-2 and its analogs toward COFP.*** *A) reaction between CORM-2 and DMSO; B) chemical structure of complex D; C) fluorescence intensity changes from COFP (10 μM) upon treatment with (1) CORM-2 and (2) reaction products from mixing CORM-2 and DMSO in PBS (pH = 7.4, 4% DMSO) at 37 ℃. (λ_{ex} = 440 nm, λ_{em}= 522 nm, slit widths: W_{ex} = W_{em} = 10 nm)*

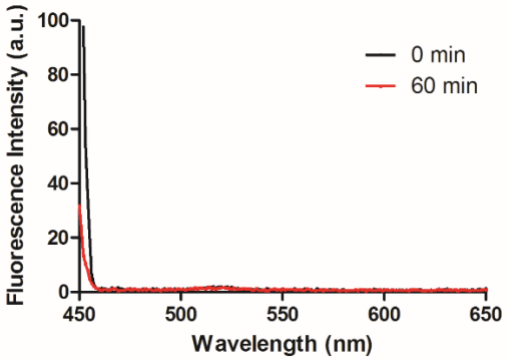

Figure 2.15 Fluorescent spectra of COFP (10 μM) upon incubation with complex D (100 μM) for 60 min in PBS (pH = 7.4, 4% DMSO) at 37 ℃. (λ_{ex} = 440 nm, slit widths: W_{ex} = W_{em} = 10 nm)

Previous NMR studies showed that one **CORM-2** molecule can dissociate into tri-carbonyl (**Complex A**) and di-carbonyl monomers (**Complex B** and **C**) by DMSO during the solubilization process (**Figure 2.14A**).[61] One carbonyl group can be displaced by DMSO to form **complex B** or **C** with loss of a CO molecule. With this in mind, we were interested in comparing the reducing ability of **CORM-2** and its products from ligand substitution with DMSO with the aim of examining if the ruthenium-coordinated CO is involved in the reduction mechanism. Following a reported procedure, **CORM-2** was dissolved in DMSO and incubated at room temperature for 30 min. Gas bubbles from the solution were observed during the incubation, which is consistent with previously published results, and indicate the transformation from **CORM-2** to **Complexes B** and **C** with the release of one CO molecule. The resulting solution was further examined with **COFP** by monitoring the fluorescence signal (**Figure 2.16**), which should be indicative of the reduction reaction. As shown in **Figure 2.14C**, both of the reduction rate and final fluorescence intensity were lower when the DMSO-**CORM-2** solution was used when compared to the fresh **CORM-2** treated control group. Such results were presumably due to the loss of CO from the ruthenium complex prior to exposure to **COFP**.

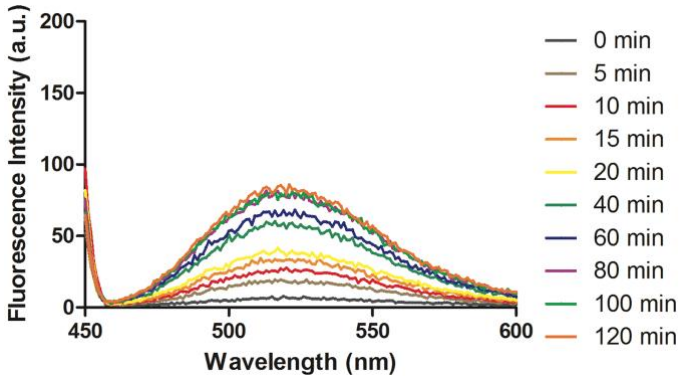

*Figure 2.16 Fluorescent spectral changes of **COFP** (10 μM) upon incubation with reaction products between **CORM-2** and DMSO (100 μM) in PBS (pH = 7.4, 4% DMSO) at 37 ℃. (λ_{ex} = 440 nm, slit widths: W_{ex} = W_{em} = 10 nm)*

Additionally, we also examined the responses of COFP upon treatment with inactive CORM-3 (iCORM-3). According to previous infrared spectroscopy studies, iCORM-3 is a dicarbonyl species formed by loss of one CO molecule from CORM-3.[58] Similar to the case of CORM-2 and DMSO-CORM-2 solution, the reduction rate and final fluorescence intensity were lower when compared with the CORM-3 treatment group (**Figure 2.17**). Such results suggest that, with the loss of one carbonyl ligand, the reducing ability of the ruthenium complex also decreased. Such results also further indicate that the coordinated CO is critical for the ability to reduce an arylnitro group by the ruthenium carbonyl complex.

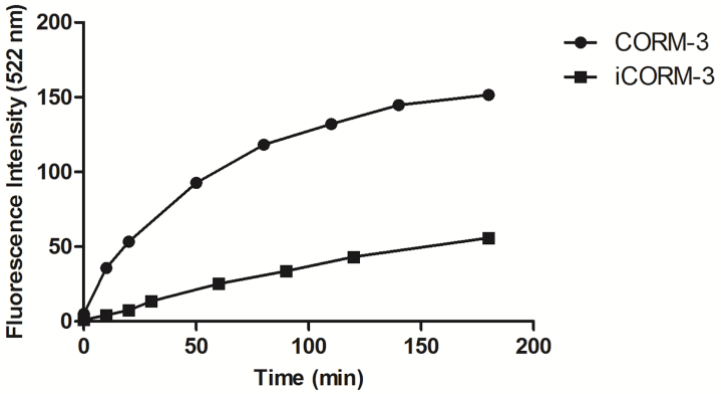

*Figure 2.17 Fluorescence intensity changes from **COFP** (10 μM) upon treatment with **CORM-3** and **iCORM-3** in PBS (pH = 7.4, 4% DMSO) at 37 ℃. (λ_{ex} = 440 nm, λ_{em} = 522 nm, slit widths: W_{ex} = W_{em} = 10 nm)*

Previously, a ruthenium (II) carbonyl complex, $Ru_3(CO)_{12}$, was extensively reported to quantitatively reduce nitrobenzene to aniline in the presence of an amine under high CO pressure (20 to 50 bar) and at high temperature (150 to 180 °C).[117-119] The mechanism was interpreted as involving nitrene formation from the nitro moiety via ruthenium carbonyl complex-mediated metallacyclization and extrusion of CO_2, followed by reaction with CO/H_2O to yield the aromatic amine.[118] In this case, it might be possible that CORM-2 and CORM-3 would lead to the reduction of an arylnitro group through a similar mechanism as presented in **Figure 2.18**.

However, detailed mechanistic studies remain scarce. It should be noted that the most important aspect of all these studies is the demonstration of a ruthenium complex as a prerequisite for probe reduction, not necessarily in the detailed steps of the reaction. Such findings suggest that COFP and other related nitro-based CO probes are capable of sensing only CO from ruthenium-based CO-RMs, as described in the original papers, but is not a general CO probe.

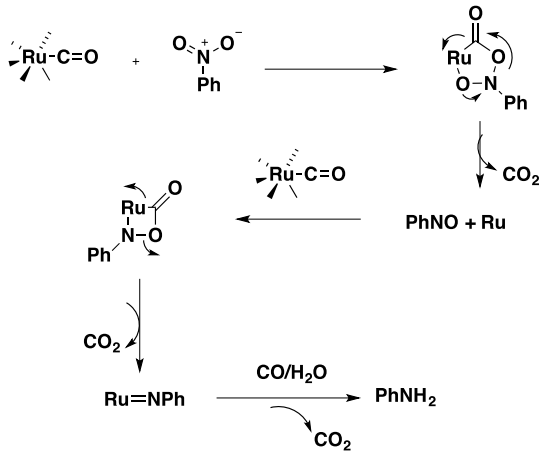

Figure 2.18 A literature proposed mechanism for the reduction of a nitro group to an amine by ruthenium-CO complexes.[118]

2.2.5 Resazurin assay

Resazurin (Alamar Blue) is an *N*-oxide-based dye, widely used in cytotoxicity studies by measuring mammalian cell viability and mitochondrial activity.[120-122] The blue and weakly fluorescent resazurin can be intracellularly reduced to a pink and highly fluorescent compound, resorufin, in metabolically active cells (Figure **2.19A**). In CO and CO-RMs related studies, the resazurin reduction assay has been used to evaluate cytotoxicity.[88, 120] Previously, we reported that **CORM-2** and **CORM-3** could directly reduce the aromatic nitro group to an amino group under physiological conditions *via* a CO-independent pathway. We wonder whether ruthenium-based CO-RMs would also lead to the reduction of *N*-oxide compounds, such as resazurin. If so,

such property would affect the ability for resazurin to be as a reliable indicator of cell viability, when CORM-2 or CORM-3 is present.

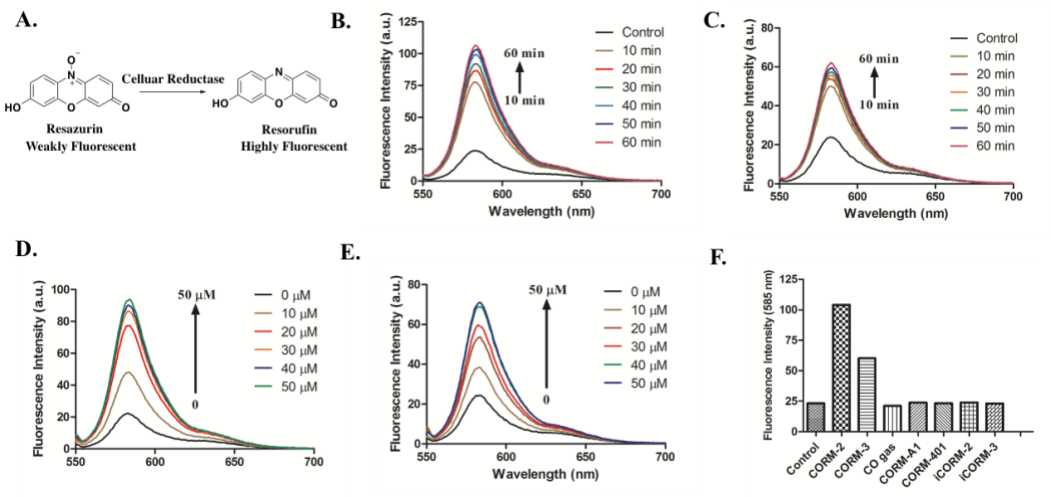

Figure 2.19 ***Responses of resazurin to treatment with various CO donors in PBS (0.01 M, pH = 7.4).*** *A. Mechanism of resazurin-based bioassay. B. The turn-on fluorescence response of 5 μM resazurin to 50 μM CORM-2 in PBS at 37 ℃ (λ_{ex}= 550 nm). C. The turn-on fluorescence response of 5 μM resazurin to 50 μM CORM-3 in PBS at 37 ℃ (λ_{ex}= 550 nm). D. Fluorescence response of 5 μM resazurin to various concentrations of CORM-2 in PBS at 37 ℃ (λ_{ex}= 550 nm). E. Fluorescence response of 5 μM resazurin to various concentrations of CORM-3 in PBS at 37 ℃ (λ_{ex}= 550 nm). F. Fluorescence responses of 5 μM resazurin to 50 μM of various CO donors after 1 h incubation in PBS at 37 ℃ (λ_{ex}= 550 nm).*

To test the reactivity of ruthenium-based CO-RMs with resazurin, we first incubated 5 μM of resazurin with 50 μM of **CORM-2** or **CORM-3** individually in PBS. In both cases, the fluorescence signal at around 583 nm showed a significant increase within an hour (**Figure 2.19B and 2.19C**), and the color of the solution changed from blue to pink, corresponding to the formation of resorufin (Figure **2.19A**). Such changes were also dependent on the concentration of **CORM-2** and **CORM-3** from 0 to 50 μM (**Figure 2.19D and 2.19E**). Under the same conditions, resazurin was also treated with the inactive forms of CO-RMs, iCORM-2 and iCORM-3, neither of which significantly affected the fluorescence upon incubation with resazurin in PBS for 1 h (Figure **2.19F**). For additional control studies, we also injected 10 ml

pure CO gas into the resazurin solution in a sealed vial to see whether CO alone would lead to such a reduction reaction; no change in fluorescence was observed (Figure **2.19F**).

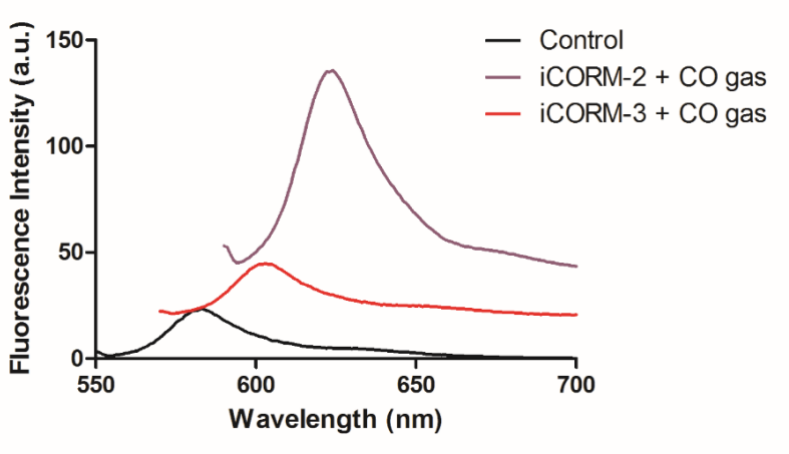

Figure 2.20 Fluorescence response of 5 μM resazurin to iCORM-2/CO gas (10 ml) or iCORM-3/CO gas (10 ml) after incubations for 1 h (λ_{ex}= 550 nm).

To examine the possible reactivity from the combination of iCORMs and CO, pure CO gas was injected together with iCORM-2 or iCORM-3 into the resazurin solution. The iCORM-3 and CO combination did not generate any fluorescent change either (Figure **2.20**). Interestingly, iCORM-2 and CO gas together led to the turn-on of resazurin (Figure **2.20**). This might suggest the catalytic role of the ruthenium core in iCORM-2, which mediates the reduction in the presence of CO. However, to fully understand the intricate details of the mechanism as to why CORM-2 and -3 are different, much more additional studies will be needed. We also examined the reactivities of other non-ruthenium CO-RMs and organic CO prodrugs toward resazurin. Manganese- and a boron-based CORMs, namely CORM-401 and CORM-A1 (Figure **2.1**), did not lead to any change in fluorescence of the resazurin solution (Figure **2.19F**). Organic CO prodrugs, **CO-103**[50] and **CO-111**,[123] also did not lead to an increase in fluorescent signal, indicating a lack of chemical reaction with resazurin (**Figure 2.21**). The above results indicate a CO-independent mechanism for the reduction of resazurin to resorufin by ruthenium-based CO-

RMs. As a result, the reduction-based resazurin assay for cytotoxicity is expected to yield convoluted results that are hard to interpret when CORM-2 or CORM-3 is present.

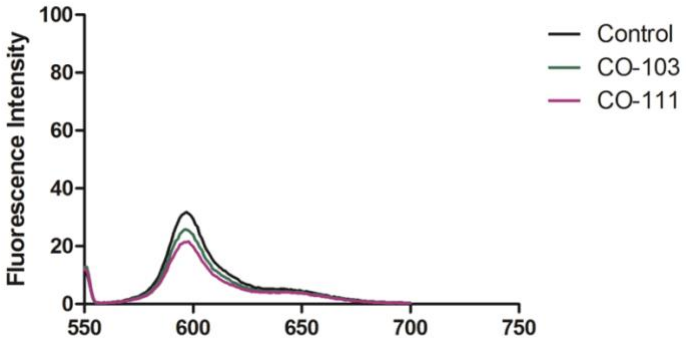

Figure 2.21 Fluorescence response of 5 μM resazurin to incubations with 100 μM of ***CO-103*** *and* ***CO-111*** *in PBS/DMSO (1:4) for 2 h (λ_{ex}= 550 nm).*

2.2.6 MTT-based assays

Another widely used cell proliferation and cytotoxicity assay is based on tetrazolium salts, which can be reduced by cellular reductase to produce the strongly colored formazan products. Among various tetrazolium salts, MTT (3-(4,5-dimethylthiazol-2-yl)-2,5-diphenyltetrazolium bromide) is the most commonly used agent, which was introduced by Mosmann nearly two decades ago.[124] In viable cells, MTT is reduced by cytoplasmic or mitochondrial reductases to form the insoluble purple MTT formazan. Therefore, an increase in absorbance between 550-600 nm is proportional to cell viability. The MTT assay has also been used in studies of CO and CO donors.[125-132] With the discovery of the reducing activities of ruthenium-based CO-RMs toward aromatic nitro compound and resazurin, we also speculate whether there is any interaction between MTT and ruthenium-based CO-RMs.

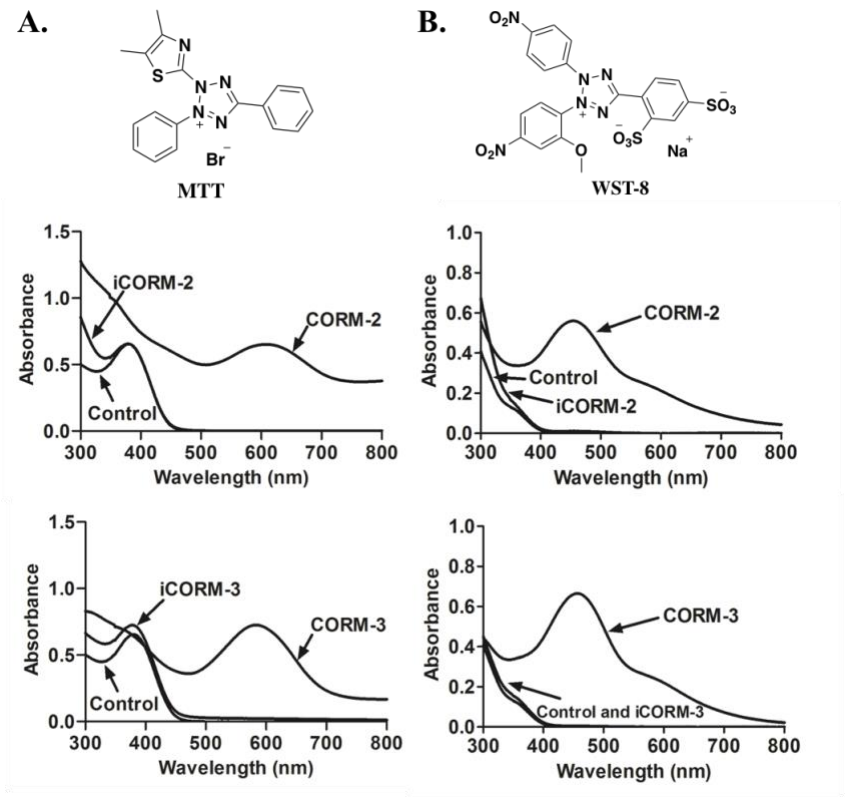

Figure 2.22 ***Responses of MTT derivatives toward ruthenium-based CO-RMs.*** *A. The structure of MTT; UV absorption changes of 100 μM MTT upon treatment with 200 μM CORM-2/3 and iCORM-2/3 for 30 min in PBS (0.01 M, pH = 7.4) at 37 ℃. B. The structure of WST-8; UV absorption changes of 50 μM WST upon treatment with 100 μM CORM-2/3 and iCORM-2/3 for 30 min in PBS (0.01 M, pH = 7.4) at 37 ℃.*

As an initial test, we simply mixed CORM-2 or CORM-3 with an MTT solution and observed almost instantaneous color change from yellow to dark purple. Such a phenomenon is very similar to what is expected from MTT reduction through cellular respiration. Therefore, we conducted further characterizations by using UV spectroscopy. 100 μM of MTT shows a distinct absorption at around 400 nm in PBS solution (Figure **2.22A**). Upon the addition of two equivalents of CORM-2 or CORM-3, a new absorption peak at around 600 nm formed, corresponding to the visible purple color (**Figure 2.22A**). As control experiments, we also incubated CO-depleted iCORM-2 or iCORM-3 with MTT under the same conditions. However, we did not observe any absorption change above 500 nm (Figure **2.22A**). As a second control

study, we added CO gas to the mixture of iCORMs (iCORM-2 or iCORM-3) and MTT to mimic the released products from CORM-2 and CORM-3. The combination of iCORM-3 and CO gas did not lead to UV absorption change (Figure **2.23**). In contrast, 1 ml of pure CO gas caused a slight increase in absorption at around 600 nm (Figure **2.24**) when added to the mixture of iCORM-2 and MTT. However, this change was much smaller than that caused by CORM-2. We also treated MTT with other CO-RMs (CORM-A1 and CORM-401) and did not observe any spectroscopic changes (**Figure 2.25**).

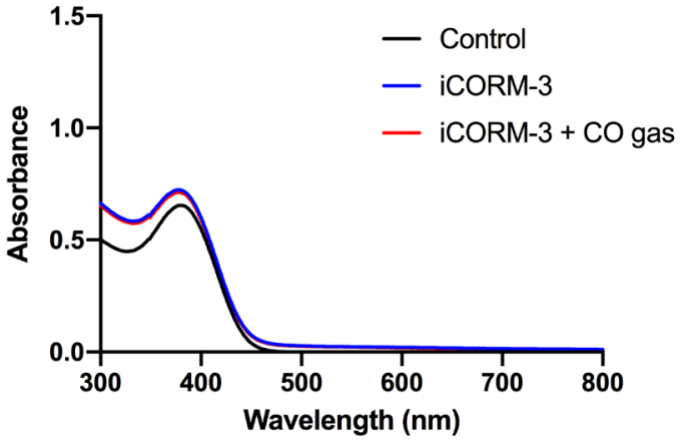

Figure 2.23 UV-vis spectra of MTT (100 μM) after treatment with iCORM-3 (200 μM) or iCORM-3 and CO gas (10 ml) for 30 min in PBS (0.01 M, pH = 7.4) at 37 ℃.

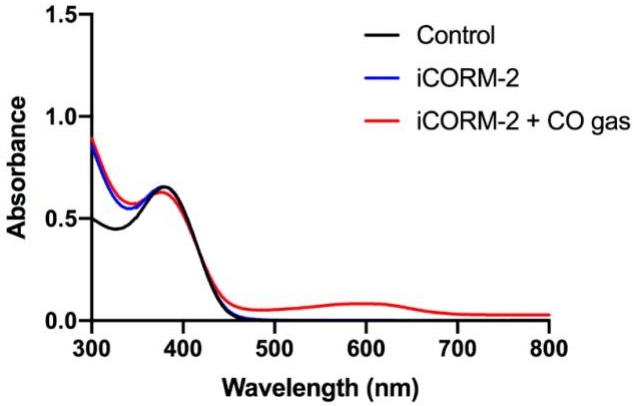

Figure 2.24 UV-vis spectra of MTT (100 μM) after treatment with iCORM-2 (200 μM) or iCORM-2 and CO gas (1 ml) for 30 min in PBS (0.01 M, pH = 7.4) at 37 ℃.

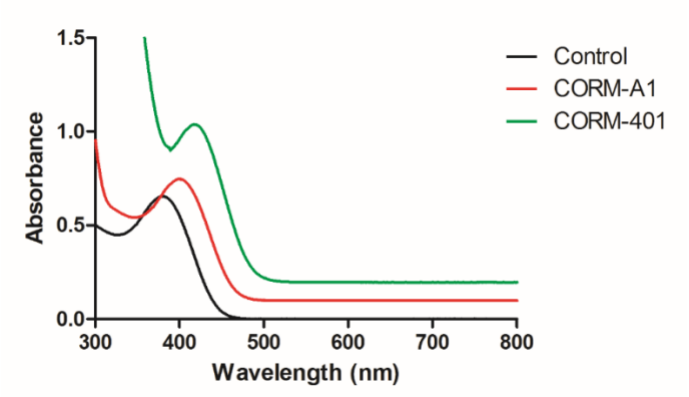

Figure 2.25 UV-vis spectra of MTT (100 μM) after treatment with CORM-A1 (200 μM) or CORM-401 (200 μM) for 30 min in PBS (0.01 M, pH = 7.4) at 37 ℃.

To check whether the color change of MTT caused by ruthenium based CO-RMs was due to the MTT formazan production, the mixture of CORM-2 and MTT in DSMS-d_6 (10% PBS) was monitored by ^{1}H-NMR. Interestingly, the chemical shift of MTT did not show any difference after incubating with CORM-2 (Figure **2.26**), although the corresponding color change was observed. Such results indicate that the UV absorption increase between 500-600 nm was not caused by the presumptive chemical reduction of MTT to its formazan product. We also compared the UV spectrum of the MTT-CORM-2 mixture with that of MTT formazan, and observed some differences in UV absorbance patterns (Figure **2.27**). There are earlier literature reports that tetrazole and formazan are able to chelate to ruthenium (II),[133, 134] which might explain the spectroscopic changes observed.

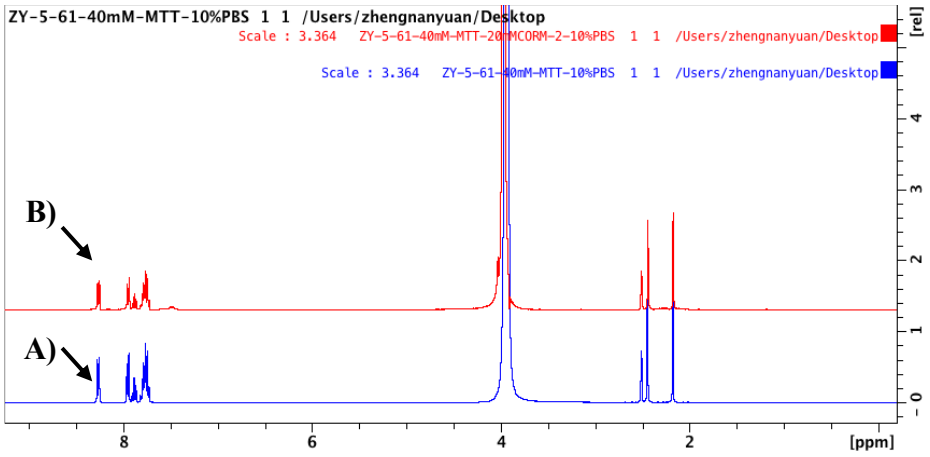

Figure 2.26 ^{1}H NMR spectrum of A) 40 mM MTT and B) Mixture of 40 mM MTT/20 mM CORM-2 (2:1) in DMSO-d6 (10% PBS in D_2O, pH = 7.4).

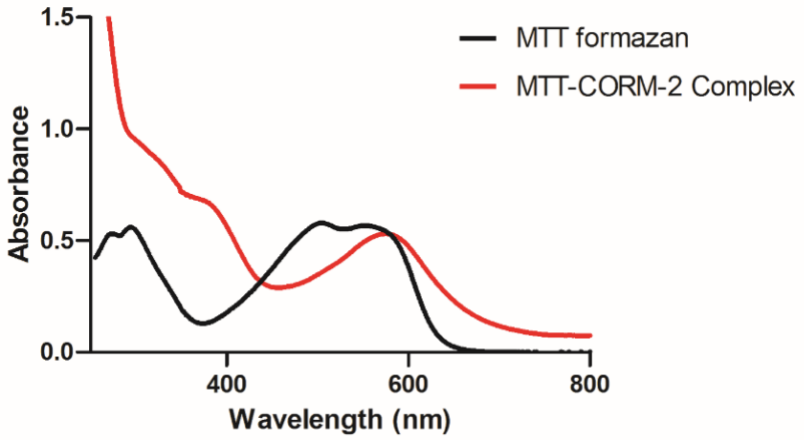

Figure 2.27 UV-vis spectra of MTT formazan (100 μM) and MTT-CORM-2 mixture (100 μM MTT upon treatment with 50 μM CORM-2 for 30 min at 37 ℃) in ACN.

For the next step, we also studied the UV spectroscopic changes of MTT formazan when treated with CORM-2 and CORM-3. As shown in Figure **2.28A**, in the presence of 100 μM of CORM-2, the peak intensity of MTT formazan gradually decreased. At the 50-min time point, the peak at 600 nm almost disappeared completely. 100 μM of CORM-3 also led to the disappearance of the peak corresponding to MTT formazan within 1 h (Figure **2.28B**). Additionally, we also used iCORM-2 and iCORM-3 in control studies. iCORM-2 also led to a decrease of the MTT formazan absorption peak. However, the effect was only 40% of that of

CORM-2 at the 90-min time point (Figure **2.29C**). iCORM-3, on the other hand, induced spectroscopic changes of MTT formazan to the same magnitude as that of CORM-3 (Figure **2.28D**). Such results mean that when MTT is used in cytotoxicity studies, CORM-2 and CORM-3 will interfere with the outcome by perturbing the spectroscopic properties of MTT and MTT formazan.

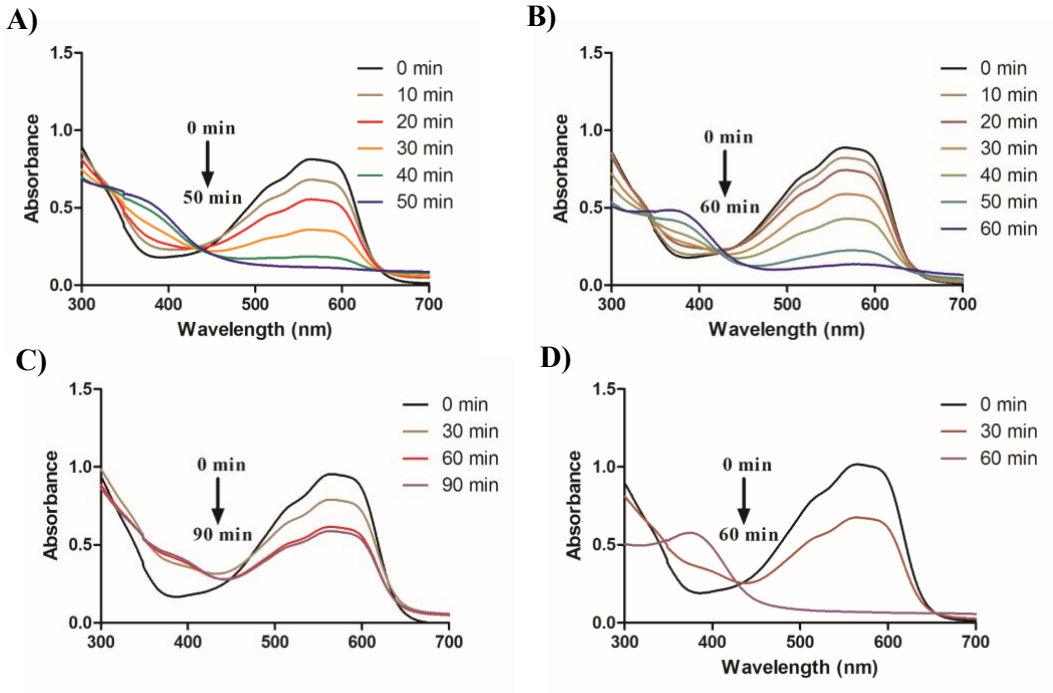

Figure 2.28 UV-vis spectra of MTT formazan (50 μM) upon treatment with 100 μM of A) CORM-2; B) CORM-3; C) iCORM-2; D) iCORM-3 in isopropanol/PBS=1:1 at 37 ℃.

Ruthenium-based CO-RMs have also been tested with another commonly used water-soluble tetrazolium compound, WST-8, which is the active ingredient in the commonly used CCK-8 assay. Similar to MTT, WST-8 also serves as a redox indicator to represent cell viability and has been widely used in CORM-based cytotoxicity studies.[135-139] Upon addition of 100 μM of CORM-2 or CORM-3 to WST-8 in PBS, a new peak at 450 nm appeared within 30 min of incubation at 37 °C (Figure **2.22B**). However, inactive forms of CORM-2 and CORM-3, iCORM-2 and iCORM-3 failed to produce any response under the same conditions (Figure

2.22B). It should be noted that the readouts from CCK-8 is based on the absorbance change of WST-8 at 460 nm in a generally accepted protocol. As such, the spectroscopic changes caused by CORM-2 and CORM-3 are expected to interfere with the results and interpretation of cytotoxicity studies using the CCK-8 assay. Our results show that ruthenium-based CO-RMs can cause significant changes on the spectroscopic properties of tetrazolium salts (MTT and WST-8) and the MTT formazan product, and are expected to affect the absorption readout in MTT- and WST-8-based assays.

2.2.7 Consumption of nitrite

CORM-2 and CORM-3 have been extensively reported to inhibit NO production triggered by various inflammatory stimulators *in vivo*.[140, 141] Due to the rapid oxidation of NO to nitrite by oxygen, the NO concentration in biological studies is usually determined by measuring its nitrite content as a surrogate. Acting as reducing agents to both aryl nitro and *N*-oxide groups, we are interested in evaluating if CORM-2/CORM-3 can also directly react with nitrite, which is the key analyte/ingredient for determining NO concentration. To start with, 100 μM of nitrite was incubated with CORM-2 in PBS for 5 h and 24 h at 37 °C, followed by determining the nitrite concentration using the Griess test. To our surprise, 50 and 100 μM CORM-2 dropped the nitrite concentration by 14% and 15% at the 5-h point and 21% and 34% at the 24-h point, respectively (Figure **2.29A**, **2.30A**). iCORM-2 also caused a comparable decrease in nitrite concentration. 100 μM iCORM-2 decreased the nitrite concentration by almost 48% after 24 h incubation, which was even lower than that caused by CORM-2 (Figure **2.29A**).

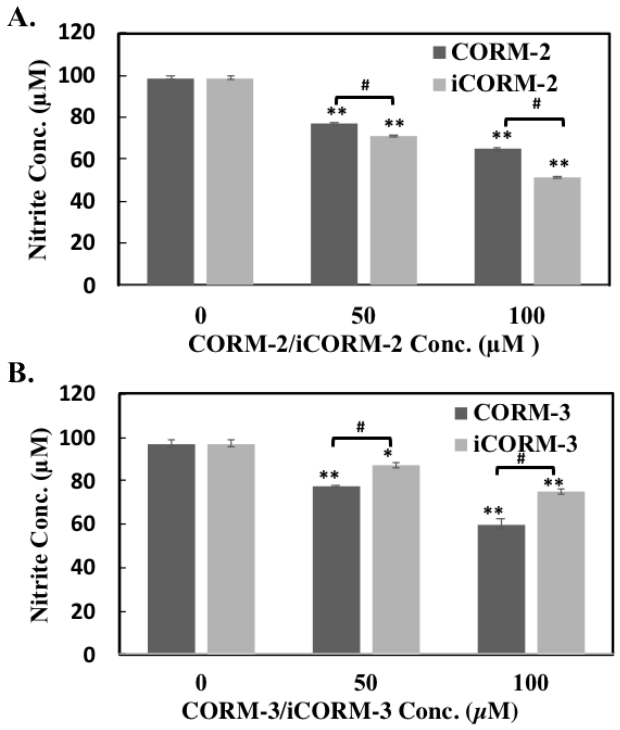

Figure 2.29 ***Effects of ruthenium-based CO-RMs of on nitrite.*** *A. A solution of 100 μM nitrite in PBS was incubated with CORM-2 and iCORM-2 for 24 h at 37 ℃ and then nitrite concentrations were determined by the Griess test. B. A solution of 100 μM nitrite in PBS was incubated with CORM-3 and iCORM-3 for 24 h at 37 ℃ and then nitrite concentrations were determined by the Griess test. Values are means ± SD. n = 3. *P<0.01, **P<0.001 versus the vehicle group. #P<0.001 between CORMs and iCORMs.*

CORM-3 was also examined under the same conditions. Upon treatment with 100 μM of CORM-3 for 5 h and 24 h, the nitrite concentration was reduced by 14% and 38%, respectively (Figure **2.29B**, **2.30B**). Under the same conditions, iCORM-3 did not lead to a significant decrease after 5 h of treatment; however, at the 24-h point, the nitrite concentration decreased by 22%. Such results suggest a weaker reactivity of iCORM-3 compared with CORM-3 (Figure **2.30B**). Our results indicate that both CORM-2 and CORM-3 directly consume nitrite *in vitro*. iCORM-2 and iCORM-3 are not considered to be suitable controls for CORM-2,3 in studying CO's effect on NO production.

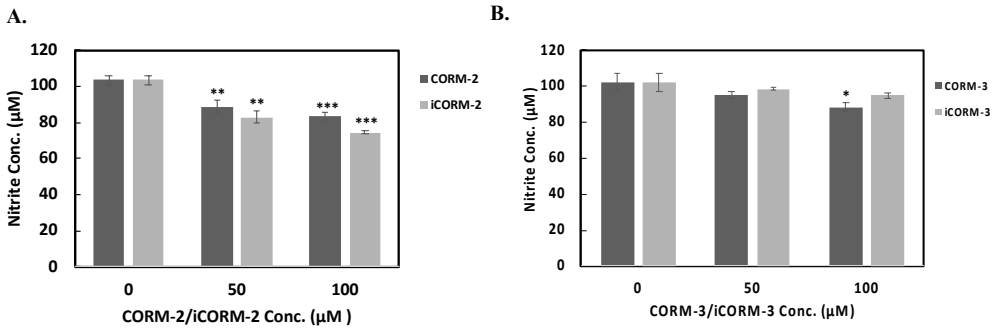

Figure 2.30 ***Effect of ruthenium-based CO-RMs on nitrite.*** *A. 100 μM nitrite PBS solution was incubated with CORM-2 or iCORM-2 for 5 h at 37 ℃ and nitrite concentrations were determined by the Griess test. B. 100 μM nitrite PBS solution was incubated with CORM-3 or iCORM-3 for 5 h at 37 ℃. Nitrite concentrations were determined by the Griess test. Values are means ± SD. n = 3. *P<0.05, **P<0.01, ***P<0.001 versus the vehicle group.*

2.2.8 Azide-based H_2S probe

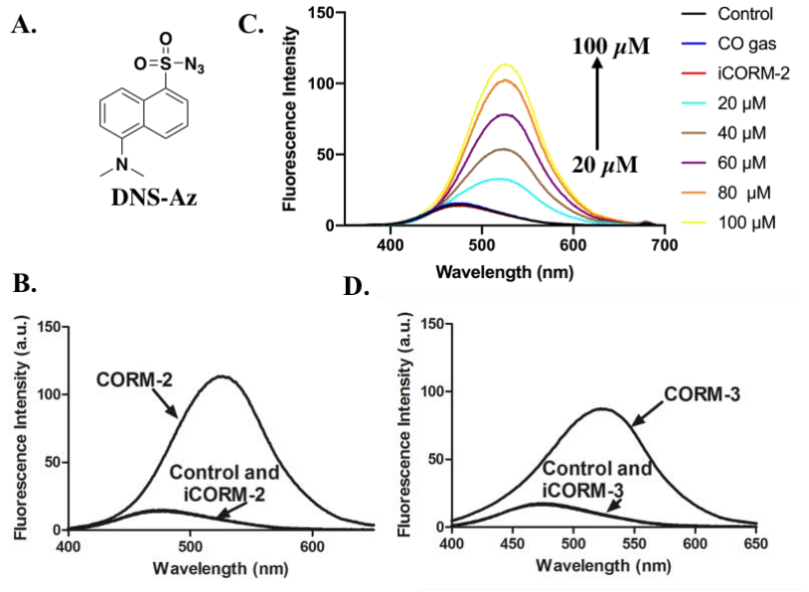

Figure 2.31 ***Responses of DNS-Az toward ruthenium-based CO-RMs.*** *A. The structure of DNS-Az. B. Fluorescence response of 100 μM DNS-Az to 100 μM CORM-2 and iCORM-2 in PBS/ACN (1:1) after incubation for 20 min at r.t. (λ_{ex}= 360 nm). C. Fluorescence response of 100 μM DNS-Az to various concentrations of CORM-2, 100 μM iCORM-2 and 10 ml CO gas in PBS/ACN (1:1) after incubation for 20 min at r.t. (λ_{ex}= 360 nm). D. Fluorescence response of 100 μM DNS-Az to 100 μM CORM-3 and iCORM-3 in PBS/ACN (1:1) after incubation for 20 min at r.t. (λ_{ex}= 360 nm).*

Activated azido groups are known to be reduced by H_2S, and such reactivity is widely used in designing H_2S fluorescent probes.[142-144] Both of DNS-Az[142] and AzMc[145] are H_2S fluorescent probes bearing an azido group attached to a fluorophore (Figure **2.31A, 2.32A**). The reduction of such an azido group to the corresponding amino group by H_2S is the basis for fluorescence turn-on and thus sulfide detection. We were interested in seeing if ruthenium-based CO-RMs could reduce these probes. Therefore, we first studied the response from DNS-Az in the presence of CORM-2. Upon incubation with 100 μM of CORM-2 in PBS/ACN (1:1), the fluorescence intensity of DNS-Az significantly increased within the first 20 min to reach a plateau (Figure **2.31B, 2.32A**). Concentration-dependent fluorescence intensity changes were also observed in the presence of 20 to 100 μM CORM-2 (Figure **2.31C**). Incubations with either iCORM-2 or CO gas did not lead to any fluorescence changes (Figure **2.31C**). 100 μM of CORM-3 also caused an increase in fluorescence intensity of the DNS-Az solution within 20 min, while iCORM-3 did not show any reactivity (Figure **2.31D, 2.31B**).

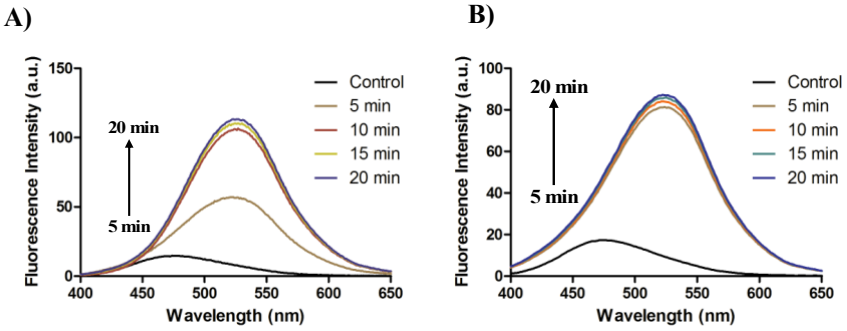

Figure 2.32 Turn-on fluorescence response of 100 μM DNS-Az to 100 μM of A) CORM-2 and B) CORM-3 in PBS (0.01 M, pH = 7.4)/ACN (1:1) at r.t. (λ_{ex}= 360 nm).

Next, AzMC was tested with CORM-2 and CORM-3. Both CORM-2 and CORM-3 led to an increase of the fluorescence intensity of AzMC within 1 h of incubation at room temperature, while incubation with iCORM-2 and iCORM-3 resulted in minimal increases in the

fluorescent intensity (Figure **2.33**). These results suggest that CORM-2 and CORM-3 are capable of reducing the azido groups presented in two representative H_2S probes, DNS-Az and AzMc, while iCORM-2/3 failed to do so. As a result, we recommend azido-based H_2S probes and CORM-2/3 not be used together in studying the cross-talk between CO and H_2S.

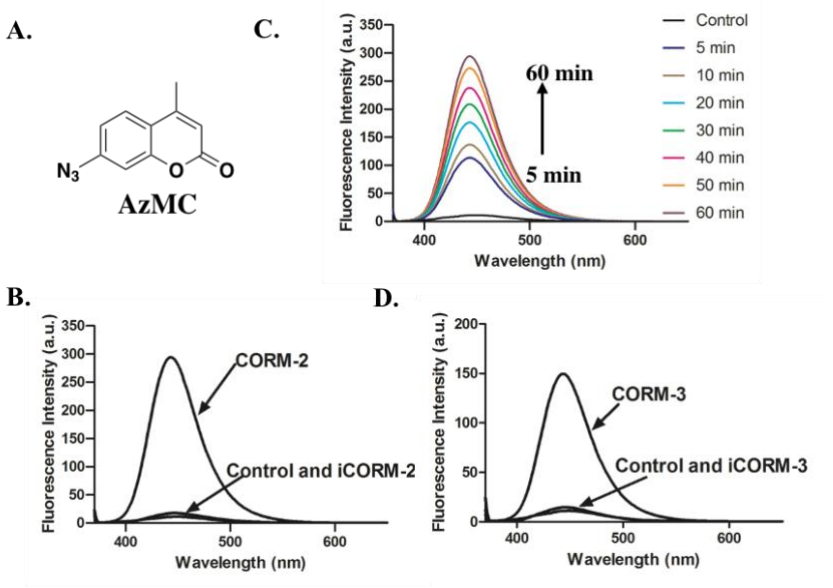

Figure 2.33 ***Responses of AzMc toward ruthenium-based CO-RMs in PBS (0.01 M, pH = 7.4).*** *A. The structure of AzMC. B. Fluorescence response of 10 μM AzMC to 100 μM CORM-2 and iCORM-2 in PBS after incubation for 1 h at r.t. (λ_{ex}= 365 nm). C. Turn-on fluorescence response of 10 μM AzMC to 100 μM CORM-2 in PBS at r.t. (λ_{ex}= 365 nm). D. Fluorescence response of 10 μM AzMC to 100 μM CORM-3 and iCORM-3 in PBS after incubation for 1 h at r.t. (λ_{ex}= 365 nm).*

2.3 Conclusions

In this chapter, we studied CO-independent reactivities of ruthenium-based CO-RMs including: i) reduction of nitro-based CO probes; ii) reduction of resazurin; iii) perturbation of the spectroscopic properties of tetrazolium salts, MTT and WST-8; iv) consumption of nitrites *in vitro* and v) and reduction of azide-based H_2S fluorescent probes, DNS-Az and AzMc. These reagents and related assays have been used in assessing CO's biological effects. As such, we

recommend cautious evaluation of the results when CORM-2/-3 are used in combination of these reagents.

2.4 Experimental part

2.4.1 General information

All reagents and solvents were of reagent grade from commercial suppliers (Sigma Aldrich and etc.). ^{1}H (400 MHz) and ^{13}C (100 MHz) NMR spectra were performed on a Bruker-400 spectrometer. Mass spectral analyses were performed on an ABI API 3200 (ESI-Triple Quadruple) by the Georgia State University Mass Spectrometry Facilities. Fluorescence spectra were recorded on a Shimadzu RF-5301PC fluorometer. Absorption spectra were measured on Varian Cary 100 Bio UV-Visible spectrophotometer. CO-RMs (CORM-2, CORM-3, CORM-A1 and CORM-401) and H_2S probe (AzMC) were purchased from Sigma-Aldrich and were used without purification. Pure CO gas was purchased from Airgas company. iCORM-2 and iCORM-3 were prepared according to the literature procedures.[58, 146] CO prodrugs (CO-103 and CO-111)[73, 123], COP-1[78] and H_2S probe (DNS-Az)[142] were synthesized according to the literature procedures. 2-Dicyanomethylen-3-cyano-4,5,5-trimethyl-2, 5-dihydrofurane was synthesized according to the reported procedures.[147]

2.4.2 Synthesis

5-nitro-2-phenyl-1*H*-benzo[*de*]isoquinoline-1,3(2*H*)-dione (**COFP**) was synthesized according to a reported procedure.[148] 3-Nitro-1,8-naphthalic anhydride (0.62 mmol, 150 mg) and aniline (0.62 mmol, 58 mg) were refluxed in 4 ml acetic acid for 4 h. 20 ml water was added at room temperature and the formed yellow solid was filtered and washed with water. The crude product was purified by silica gel column chromatography to yield the pure product as white solid (103 mg, 52 %). ^{1}H NMR (DMSO-D6) δ 9.51 (s, 1H), 8.95 (s, 1H), 8.81 (d, J = 8.4 Hz,

1H), 8.68 (d, J = 7.2 Hz, 1H), 8.08 (t, J = 8.0 Hz, 1H), 7.56-7.48 (m, 3H), 7.41 (d, J = 7.2 Hz, 2H). ^{13}C NMR (DMSO) δ 163.2, 162.7, 145.9, 136.5, 135.7, 134.0, 131.1, 130.1, 129.9, 129.4, 129.1, 128.6, 124.7, 123.3, 122.9. HRMS calculated for $C_{18}H_{10}N_2O_4Na$ $[M+Na]^+$: m/z 341.0540, found 341.0538. HRMS calculated for $C_{18}H_{10}N_2O_4Na$ $[M+Na]^+$: m/z 341.0540, found 341.0538.

2-(2-morpholinoethyl)-5-nitro-*1H*-benzo[de]isoquinoline-1,3(*2H*)-dione (**LysoFP-NO$_2$**) was synthesized following a modified reported procedure.[85] To a solution of 3-nitro-1,8-naphthalic anhydride (0.33 mmol, 80 mg) in 20 ml ethanol was added 4-(2-aminoethyl) morpholine (0.39 mmol, 51 mg) dropwise in 3 ml ethanol. The solution was allowed to stir for 40 min at r.t. and then heated to reflux for another 2 h. The formed solid was filtered and washed with 5 ml cold ethanol. The crude product was purified by silica gel column chromatography to yield the pure product (42 mg, 36%). ^{1}H NMR ($CDCl_3$) δ 9.30 (d, *J* = 2.2 Hz, 1H), 9.13 (d, *J* = 2.2 Hz, 1H), 8.93-8.61 (m, 1H), 8.43 (d, *J* = 8.2 Hz, 1H), 8.07-7.77 (m, 1H), 4.36 (t, *J* = 6.7 Hz, 2H), 3.80-3.50 (m, 4H), 2.72 (t, *J* = 6.6 Hz, 2H), 2.58 (s, 4H). ^{13}C NMR ($CDCl_3$) δ 163.27, 146.51, 135.71, 134.57, 131.1, 130.3, 129.1, 124.8, 124.3, 123.3, 77.4, 77.1, 76.8, 67.1, 56.1, 53.9, 37.7. HRMS calculated for $C_{18}H_{18}N_3O_5$ $[M+H]^+$: m/z 356.1237, found 356.1246.

(E)-2-(3-cyano-4-(3-hydroxy-4-nitrostyryl)-5,5-dimethylfuran-2(5H)-ylidene)malononitrile (**NIR-CO**) was synthesized following a literature procedure.[86] To a solution of 3-hydroxy-4-nitrobenzaldehyde (105 mg, 0.63 mmol) in 5 ml ethanol was added piperidine (53 mg, 0.63 mmol) and 2-dicyanomethylen-3-cyano-4,5,5-trimethyl-2, 5-dihydrofurane (125 mg, 0.63 mmol). The mixture was allowed to stir at r.t. for 12 h and then filtrated. The residue was purified by silica gel column chromatography to yield the pure product (80 mg, 36%). ^{1}H NMR (DMSO-D6) δ 7.98 (d, *J* = 8.8 Hz, 1H), 7.81 (d, *J* = 16.8 Hz, 1H), 7.51 (d, *J* = 8.4 Hz, 2H), 7.24 (d, *J* = 16.4 Hz, 1H), 1.78 (s, 6H). ^{13}C NMR (DMSO-D6) δ 40.15 (s),

39.88 (d, J = 11.4 Hz), 39.73 (s), 39.52 (s), 39.23 (d, J = 15.8 Hz), 39.10 (s), 38.82 (d, J = 14.8 Hz). HRMS calcd for $C_{18}H_{11}N_4O_4$ $[M-H]^-$: m/z 347.0780, found 347.0774.

cis-$RuCl_2(DMSO)_4$ (**Complex D**) was synthesized according to a reported procedure.[116] Briefly, 100 mg $RuCl_3.xH_2O$ was dissolved in 4 ml DMSO and stirred at reflux for 1 h. The color of the reaction mixture changed from deep brown to light yellow. After cooling to room temperature, the reaction mixture was cooled at -20 °C; the crystalized bright yellow solid was filtered and washed with acetone followed by drying in vacuum to afford 147 mg (63%) of a bright yellow solid. NMR shown the aqua species *cis*,*fac*-$[RuCl_2(dmso\text{-}S)_3(H_2O)]$ after dissolved in D_2O as suggested. ^1H NMR (D_2O) δ 3.48 (s, 6H), 3.46 (s, 6H), 3.37 (s, 6H), 2.70 (s, 6H). ^{13}C NMR (D_2O) δ 46.73, 45.70, 44.31, 38.67.

N-isobutyl-4-nitrobenzamide (**PNB**) To a solution of 4-nitrobenzoic acid (200 mg, 1.2 mmol) in 5 ml DCM was added EDC (343 mg, 1.8 mmol), DMAP (219 mg, 1.8 mmol), triethylamine (181 mg, 1.8 mmol) and isobutylamine (87.6 mg, 1.2 mmol). The mixture was allowed to stir at r.t. for 12 h. The reaction solution was diluted with 15 ml DCM and washed with 10 ml 0.1 M HCl. The organic layer was dried over anhydrous Na_2SO_4 and concentrated under reduced pressure. The residue was purified by silica gel column chromatography to yield the pure product as a white solid (205 mg, 77 %). ^1H NMR ($CDCl_3$) δ 8.15 (d, *J* = 8.8 Hz, 2H), 7.90 (d, *J* = 8.4 Hz, 2H), 7.09 (s, 1H), 3.21 (t, *J* = 6.4 Hz, 2H), 1.87-1.84 (m, 1H), 0.90 (d, *J* = 6.8 Hz, 6H). ^{13}C NMR ($CDCl_3$) δ 165.8, 149.6, 140.6, 128.2, 123.9, 47.78, 28.7 20.3. HRMS calcd for $C_{11}H_{14}N_2O_3$ $[M+H]^+$ 223.1083, found 223.1093.

4-amino-*N*-isobutylbenzamide (**PAB**) To a solution of PNB (45 mg, 0.18 mmol) in 1.8 ml acetone/water (5:1) was added zinc powder (117 mg, 1.8 mmol) and ammonium chloride (144 mg. 2.7 mmol). The mixture was vigorously shaken at room temperature for 1 min and then

filtered. The filtrate was diluted with 10 ml ethyl acetate and washed with 5 ml saturated $NaHCO_3$ solution. The organic layer was dried over anhydrous Na_2SO_4 and concentrated under reduced pressure. The residue was purified by silica gel column chromatography to yield the pure product as a white solid (23 mg, 67%). ^{1}H NMR (Methanol-d4) δ 8.13 (s, 1H), 7.59 (d, *J* = 8.4 Hz, 2H), 6.66 (d, *J* = 8.8 Hz, 2H), 3.15 (t, *J* = 6.4 Hz, 2H), 1.92-1.86 (m, 1H), 0.94 (d, *J* = 6.8 Hz, 6H). ^{13}C NMR (Methanol-d4) δ 170.6, 153.0, 129.8, 123.5, 114.7, 48.3, 29.9, 20.6. HRMS calcd for $C_{11}H_{16}N_2O$ $[M-H]^-$: m/z 191.1186, found 191.1184.

2.4.3 Preparation of stock solutions

COFP, LysoFP-NO_2 and NIR-CO were dissolved in DMSO to afford a 500-μM stock solution; COP-1 was dissolved in DMSO to afford a 200-μM stock solution. Stock solutions of CORM-2 (10 mM), CORM-401 (10 mM), CO-103 (10 mM), CO-111 (10 mM), resazurin (1 mM) and AzMC (1 mM) were prepared in DMSO. 10 mM Stock solutions of CORM-3, CORM-A1, MTT and WST-8 were prepared in water. MTT formazan was dissolved in isopropanol to afford a 2 mM stock solution. DNS-Az was dissolved in ethanol to afford a 30 mM stock solution.

2.4.4 HPLC and LC-MS analysis of reduction of PNB by CORM-3

Stock solution preparation: PNB was dissolved in DMSO to afford a 10 mM stock solution. CORM-3 was dissolved in distilled water to afford a 100 mM stock solution.

20 μL of PNB stock solution was diluted with 360 μL PBS (pH 7.4), followed by addition of 20 μL of the CORM-3 stock solution. The final concentrations of PNB and CORM-3 were 500 μM and 5 mM respectively. The reaction mixture was incubated at 37°C and monitored by HPLC (gradient: ACN in water (0.1%TFA) 5-95% in 10 min, C18 4.6*150 mm column). For CO gas treatment, pure CO gas was bubbled through the PNB solution (500 μM in

PBS, pH 7.4 with 5% DMSO) for 2 h at 37 °C. The formation of PAB was identified by HPLC (with PAB reference compound) and LC/MS.

2.4.5 CO gas treatment

To a 6-ml headspace vial, 2 ml of the sample solution was added. 1 to 10 ml of pure CO gas was directly bubbled into the solution by a headspace gas syringe. The resulting solution was further incubated under various conditions followed by acquisition of the spectroscopic spectra.

2.4.6 Griess test

Nitrite concentrations were measured by the Griess method. According to the vendor's procedure, 50 μL sample solution was mixed with 25 μL Griess reagent R1 (No. 780018, Cayman Chemical) and 25 μL Griess reagent R2 (No. 780020, Cayman Chemical). The resulting mixture was incubated for 10 min before measuring the absorbance at 530 nm. The nitrite concentrations were quantified by using a standard curve.

REFERENCES

1. Ghezzi, P., Protein glutathionylation in health and disease. *Biochim. Biophys. Acta* **2013,** *1830*, 3165-72.
2. Checconi, P.; Limongi, D.; Baldelli, S.; Ciriolo, M. R.; Nencioni, L.; Palamara, A. T., Role of Glutathionylation in Infection and Inflammation. *Nutrients* **2019,** *11*.
3. Young, A.; Gill, R.; Mailloux, R. J., Protein S-glutathionylation: The linchpin for the transmission of regulatory information on redox buffering capacity in mitochondria. *Chem. Biol. Interact.* **2019,** *299*, 151-162.
4. Mailloux, R. J.; Treberg, J. R., Protein S-glutathionlyation links energy metabolism to redox signaling in mitochondria. *Redox Biol.* **2016,** *8*, 110-8.
5. Yang, J.; Gupta, V.; Tallman, K. A.; Porter, N. A.; Carroll, K. S.; Liebler, D. C., Global, in situ, site-specific analysis of protein S-sulfenylation. *Nat. Protoc.* **2015,** *10* (7), 1022-37.
6. Fu, L.; Liu, K.; Ferreira, R. B.; Carroll, K. S.; Yang, J., Proteome-Wide Analysis of Cysteine S-Sulfenylation Using a Benzothiazine-Based Probe. *Curr. Protoc. Protein Sci.* **2019,** *95*, e76.
7. Paul, B. D.; Snyder, S. H., Gasotransmitter hydrogen sulfide signaling in neuronal health and disease. *Biochem. Pharmacol.* **2018,** *149*, 101-109.
8. Kimura, H., Hydrogen Sulfide and Polysulfide Signaling. *Antioxid. Redox Signal* **2017,** *27*, 619-621.
9. Filipovic, M. R.; Zivanovic, J.; Alvarez, B.; Banerjee, R., Chemical Biology of H2S Signaling through Persulfidation. *Chem. Rev.* **2018,** *118*, 1253-1337.
10. Kabil, O.; Banerjee, R., Enzymology of H2S Biogenesis, Decay and Signaling. *Antioxid. Redox Signal.* **2013,** *20* (5), 770-782.
11. Filipovic, M. R., Persulfidation (S-sulfhydration) and H2S. *Handb Exp Pharmacol* **2015,** *230*, 29-59.
12. Fu, L.; Liu, K.; He, J.; Tian, C.; Yu, X.; Yang, J., Direct Proteomic Mapping of Cysteine Persulfidation. *Antioxid. Redox Signal.* **2019**.
13. Yu, B.; Zheng, Y.; Yuan, Z.; Li, S.; Zhu, H.; De La Cruz, L. K.; Zhang, J.; Ji, K.; Wang, S.; Wang, B., Toward Direct Protein S-Persulfidation: A Prodrug Approach That Directly Delivers Hydrogen Persulfide. *J. Am. Chem. Soc.* **2018,** *140* (1), 30.
14. Jarosz, A. P.; Wei, W.; Gauld, J. W.; Auld, J.; Ozcan, F.; Aslan, M.; Mutus, B., Glyceraldehyde 3-phosphate dehydrogenase (GAPDH) is inactivated by S-sulfuration in vitro. *Free Radic. Biol. Med.* **2015,** *89*, 512-21.
15. Zivanovic, J.; Kouroussis, E.; Kohl, J. B.; Adhikari, B.; Bursac, B.; Schott-Roux, S.; Petrovic, D.; Miljkovic, J. L.; Thomas-Lopez, D.; Jung, Y.; Miler, M.; Mitchell, S.; Milosevic, V.; Gomes, J. E.; Benhar, M.; Gonzalez-Zorn, B.; Ivanovic-Burmazovic, I.; Torregrossa, R.; Mitchell, J. R.; Whiteman, M.; Schwarz, G.; Snyder, S. H.; Paul, B. D.; Carroll, K. S.; Filipovic, M. R., Selective Persulfide Detection Reveals Evolutionarily Conserved Antiaging Effects of S-Sulfhydration. *Cell Metab.* **2019,** *30* (6), 1152-1170.e13.
16. Zheng, Y.; Yu, B.; Li, Z.; Yuan, Z.; Organ, C. L.; Trivedi, R. K.; Wang, S.; Lefer, D. J.; Wang, B., An Esterase-Sensitive Prodrug Approach for Controllable Delivery of Persulfide Species. *Angew. Chem. Int. Ed.* **2017,** *56* (39), 11749-11753.

17. Pan, J.; Carroll, K. S., Persulfide Reactivity in the Detection of Protein S-Sulfhydration. *ACS Chem. Biol.* **2013,** *8* (6), 1110.
18. Zhang, D.; Macinkovic, I.; Devarie-Baez, N. O.; Pan, J.; Park, C. M.; Carroll, K. S.; Filipovic, M. R.; Xian, M., Detection of Protein S-Sulfhydration by a Tag-Switch Technique. *Angew. Chem. Int. Ed.* **2014,** *53* (2), 575-581.
19. Kang, J.; Xu, S.; Radford, M. N.; Zhang, W.; Kelly, S. S.; Day, J. J.; Xian, M., O-->S Relay Deprotection: A General Approach to Controllable Donors of Reactive Sulfur Species. *Angew. Chem. Int. Ed.* **2018,** *57* (20), 5893-5897.
20. Khodade, V. S.; Toscano, J. P., Development of S-Substituted Thioisothioureas as Efficient Hydropersulfide Precursors. *J. Am. Chem. Soc.* **2018,** *140* (50), 17333-17337.
21. Powell, C. R.; Dillon, K. M.; Wang, Y.; Carrazzone, R. J.; Matson, J. B., A Persulfide Donor Responsive to Reactive Oxygen Species: Insights into Reactivity and Therapeutic Potential. *Angew. Chem. Int. Ed.* **2018,** *57* (21), 6324-6328.
22. Bora, P.; Chauhan, P.; Manna, S.; Chakrapani, H., A Vinyl-Boronate Ester-Based Persulfide Donor Controllable by Hydrogen Peroxide, a Reactive Oxygen Species (ROS). *Org. Lett.* **2018,** *20* (24), 7916-7920.
23. Chaudhuri, A.; Venkatesh, Y.; Das, J.; Gangopadhyay, M.; Maiti, T. K.; Singh, N. D. P., One- and Two-Photon-Activated Cysteine Persulfide Donors for Biological Targeting. *J. Org. Chem.* **2019,** *84* (18), 11441-11449.
24. Ida, T.; Sawa, T.; Ihara, H.; Tsuchiya, Y.; Watanabe, Y.; Kumagai, Y.; Suematsu, M.; Motohashi, H.; Fujii, S.; Matsunaga, T.; Yamamoto, M.; Ono, K.; Devarie-Baez, N. O.; Xian, M.; Fukuto, J. M.; Akaike, T., Reactive cysteine persulfides and S-polythiolation regulate oxidative stress and redox signaling. *Proc. Natl. Acad. Sci. U.S.A.* **2014,** *111* (21), 7606-7611.
25. Rao, G. S.; Gorin, G., Reaction of Cystine with Sodium Sulfide in Sodium Hydroxide Solution. *J. Org. Chem.* **1959,** *24* (6), 749-753.
26. Smith, D. J.; Venkatraghavan, V., Synthesis and Stability of Thiocysteine. *Synth. Commun.* **1985,** *15* (10), 945-950.
27. Navath, R. S.; Kurtoglu, Y. E.; Wang, B.; Kannan, S.; Romero, R.; Kannan, R. M., Dendrimer−Drug Conjugates for Tailored Intracellular Drug Release Based on Glutathione Levels. *Bioconjug. Chem.* **2008,** *19* (12), 2446-2455.
28. Amsberry, K. L.; Borchardt, R. T., The lactonization of 2'-hydroxyhydrocinnamic acid amides: a potential prodrug for amines. *J. Org. Chem.* **1990,** *55* (23), 5867-5877.
29. Zheng, Y.; Yu, B.; Ji, K.; Pan, Z.; Chittavong, V.; Wang, B., Esterase-Sensitive Prodrugs with Tunable Release Rates and Direct Generation of Hydrogen Sulfide. *Angew. Chem. Int. Ed.* **2016,** *55* (14), 4514-4518.
30. Yu, B.; Zheng, Y.; Yuan, Z.; Li, S.; Zhu, H.; De La Cruz, L. K.; Zhang, J.; Ji, K.; Wang, S.; Wang, B., Toward Direct Protein S-Persulfidation: A Prodrug Approach That Directly Delivers Hydrogen Persulfide. *J. Am. Chem. Soc.* **2018,** *140* (1), 30-33.
31. Peng, H.; Chen, W.; Burroughs, S.; Wang, B., Recent Advances in Fluorescent Probes for the Detection of Hydrogen Sulfide. *Curr. Org. Chem.* **2013,** *17* (6), 641-653.
32. Lin, V. S.; Chen, W.; Xian, M.; Chang, C. J., Chemical probes for molecular imaging and detection of hydrogen sulfide and reactive sulfur species in biological systems. *Chem. Soc. Rev.* **2015,** *44* (14), 4596-4618.
33. Sawahata, T.; Neal, R. A., Use of 1-fluoro-2,4-dinitrobenzene as a probe for the presence of hydrodisulfide groups in proteins. *Anal. Biochem.* **1982,** *126* (2), 360-364.

34. Park, C.-M.; Weerasinghe, L.; Day, J. J.; Fukuto, J. M.; Xian, M., Persulfides: current knowledge and challenges in chemistry and chemical biology. *Mol. BioSyst.* **2015,** *11* (7), 1775-1785.
35. Nakabayashi, T.; Tsurugi, J.; Yabuta, T., Organic Polysulfides.1 IV. Synthesis of Bis(triphenylmethyl) Polysulfides. *J. Org. Chem.* **1964,** *29* (5), 1236-1238.
36. Kawamura, S.; Otsuji, Y.; Nakabayashi, T.; Kitao, T.; Tsurugi, J., Aralkyl Hydrodisulfides. IV. The Reaction of Benzyl Hydrodisulfide with Several Nucleophiles. *J. Org. Chem.* **1965,** *30* (8), 2711-2714.
37. Chatterji, T.; Keerthi, K.; Gates, K. S., Generation of reactive oxygen species by a persulfide (BnSSH). *Bioorg. Med. Chem. Lett.* **2005,** *15* (17), 3921-3924.
38. Bailey, T. S.; Zakharov, L. N.; Pluth, M. D., Understanding Hydrogen Sulfide Storage: Probing Conditions for Sulfide Release from Hydrodisulfides. *J. Am. Chem. Soc.* **2014,** *136* (30), 10573-10576.
39. Bailey, T. S.; Pluth, M. D., Reactions of isolated persulfides provide insights into the interplay between H2S and persulfide reactivity. *Free Radic. Biol. Med.* **2015,** *89*, 662-667.
40. Pan, J.; Carroll, K. S., Persulfide Reactivity in the Detection of Protein S-Sulfhydration. *ACS Chem. Biol.* **2013,** *8* (6), 1110-1116.
41. Zheng, Y.; Yu, B.; La Cruz, L. K.; Roy Choudhury, M.; Anifowose, A.; Wang, B., Toward Hydrogen Sulfide Based Therapeutics: Critical Drug Delivery and Developability Issues. *Med. Res. Rev.* **2018,** *38* (1), 57-100.
42. Martelli, A.; Testai, L.; Breschi, M. C.; Blandizzi, C.; Virdis, A.; Taddei, S.; Calderone, V., Hydrogen sulphide: novel opportunity for drug discovery. *Med. Res. Rev.* **2010,** *32* (6), 1093-1130.
43. Mustafa, A. K.; Gadalla, M. M.; Sen, N.; Kim, S.; Mu, W.; Gazi, S. K.; Barrow, R. K.; Yang, G.; Wang, R.; Snyder, S. H., H₂S Signals Through Protein S-Sulfhydration. *Sci. Signal.* **2009,** *2* (96), ra72-ra72.
44. Jarosz, A. P.; Wei, W.; Gauld, J. W.; Auld, J.; Özcan, F.; Aslan, M.; Mutus, B., Glyceraldehyde 3-phosphate dehydrogenase (GAPDH) is inactivated by S-sulfuration in vitro. *Free Radic. Biol. Med.* **2015,** *89*, 512-521.
45. Liu, C.; Chen, W.; Shi, W.; Peng, B.; Zhao, Y.; Ma, H.; Xian, M., Rational design and bioimaging applications of highly selective fluorescence probes for hydrogen polysulfides. *J. Am. Chem. Soc.* **2014,** *136* (20), 7257-7260.
46. Navath, R. S.; Kurtoglu, Y. E.; Wang, B.; Kannan, S.; Romero, R.; Kannan, R. M., Dendrimer−Drug Conjugates for Tailored Intracellular Drug Release Based on Glutathione Levels. *Bioconjugate Chem.* **2008,** *19* (12), 2446-2455.
47. Wu, L.; Wang, R., Carbon monoxide: endogenous production, physiological functions, and pharmacological applications. *Pharmacol. Rev.* **2005,** *57*, 585-630.
48. Motterlini, R.; Otterbein, L. E., The therapeutic potential of carbon monoxide. *Nat. Rev. Drug Discov.* **2010,** *9*, 728-743.
49. Tayem, Y.; Johnson, T. R.; Mann, B. E.; Green, C. J.; Motterlini, R., Protection against cisplatin-induced nephrotoxicity by a carbon monoxide-releasing molecule. *Am. J. Physiol. Renal Physiol.* **2006,** *290* (4), F789-F794.
50. Steiger, C.; Uchiyama, K.; Takagi, T.; Mizushima, K.; Higashimura, Y.; Gutmann, M.; Hermann, C.; Botov, S.; Schmalz, H.-G.; Naito, Y.; Meinel, L., Prevention of colitis by controlled oral drug delivery of carbon monoxide. *J. Control. Release* **2016,** *239*, 128-136.

51. Hoetzel, A.; Dolinay, T.; Schmidt, R.; Choi, A. M. K.; Ryter, S. W., Carbon Monoxide in Sepsis. *Antioxid. Redox Signal.* **2007,** *9* (11), 2013-2026.
52. Bakalarz, D.; Surmiak, M.; Yang, X.; Wójcik, D.; Korbut, E.; Śliwowski, Z.; Ginter, G.; Buszewicz, G.; Brzozowski, T.; Cieszkowski, J.; Głowacka, U.; Magierowska, K.; Pan, Z.; Wang, B.; Magierowski, M., Organic carbon monoxide prodrug, BW-CO-111, in protection against chemical-induced gastric mucosal damage. *Acta Pharm. Sin. B* **2020,** *in press*.
53. Yang, X.; de Caestecker, M.; Otterbein, L. E.; Wang, B., Carbon monoxide: An emerging therapy for acute kidney injury. *Med. Res. Rev.* **2019,** *40* (4), 1147-1177.
54. Ji, X.; Damera, K.; Zheng, Y.; Yu, B.; Otterbein, L. E.; Wang, B., Toward CO-based Therapeutics: Critical Drug Delivery and Developability Issues. *J. Pharm. Sci.* **2016,** *105*, 405-416 and references cited therein.
55. Soboleva, T.; Esquer, H. J.; Anderson, S. N.; Berreau, L. M.; Benninghoff, A. D., Mitochondrial-Localized Versus Cytosolic Intracellular CO-Releasing Organic PhotoCORMs: Evaluation of CO Effects Using Bioenergetics. *ACS Chem. Biol.* **2018,** *13*, 2220-2228.
56. Soboleva, T.; Simons, C. R.; Arcidiacono, A.; Benninghoff, A. D.; Berreau, L. M., Extracellular vs Intracellular Delivery of CO: Does It Matter for a Stable, Diffusible Gasotransmitter? *J Med Chem* **2019,** *62*, 9990-9995.
57. Zheng, Y.; Ji, X.; Yu, B.; Ji, K.; Gallo, D.; Csizmadia, E.; Zhu, M.; de la Cruz, L. K. C.; Choudhary, M. R.; Chittavong, V.; Pan, Z.; Yuan, Z.; Otterbein, L. E.; Wang, B., Enrichment-triggered Prodrug Activation Demonstrated through Mitochondria-targeted Delivery of Doxorubicin and Carbon Monoxide. *Nat. Chem.* **2018,** *10*, 787-794.
58. Clark James, E.; Naughton, P.; Shurey, S.; Green Colin, J.; Johnson Tony, R.; Mann Brian, E.; Foresti, R.; Motterlini, R., Cardioprotective Actions by a Water-Soluble Carbon Monoxide–Releasing Molecule. *Circ. Res.* **2003,** *93* (2), e2-e8.
59. Crook, S. H.; Mann, B. E.; Meijer, A. J. H. M.; Adams, H.; Sawle, P.; Scapens, D.; Motterlini, R., [Mn(CO)4{S2CNMe(CH2CO2H)}], a new water-soluble CO-releasing molecule. *Dalton Trans.* **2011,** *40* (16), 4230-4235.
60. Mann, B. E., CO-Releasing Molecules: A Personal View. *Organometallics* **2012,** *31*, 5728-5735.
61. Motterlini, R.; Clark James, E.; Foresti, R.; Sarathchandra, P.; Mann Brian, E.; Green Colin, J., Carbon Monoxide-Releasing Molecules. *Circ. Res.* **2002,** *90* (2), e17-e24.
62. Heinemann, S. H.; Hoshi, T.; Westerhausen, M.; Schiller, A., Carbon monoxide--physiology, detection and controlled release. *Chem. Commun.* **2014,** *50* (28), 3644-60.
63. Carrington, S. J.; Chakraborty, I.; Bernard, J. M.; Mascharak, P. K., Synthesis and Characterization of a "Turn-On" photoCORM for Trackable CO Delivery to Biological Targets. *ACS Med. Chem. Lett.* **2014,** *5*, 1324-8.
64. Romão, C. C.; Blättler, W. A.; Seixas, J. D.; Bernardes, G. J., Developing drug molecules for therapy with carbon monoxide. *Chem. Soc. Rev.* **2012,** *41*, 3571-83.
65. Santos-Silva, T.; Mukhopadhyay, A.; Seixas, J. D.; Bernardes, G. J.; Romão, C. C.; Romão, M. J., Towards improved therapeutic CORMs: understanding the reactivity of CORM-3 with proteins. *Curr. Med. Chem.* **2011,** *18*, 3361-6.
66. Popova, M.; Soboleva, T.; Ayad, S.; Benninghoff, A. D.; Berreau, L. M., Visible-Light-Activated Quinolone Carbon-Monoxide-Releasing Molecule: Prodrug and Albumin-Assisted Delivery Enables Anticancer and Potent Anti-Inflammatory Effects. *J. Am. Chem. Soc.* **2018,** *140* (30), 9721-9729.

67. Soboleva, T.; Berreau, L. M., 3-Hydroxyflavones and 3-Hydroxy-4-oxoquinolines as Carbon Monoxide-Releasing Molecules. *Molecules* **2019,** *24*, 1252.
68. Soboleva, T.; Esquer, H. J.; Benninghoff, A. D.; Berreau, L. M., Sense and Release: A Thiol-Responsive Flavonol-Based Photonically Driven Carbon Monoxide-Releasing Molecule That Operates via a Multiple-Input AND Logic Gate. *J Am Chem Soc* **2017,** *139* (28), 9435-9438.
69. Peng, P.; Wang, C.; Shi, Z.; Johns, V. K.; Ma, L.; Oyer, J.; Copik, A.; Igarashi, R.; Liao, Y., Visible-light activatable organic CO-releasing molecules (PhotoCORMs) that simultaneously generate fluorophores. *Org. Biomol. Chem.* **2013,** *11* (39), 6671-4.
70. Palao, E.; Slanina, T.; Muchova, L.; Solomek, T.; Vitek, L.; Klan, P., Transition-Metal-Free CO-Releasing BODIPY Derivatives Activatable by Visible to NIR Light as Promising Bioactive Molecules. *J. Am. Chem. Soc.* **2016,** *138* (1), 126-33.
71. Urdabayev, N. K.; Poloukhtine, A.; Popik, V. V., Two-photon induced photodecarbonylation reaction of cyclopropenones. *Chem. Commun.* **2006**, 454-6.
72. Antony, L. A.; Slanina, T.; Šebej, P.; Šolomek, T.; Klán, P., Fluorescein analogue xanthene-9-carboxylic acid: a transition-metal-free CO releasing molecule activated by green light. *Org. Lett.* **2013,** *15*, 4552-5.
73. Ji, X.; Zhou, C.; Ji, K.; Aghoghovbia, R. E.; Pan, Z.; Chittavong, V.; Ke, B.; Wang, B., Click and Release: A Chemical Strategy toward Developing Gasotransmitter Prodrugs by Using an Intramolecular Diels–Alder Reaction. *Angew. Chem. Int. Ed.* **2016,** *55* (51), 15846-15851.
74. Ji, X.; Pan, Z.; Li, C.; Kang, T.; De La Cruz, L. K. C.; Yang, L.; Yuan, Z.; Ke, B.; Wang, B., Esterase-Sensitive and pH-Controlled Carbon Monoxide Prodrugs for Treating Systemic Inflammation. *J. Med. Chem.* **2019,** *62* (6), 3163-3168.
75. Ji, X.; Wang, B., Strategies toward Organic Carbon Monoxide Prodrugs. *Acc. Chem. Res.* **2018,** *51*, 1377-1385.
76. Kueh, J. T. B.; Stanley, N. J.; Hewitt, R. J.; Woods, L. M.; Larsen, L.; Harrison, J. C.; Rennison, D.; Brimble, M. A.; Sammut, I. A.; Larsen, D. S., Norborn-2-en-7-ones as physiologically-triggered carbon monoxide-releasing prodrugs. *Chem. Sci.* **2017,** *8* (8), 5454-5459.
77. Hess, D. R., Inhaled Carbon Monoxide: From Toxin to Therapy. *Respir. Care* **2017,** *62* (10), 1333-1342.
78. Michel, B. W.; Lippert, A. R.; Chang, C. J., A Reaction-Based Fluorescent Probe for Selective Imaging of Carbon Monoxide in Living Cells Using a Palladium-Mediated Carbonylation. *J. Am. Chem. Soc.* **2012,** *134* (38), 15668-15671.
79. Zheng, K.; Lin, W.; Tan, L.; Chen, H.; Cui, H., A unique carbazole–coumarin fused two-photon platform: development of a robust two-photon fluorescent probe for imaging carbon monoxide in living tissues. *Chem. Sci.* **2014,** *5* (9), 3439-3448.
80. Li, Y.; Wang, X.; Yang, J.; Xie, X.; Li, M.; Niu, J.; Tong, L.; Tang, B., Fluorescent Probe Based on Azobenzene-Cyclopalladium for the Selective Imaging of Endogenous Carbon Monoxide under Hypoxia Conditions. *Anal. Chem.* **2016,** *88* (22), 11154-11159.
81. Feng, W.; Liu, D.; Feng, S.; Feng, G., Readily Available Fluorescent Probe for Carbon Monoxide Imaging in Living Cells. *Anal. Chem.* **2016,** *88* (21), 10648-10653.
82. Pal, S.; Mukherjee, M.; Sen, B.; Mandal, S. K.; Lohar, S.; Chattopadhyay, P.; Dhara, K., A new fluorogenic probe for the selective detection of carbon monoxide in aqueous medium based on Pd(0) mediated reaction. *Chem. Commun.* **2015,** *51* (21), 4410-4413.

83. Wang, J.; Karpus, J.; Zhao, B. S.; Luo, Z.; Chen, P. R.; He, C., A Selective Fluorescent Probe for Carbon Monoxide Imaging in Living Cells. *Angew. Chem. Int. Ed.* **2012,** *51* (38), 9652-9656.
84. Das, B.; Lohar, S.; Patra, A.; Ahmmed, E.; Mandal, S. K.; Bhakta, J. N.; Dhara, K.; Chattopadhyay, P., A naphthalimide-based fluorescence ''turn-on'' chemosensor for highly selective detection of carbon monoxide: imaging applications in living cells. *New J. Chem.* **2018,** *42* (16), 13497-13502.
85. Dhara, K.; Lohar, S.; Patra, A.; Roy, P.; Saha, S. K.; Sadhukhan, G. C.; Chattopadhyay, P., A New Lysosome-Targetable Turn-On Fluorogenic Probe for Carbon Monoxide Imaging in Living Cells. *Anal. Chem.* **2018,** *90* (4), 2933-2938.
86. Wang, Z.; Liu, C.; Wang, X.; Duan, Q.; Jia, P.; Zhu, H.; Li, Z.; Zhang, X.; Ren, X.; Zhu, B.; Sheng, W., A metal-free near-infrared fluorescent probe for tracking the glucose-induced fluctuations of carbon monoxide in living cells and zebrafish. *Sens. Actuators B Chem.* **2019,** *291*, 329-336.
87. Southam, H. M.; Smith, T. W.; Lyon, R. L.; Liao, C.; Trevitt, C. R.; Middlemiss, L. A.; Cox, F. L.; Chapman, J. A.; El-Khamisy, S. F.; Hippler, M.; Williamson, M. P.; Henderson, P. J. F.; Poole, R. K., A thiol-reactive Ru(II) ion, not CO release, underlies the potent antimicrobial and cytotoxic properties of CO-releasing molecule-3. *Redox Biol.* **2018,** *18*, 114-123.
88. Juszczak, M.; Kluska, M.; Wysokiński, D.; Woźniak, K., DNA damage and antioxidant properties of CORM-2 in normal and cancer cells. *Sci Rep* **2020,** *10*, 12200.
89. Nielsen, V. G., The anticoagulant effect of Apis mellifera phospholipase A(2) is inhibited by CORM-2 via a carbon monoxide-independent mechanism. *J Thromb. Thrombolysis* **2020,** *49*, 100-107.
90. Nielsen, V. G.; Wagner, M. T.; Frank, N., Mechanisms Responsible for the Anticoagulant Properties of Neurotoxic Dendroaspis Venoms: A Viscoelastic Analysis. *Int. J. Mol. Sci.* **2020,** *21* (6), 2082.
91. Nielsen, V. G., Ruthenium, Not Carbon Monoxide, Inhibits the Procoagulant Activity of Atheris, Echis, and Pseudonaja Venoms. *Int. J. Mol. Sci.* **2020,** *21* (8), 2970.
92. Stucki, D.; Krahl, H.; Walter, M.; Steinhausen, J.; Hommel, K.; Brenneisen, P.; Stahl, W., Effects of frequently applied carbon monoxide releasing molecules (CORMs) in typical CO-sensitive model systems - A comparative in vitro study. *Arch. Biochem. Biophys.* **2020,** *687*, 108383.
93. Rossier, J.; Delasoie, J.; Haeni, L.; Hauser, D.; Rothen-Rutishauser, B.; Zobi, F., Cytotoxicity of Mn-based photoCORMs of ethynyl-α-diimine ligands against different cancer cell lines: The key role of CO-depleted metal fragments. *J. Inorg. Biochem.* **2020,** *209*, 111122.
94. Santos-Silva, T.; Mukhopadhyay, A.; Seixas, J. D.; Bernardes, G. J.; Romão, C. C.; Romão, M. J., CORM-3 reactivity toward proteins: the crystal structure of a Ru(II) dicarbonyl-lysozyme complex. *J. Am. Chem. Soc.* **2011,** *133* (5), 1192-5.
95. Nobre, L. S.; Jeremias, H.; Romao, C. C.; Saraiva, L. M., Examining the antimicrobial activity and toxicity to animal cells of different types of CO-releasing molecules. *Dalton Trans.* **2016,** *45* (4), 1455-1466.
96. Yuan, Z.; Yang, X.; De La Cruz, L. K. C.; Wang, B., Nitro reduction-based fluorescent probes for carbon monoxide require reactivity involving a ruthenium carbonyl moiety. *Chem. Commun.* **2020,** *56* (14), 2190-2193.

97. Wareham, L. K.; Poole, R. K.; Tinajero-Trejo, M., CO-releasing metal carbonyl compounds as antimicrobial agents in the post-antibiotic era. *J. Biol. Chem.* **2015,** *290* (31), 18999-19007.
98. Gessner, G.; Sahoo, N.; Swain, S. M.; Hirth, G.; Schönherr, R.; Mede, R.; Westerhausen, M.; Brewitz, H. H.; Heimer, P.; Imhof, D.; Hoshi, T.; Heinemann, S. H., CO-independent modification of K(+) channels by tricarbonyldichlororuthenium(II) dimer (CORM-2). *Eur. J. Pharmacol.* **2017,** *815*, 33-41.
99. Dong, D. L.; Chen, C.; Huang, W.; Chen, Y.; Zhang, X. L.; Li, Z.; Li, Y.; Yang, B. F., Tricarbonyldichlororuthenium (II) dimer (CORM2) activates non-selective cation current in human endothelial cells independently of carbon monoxide releasing. *Eur. J. Pharmacol.* **2008,** *590* (1-3), 99-104.
100. Nielsen, V. G.; Garza, J. I., Comparison of the effects of CORM-2, CORM-3 and CORM-A1 on coagulation in human plasma. *Blood Coagul. Fibrinolysis* **2014,** *25* (8), 801-5.
101. Correa-Costa, M.; Gallo, D.; Csizmadia, E.; Gomperts, E.; Lieberum, J.-L.; Hauser, C. J.; Ji, X.; Wang, B.; Câmara, N. O. S.; Robson, S. C.; Otterbein, L. E., Carbon monoxide protects the kidney through the central circadian clock and CD39. *Proc. Natl. Acad. Sci. U.S.A* **2018,** *115* (10), E2302-E2310.
102. Bennett, B.; Lemon, B. J.; Peters, J. W., Reversible Carbon Monoxide Binding and Inhibition at the Active Site of the Fe-Only Hydrogenase. *Biochemistry* **2000,** *39* (25), 7455-7460.
103. Piantadosi, C. A., Biological Chemistry of Carbon Monoxide. *Antioxid. Redox Signal.* **2002,** *4* (2), 259-270.
104. Bagley, K. A.; Van Garderen, C. J.; Chen, M.; Woodruff, W. H.; Duin, E. C.; Albracht, S. P. J., Infrared Studies on the Interaction of Carbon Monoxide with Divalent Nickel in Hydrogenase from Chromatium vinosum. *Biochemistry* **1994,** *33* (31), 9229-9236.
105. Ernst, A.; Zibrak, J. D., Carbon Monoxide Poisoning. *N. Engl. J. Med.* **1998,** *339* (22), 1603-1608.
106. Ryter, S. W.; Otterbein, L. E., Carbon monoxide in biology and medicine. *BioEssays* **2004,** *26* (3), 270-280.
107. Zevin, S.; Saunders, S.; Gourlay, S. G.; Jacob, P.; Benowitz, N. L., Cardiovascular effects of carbon monoxide and cigarette smoking. *J. Am. Coll. Cardiol.* **2001,** *38* (6), 1633-1638.
108. Aronow, W. S.; Dendinger, J.; Rokaw, S. N., Heart Rate and Carbon Monoxide Level After Smoking High-, Low-, and Non-Nicotine Cigarettes: A Study in Male Patients with Angina Pectoris. *Ann. Intern. Med.* **1971,** *74* (5), 697-702.
109. Cohen, S. I.; Perkins, N. M.; Ury, H. K.; Goldsmith, J. R., Carbon Monoxide Uptake in Cigarette Smoking. *Arch. Environ. Occup. Health* **1971,** *22* (1), 55-60.
110. He, L.; Wang, L.-C.; Sun, H.; Ni, J.; Cao, Y.; He, H.-Y.; Fan, K.-N., Efficient and Selective Room-Temperature Gold-Catalyzed Reduction of Nitro Compounds with CO and H2O as the Hydrogen Source. *Angew.Chem. Int. Ed.* **2009,** *48* (50), 9538-9541.
111. Liu, X.; Lu, S., Selective formation of aromatic amines by selenium-catalyzed reduction of aromatic nitro compounds with CO/H2O under atmospheric pressure. *J. Mol. Catal. A: Chem.* **2004,** *212* (1), 127-130.
112. Nomura, K.; Ishino, M.; Hazama, M., Efficient Selective Reduction of Aromatic Nitro Compounds Affording Aromatic Amines under CO/H2O Conditions Catalyzed by Amine-Added Rhodium–Carbonyl Complexes. *Bull. Chem. Soc. Jpn.* **1991,** *64* (9), 2624-2628.

113. Shvo, Y.; Czarkie, D., Catalytic reduction of nitroaromatics with carbon monoxide and water using tricarbonyltetraphenylcyclopentadienone ruthenium(0). *J. Organomet. Chem.* **1989,** *368* (3), 357-365.
114. Tafesh, A. M.; Weiguny, J., A Review of the Selective Catalytic Reduction of Aromatic Nitro Compounds into Aromatic Amines, Isocyanates, Carbamates, and Ureas Using CO. *Chem. Rev.* **1996,** *96* (6), 2035-2052.
115. Motterlini, R.; Sawle, P.; Hammad, J.; Bains, S.; Alberto, R.; Foresti, R.; Green, C. J., CORM-A1: a new pharmacologically active carbon monoxide-releasing molecule. *FASEB J.* **2004,** *19* (2), 284-286.
116. Rauchfuss, T. B., Ruthenium Complexes. In *Inorganic Syntheses*, 1 ed.; Rauchfuss, T. B., Ed. John Wiley & Sons: Hoboken, N, J, 2010; Vol. 35, pp 148-163.
117. Nomura, K., *J. Mol. Catal.* **1992,** *73*, L1-L1.
118. Nomura, K., Efficient selective reduction of aromatic nitro compounds by ruthenium catalysis under CO/H 2 O conditions. *J. Mol. Catal. A: Chem.* **1995,** *95* (3), 203-210.
119. Nomura, K., *Chem. Lett.* **1991,** *20*, 1679-1682.
120. O'Brien, J.; Wilson, I.; Orton, T.; Pognan, F., Investigation of the Alamar Blue (resazurin) fluorescent dye for the assessment of mammalian cell cytotoxicity. *Eur. J. Biochem.* **2000,** *267* (17), 5421-5426.
121. McMillian, M. K.; Li, L.; Parker, J. B.; Patel, L.; Zhong, Z.; Gunnett, J. W.; Powers, W. J.; Johnson, M. D., An improved resazurin-based cytotoxicity assay for hepatic cells. *Cell Biol. Toxicol.* **2002,** *18* (3), 157-173.
122. Abu-Amero, K. K.; Bosley, T. M., Detection of Mitochondrial Respiratory Dysfunction in Circulating Lymphocytes Using Resazurin. *Archi. Patho. Lab. Med.* **2005,** *129* (10), 1295-1298.
123. Pan, Z.; Chittavong, V.; Li, W.; Zhang, J.; Ji, K.; Zhu, M.; Ji, X.; Wang, B., Organic CO Prodrugs: Structure–CO-Release Rate Relationship Studies. *Chem. Eur. J.* **2017,** *23* (41), 9838-9845.
124. Mosmann, T., Rapid colorimetric assay for cellular growth and survival: Application to proliferation and cytotoxicity assays. *J. Immunol. Methods* **1983,** *65* (1), 55-63.
125. Selvamurugan, S.; Ramachandran, R.; Viswanathamurthi, P., Ruthenium(II) carbonyl complexes containing S-methylisothiosemicarbazone based tetradentate ligand: synthesis, characterization and biological applications. *Biometals* **2013,** *26*, 741-53.
126. Hettiarachchi, N. T.; Boyle, J. P.; Dallas, M. L.; Al-Owais, M. M.; Scragg, J. L.; Peers, C., Heme oxygenase-1 derived carbon monoxide suppresses Aβ(1-42) toxicity in astrocytes. *Cell Death Dis.* **2017,** *8*, e2884.
127. Srisook, K.; Han, S. S.; Choi, H. S.; Li, M. H.; Ueda, H.; Kim, C.; Cha, Y. N., CO from enhanced HO activity or from CORM-2 inhibits both O2- and NO production and downregulates HO-1 expression in LPS-stimulated macrophages. *Biochem. Pharmacol.* **2006,** *71*, 307-18.
128. Xu, X.; Zhang, H.; Wang, K.; Tu, T.; Jiang, Y., Protective Effect of Edaravone against Carbon Monoxide Induced Apoptosis in Rat Primary Cultured Astrocytes. *Biochem. Res. Int.* **2017,** *2017*, 5839762.
129. Wang, P.; Liu, H.; Zhao, Q.; Chen, Y.; Liu, B.; Zhang, B.; Zheng, Q., Syntheses and evaluation of drug-like properties of CO-releasing molecules containing ruthenium and group 6 metal. *Eur. J. Med. Chem.* **2014,** *74*, 199-215.

130. Luo, X.; Zhou, X.; Su, P.; Zhu, W., [Effects of Scutellaria baicalensis stem-leaf total flavonoid on proliferation of vassel smooth muscle cells stimulated by high triglyceride blood serum]. *Zhongguo Zhong Yao Za Zhi* **2009,** *34*, 2803-7.
131. Upadhyay, K. K.; Jadeja, R. N.; Vyas, H. S.; Pandya, B.; Joshi, A.; Vohra, A.; Thounaojam, M. C.; Martin, P. M.; Bartoli, M.; Devkar, R. V., Carbon monoxide releasing molecule-A1 improves nonalcoholic steatohepatitis via Nrf2 activation mediated improvement in oxidative stress and mitochondrial function. *Redox Biol.* **2020,** *28*, 101314.
132. Stamellou, E.; Storz, D.; Botov, S.; Ntasis, E.; Wedel, J.; Sollazzo, S.; Krämer, B. K.; van Son, W.; Seelen, M.; Schmalz, H. G.; Schmidt, A.; Hafner, M.; Yard, B. A., Different design of enzyme-triggered CO-releasing molecules (ET-CORMs) reveals quantitative differences in biological activities in terms of toxicity and inflammation. *Redox Biol.* **2014,** *2*, 739-48.
133. Stagni, S.; Orselli, E.; Palazzi, A.; De Cola, L.; Zacchini, S.; Femoni, C.; Marcaccio, M.; Paolucci, F.; Zanarini, S., Polypyridyl Ruthenium(II) Complexes with Tetrazolate-Based Chelating Ligands. Synthesis, Reactivity, and Electrochemical and Photophysical Properties. *Inorg. Chem.* **2007,** *46* (22), 9126-9138.
134. Jameson, G. B.; Muster, A.; Robinson, S. D.; Wingfield, J. N.; Ibers, J. A., Cyclometalated formazan derivatives of ruthenium and osmium: structure of Ru((o-C6H4)N:NC(Ph):NNPh)(CO)(PPh3)2. *Inorg. Chem.* **1981,** *20* (8), 2448-2456.
135. Lv, C.; Su, Q.; Fang, J.; Yin, H., Styrene-maleic acid copolymer-encapsulated carbon monoxide releasing molecule-2 (SMA/CORM-2) suppresses proliferation, migration and invasion of colorectal cancer cells in vitro and in vivo. *Biochem. Biophys. Res. Commun.* **2019,** *520*, 320-326.
136. Pan, Y.; Song, J.; Ma, L.; Zong, X.; Chen, H.; Zhao, B.; Yu, Q.; Song, H., Carbon Monoxide Releasing Molecule 3 Inhibits Osteoclastogenic Differentiation of RAW264.7 Cells by Heme Oxygenase-1. *Cell Physiol. Biochem.* **2018,** *50*, 1988-2003.
137. Yoon, Y. E.; Lee, K. S.; Lee, Y. J.; Lee, H. H.; Han, W. K., Renoprotective Effects of Carbon Monoxide-Releasing Molecule 3 in Ischemia-Reperfusion Injury and Cisplatin-Induced Toxicity. *Transplant Proc.* **2017,** *49*, 1175-1182.
138. Shao, L.; Gu, Y. Y.; Jiang, C. H.; Liu, C. Y.; Lv, L. P.; Liu, J. N.; Zou, Y., Carbon monoxide releasing molecule-2 suppresses proliferation, migration, invasion, and promotes apoptosis in non-small cell lung cancer Calu-3 cells. *Eur. Rev. Med. Pharmacol. Sci.* **2018,** *22*, 1948-1957.
139. Yan, Y.; Du, C.; Li, G.; Chen, L.; Yan, Y.; Chen, G.; Hu, W.; Chang, L., CO suppresses prostate cancer cell growth by directly targeting LKB1/AMPK/mTOR pathway in vitro and in vivo. *Urol. Oncol.* **2018,** *36*, 312.e1-312.e8.
140. Choi, E.-Y.; Choe, S.-H.; Hyeon, J.-Y.; Choi, J.-I.; Choi, I. S.; Kim, S.-J., Carbon monoxide-releasing molecule-3 suppresses Prevotella intermedia lipopolysaccharide-induced production of nitric oxide and interleukin-1β in murine macrophages. *Eur. J. Pharmacol.* **2015,** *764*, 22-29.
141. Sun, B.-W.; Sun, Y.; Sun, Z.-W.; Chen, X., CO liberated from CORM-2 modulates the inflammatory response in the liver of thermally injured mice. *World J Gastroenterol* **2008,** *14* (4), 547-553.
142. Peng, H.; Cheng, Y.; Dai, C.; King, A. L.; Predmore, B. L.; Lefer, D. J.; Wang, B., A Fluorescent Probe for Fast and Quantitative Detection of Hydrogen Sulfide in Blood. *Angew. Chem. Intl. Ed.* **2011,** *50* (41), 9672-9675.

143. Lippert, A. R.; New, E. J.; Chang, C. J., Reaction-Based Fluorescent Probes for Selective Imaging of Hydrogen Sulfide in Living Cells. *J. Am. Chem. Soc.* **2011,** *133* (26), 10078-10080.
144. Wang, K.; Peng, H.; Wang, B., Recent Advances in Thiol and Sulfide Reactive Probes. *J. Cell. Biochem.* **2014,** *115* (6), 1007-1022.
145. Thorson, M. K.; Majtan, T.; Kraus, J. P.; Barrios, A. M., Identification of Cystathionine β-Synthase Inhibitors Using a Hydrogen Sulfide Selective Probe. *Angew. Chem. Intl. Ed.* **2013,** *52* (17), 4641-4644.
146. Babu, D.; Leclercq, G.; Motterlini, R.; Lefebvre, R., Differential effects of CORM-2 and CORM-401 in murine intestinal epithelial MODE-K cells under oxidative stress. *Front. Pharmacol.* **2017,** *8*, 31.
147. Villemin, D.; Liao, L., RAPID AND EFFICIENT SYNTHESIS OF 2-[3-CYANO-4-(2-ARYLIDEN)-5, 5-DIMETHYL-5H-FURAN-2-YLIDENE]-MALONONITRILE UNDER FOCUSED MICROWAVE IRRADIATION. *Synth. Commun.* **2001,** *31* (11), 1771-1780.
148. Yuan, Y.-C.; Kamaraj, R.; Bruneau, C.; Labasque, T.; Roisnel, T.; Gramage-Doria, R., Unmasking Amides: Ruthenium-Catalyzed Protodecarbonylation of N-Substituted Phthalimide Derivatives. *Org. Lett.* **2017,** *19* (23), 6404-6407.

APPENDICES

Appendix A NMR Spectrum of BW-GP-401 and Trapped prodruct A.

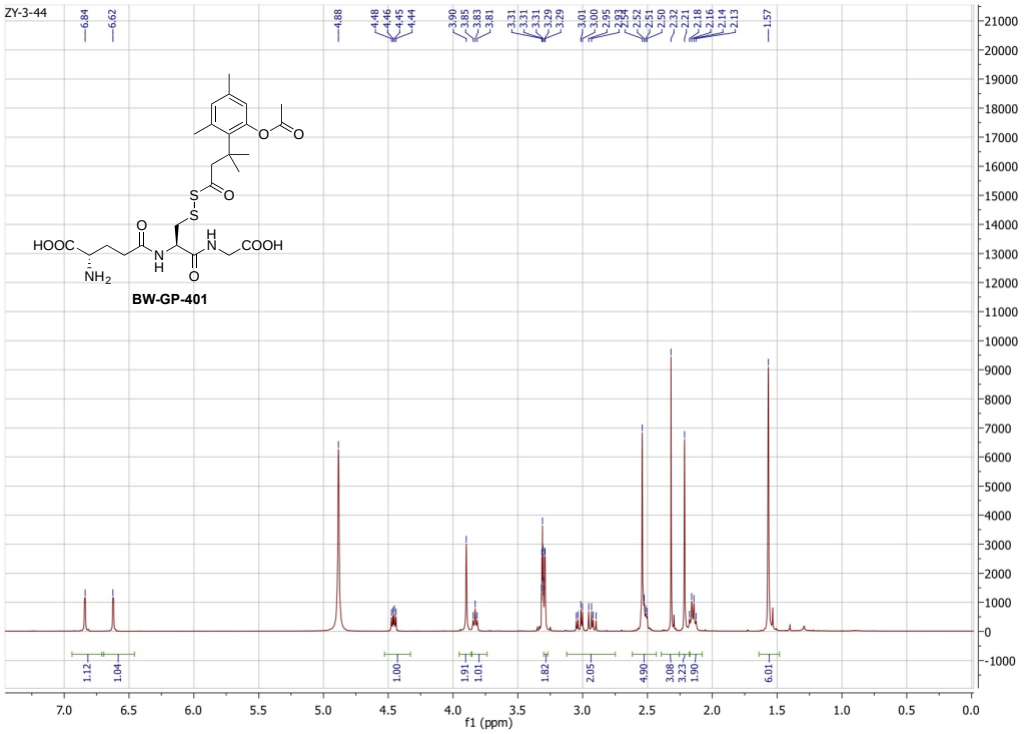

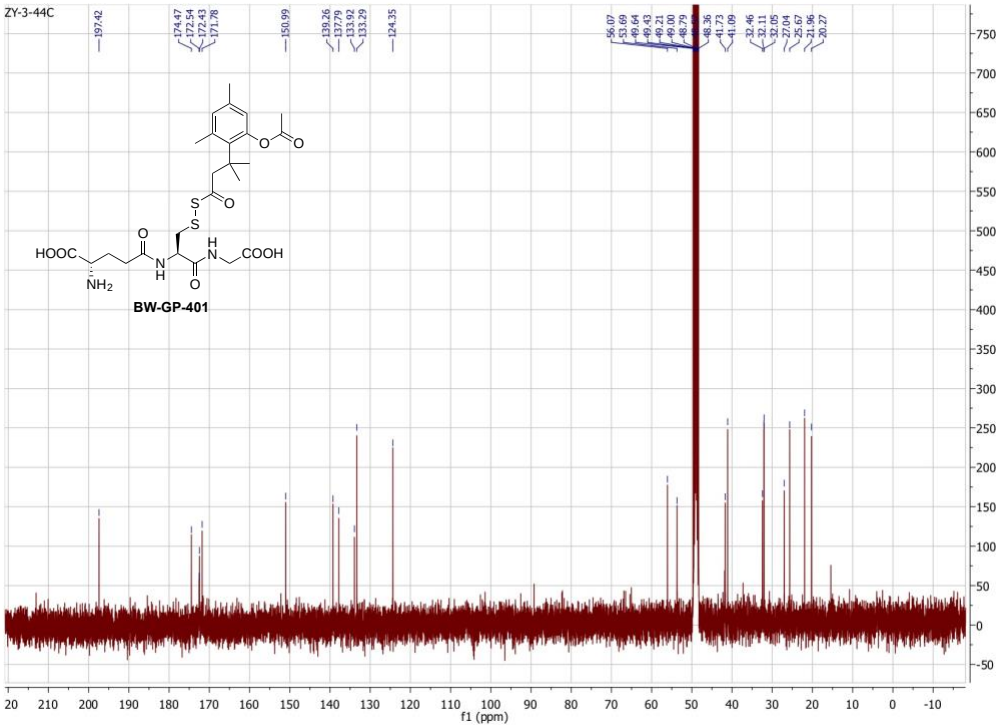

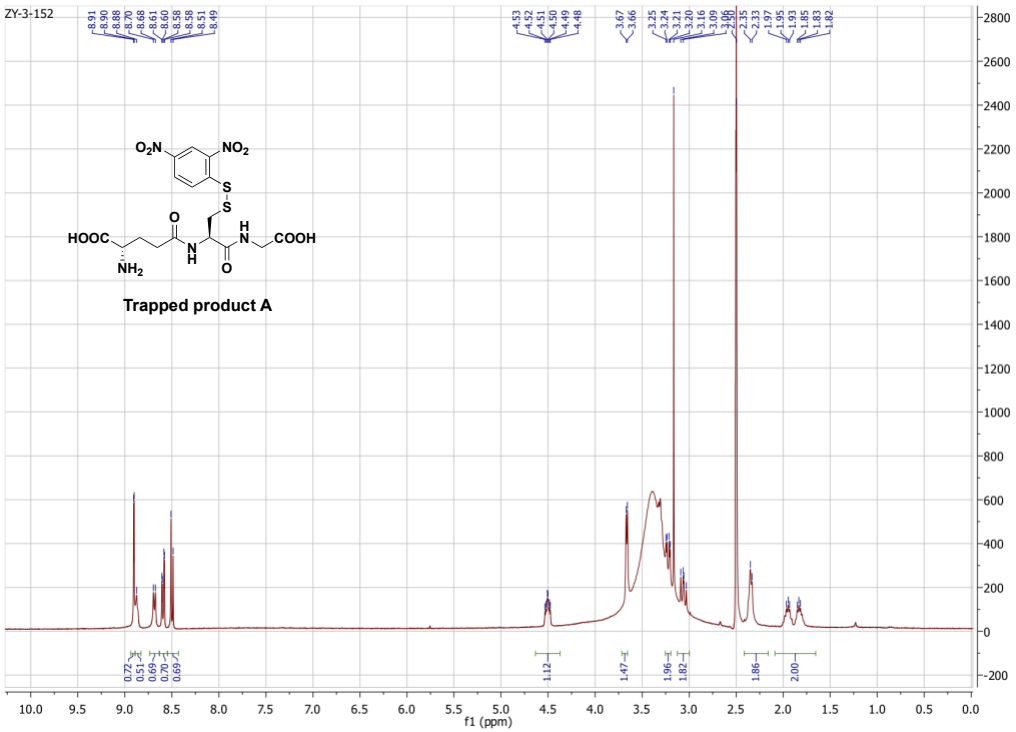
ZY-3-152
Trapped product A
f1 (ppm)

Appendix B NMR Spectrum of persulfide prodrugs and trapped products.

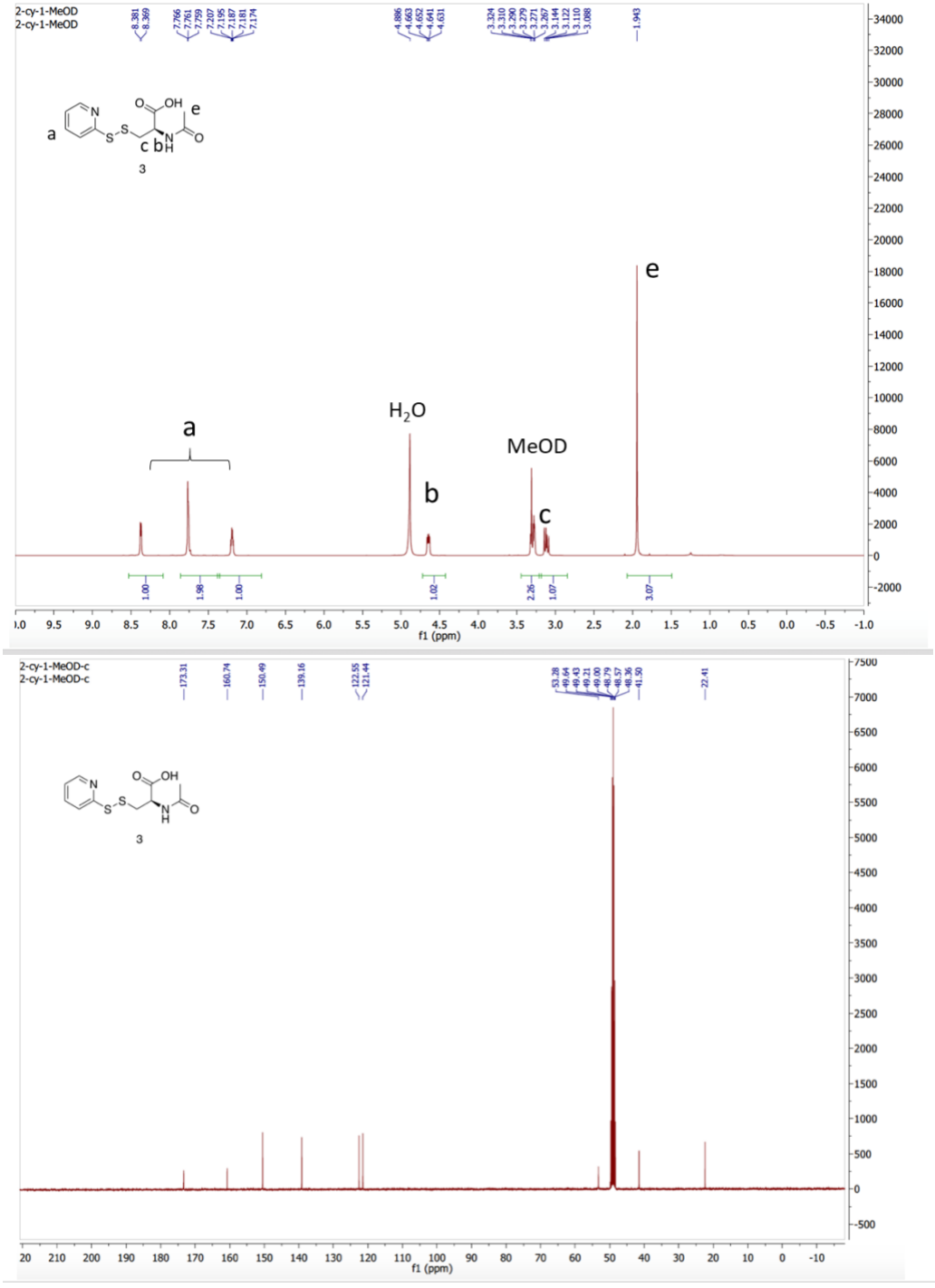

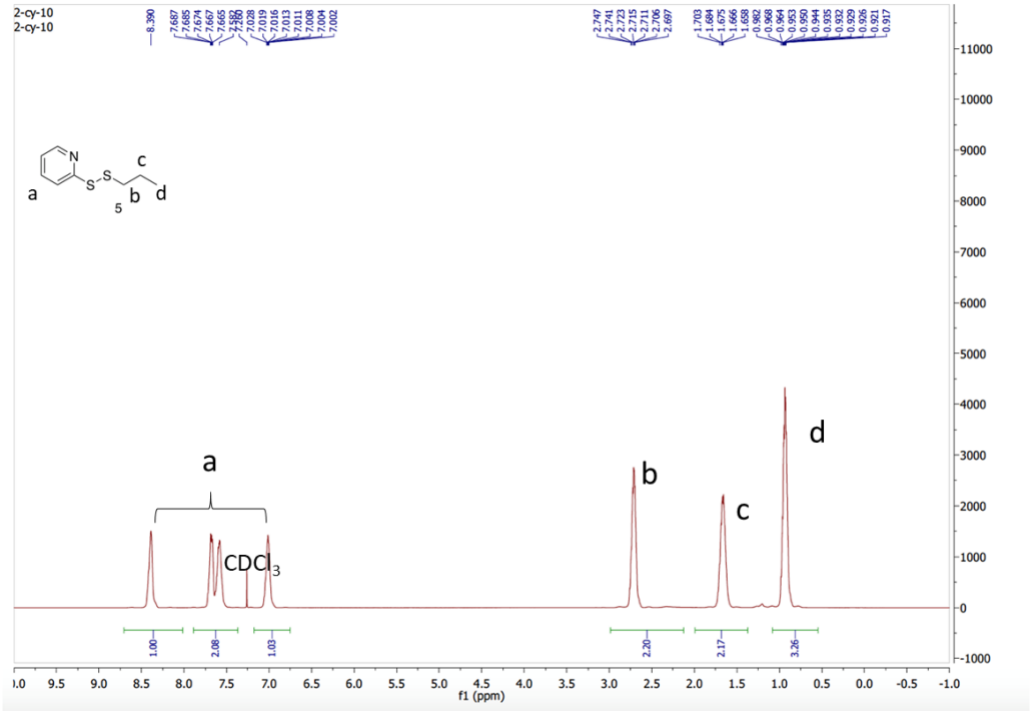
2-cy-10
2-cy-10
a
b
c
d
5
CDCl3
f1 (ppm)

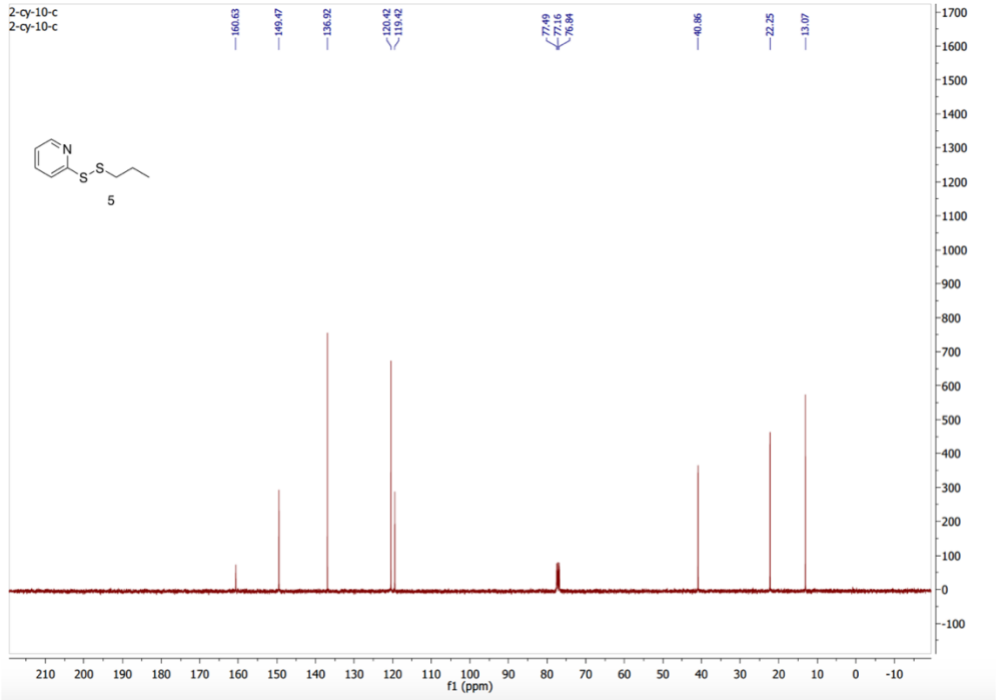
2-cy-10-c
2-cy-10-c
5
f1 (ppm)

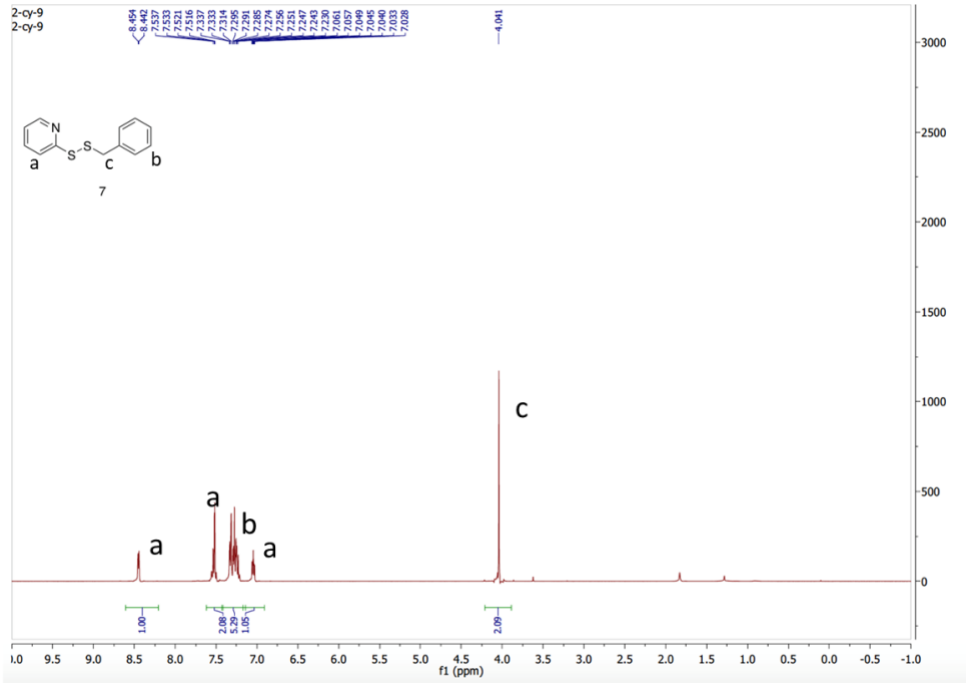
2-cy-9
2-cy-9
a
b
c
7
f1 (ppm)

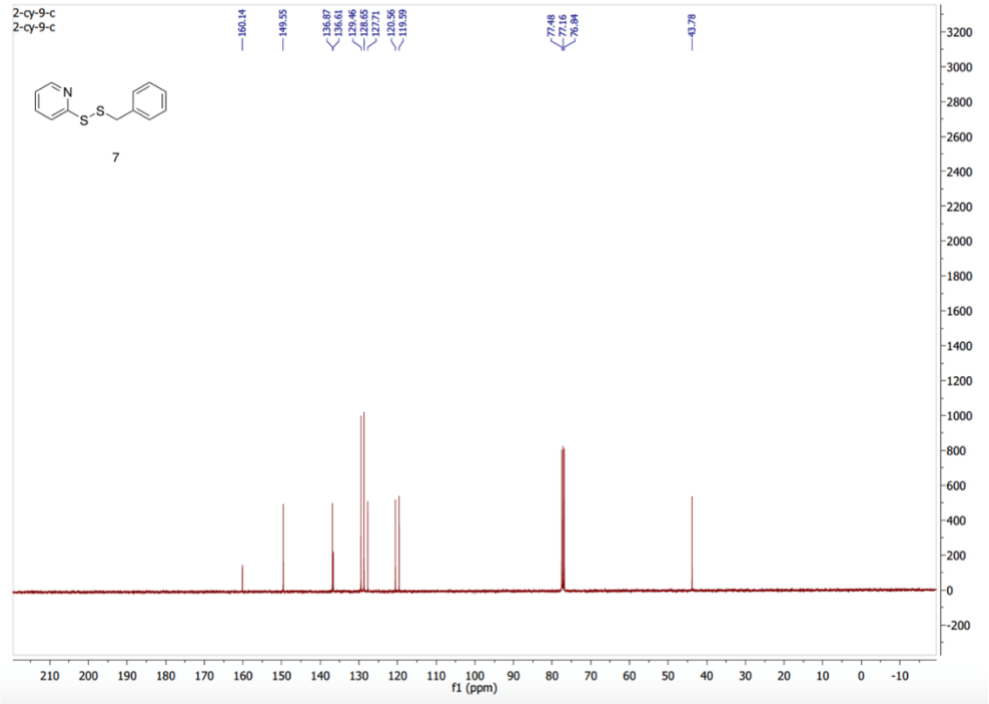
2-cy-9-c
2-cy-9-c
7
f1 (ppm)

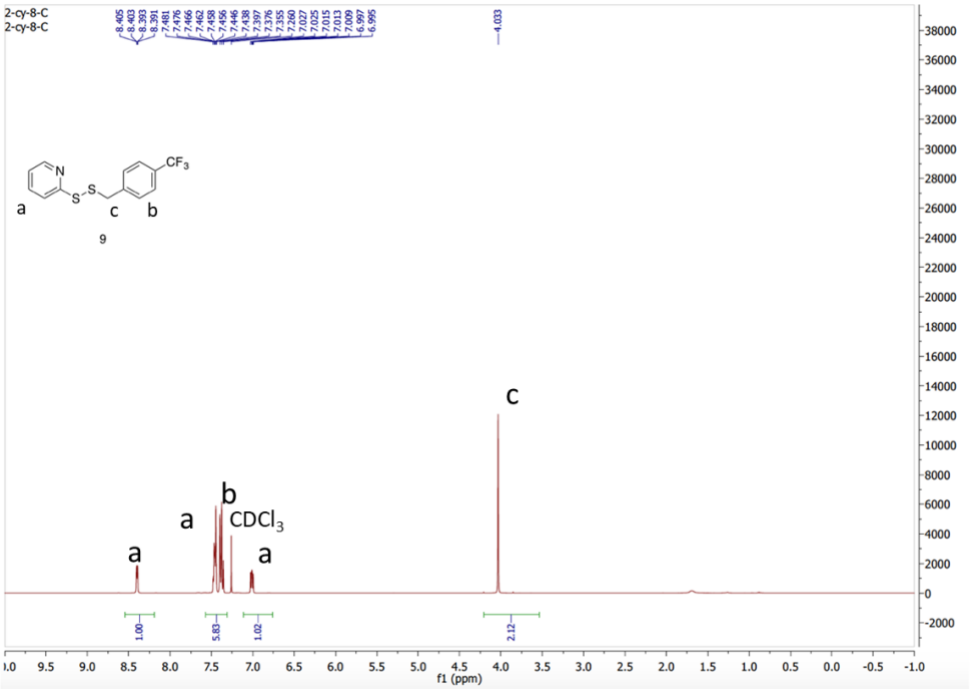
2-cy-8-C
2-cy-8-C
8.405
8.403
8.393
8.391
7.481
7.476
7.466
7.462
7.458
7.456
7.446
7.438
7.397
7.376
7.355
7.260
7.027
7.025
7.015
7.013
7.009
6.997
6.995
4.033
CF3
N
S
S
a
c
b
9
c
b
a
CDCl3
a
a
1.00
5.83
1.02
2.12
f1 (ppm)

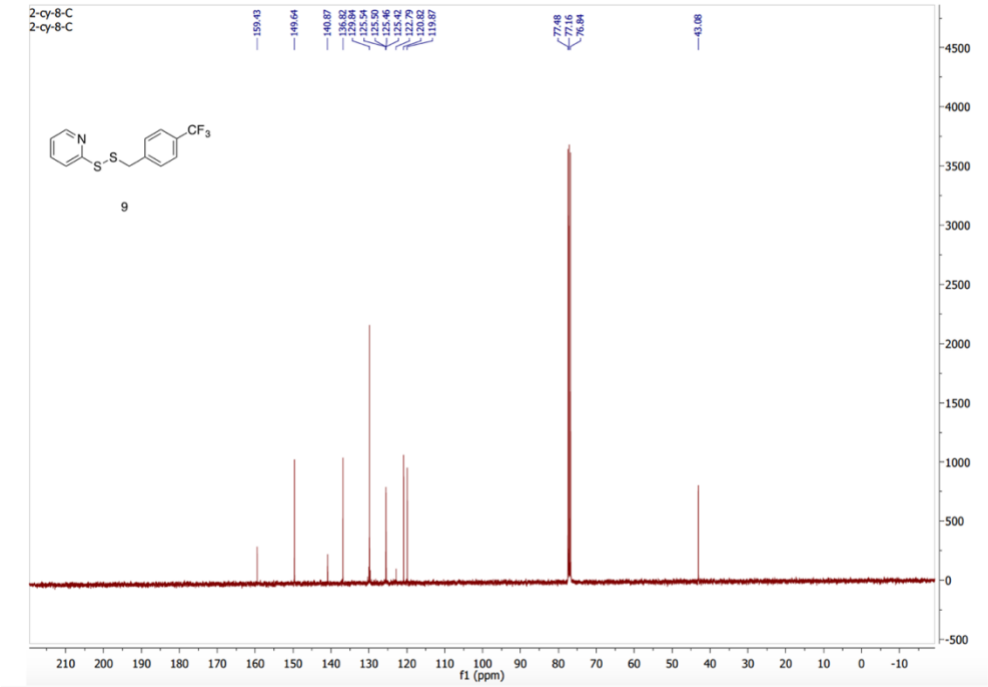
2-cy-8-C
2-cy-8-C
159.43
149.64
140.87
136.82
129.84
125.54
125.50
125.46
125.43
122.79
120.82
119.87
77.48
77.16
76.84
43.08
CF3
N
S
S
9
f1 (ppm)

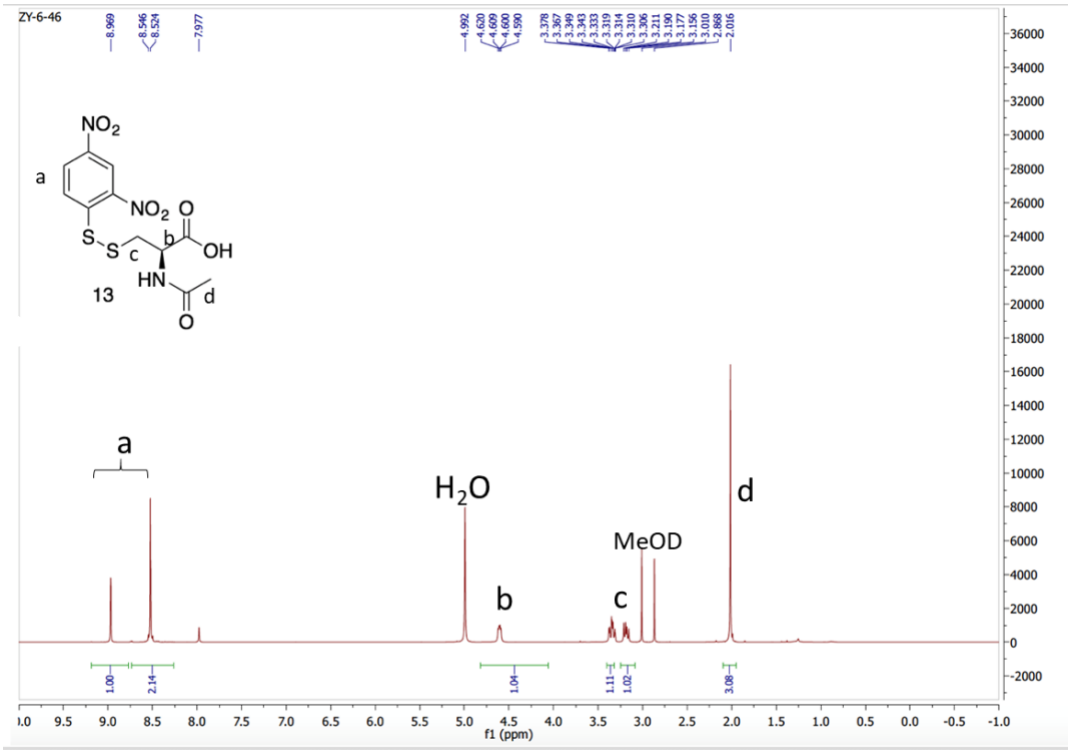
ZY-6-46
NO2
NO2
O
OH
S
S
HN
O
13
a
b
c
d
H2O
MeOD
f1 (ppm)

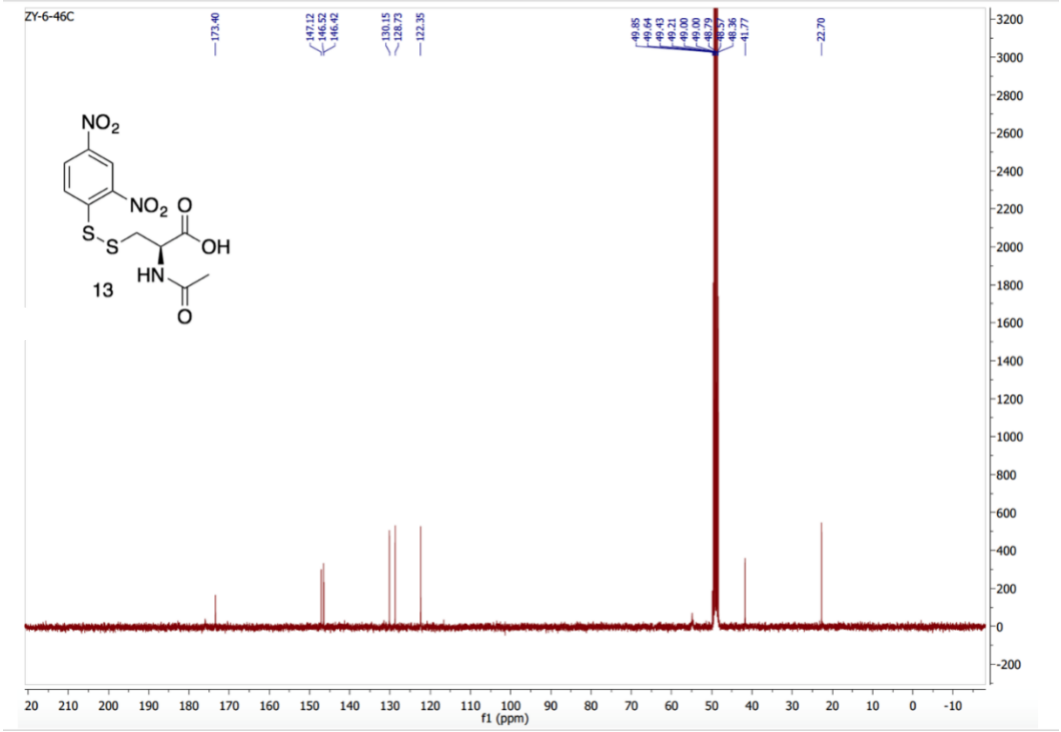
ZY-6-46C
NO2
NO2
O
OH
S
S
HN
O
13
f1 (ppm)

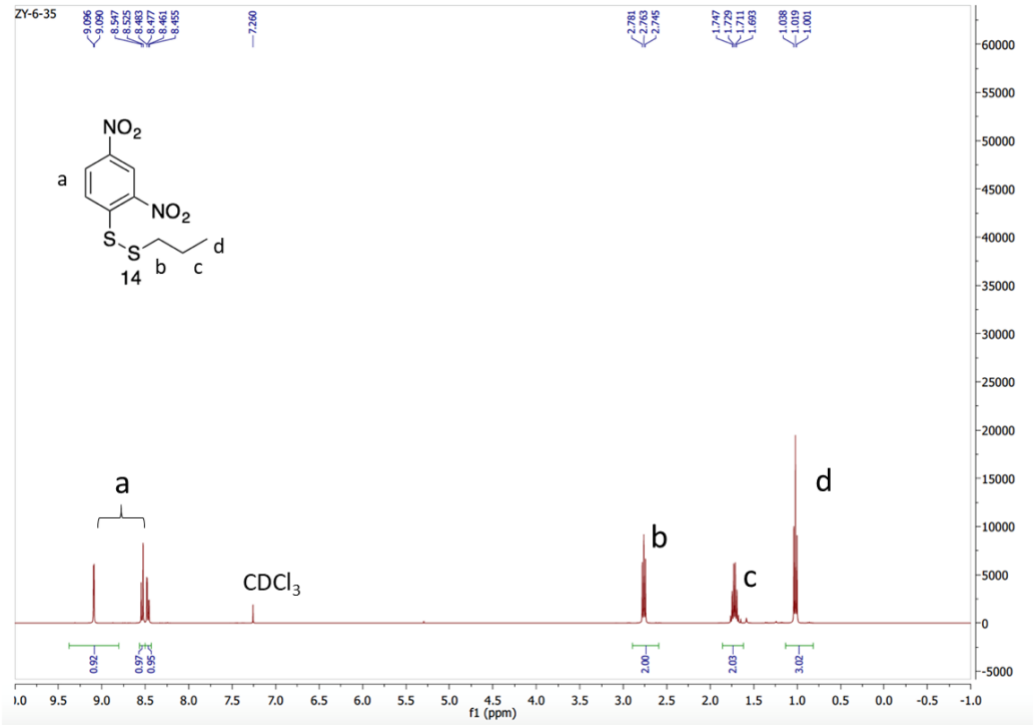
ZY-6-35
NO2
NO2
a
S
S
b
c
d
14
a
CDCl3
b
c
d
f1 (ppm)

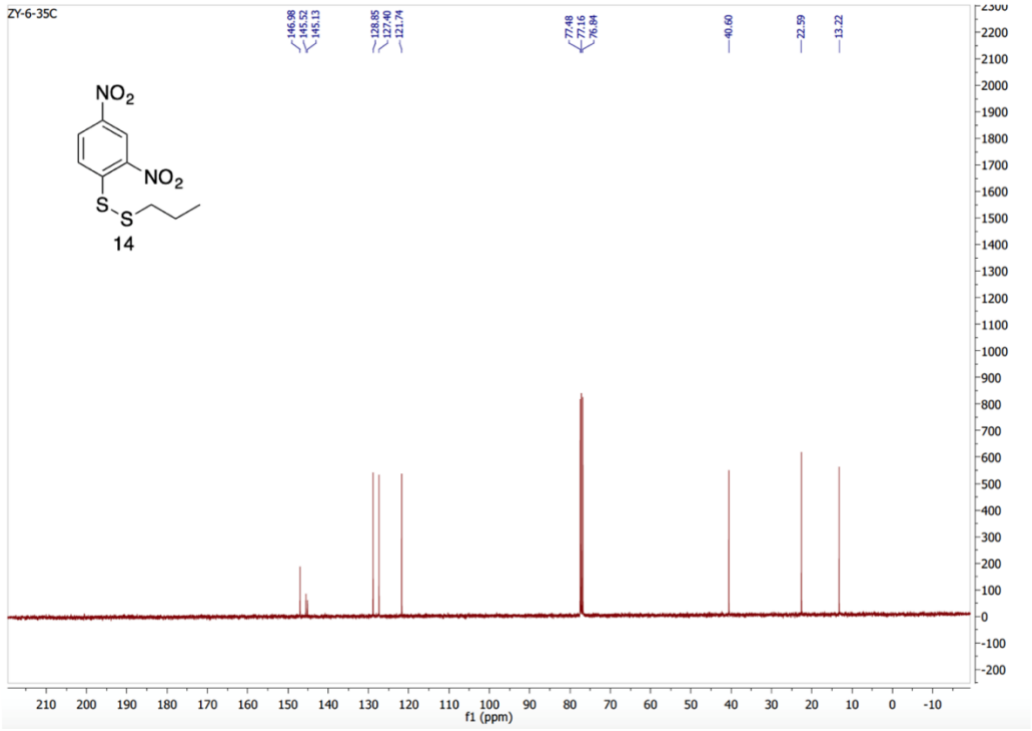
ZY-6-35C
NO2
NO2
S
S
14
f1 (ppm)

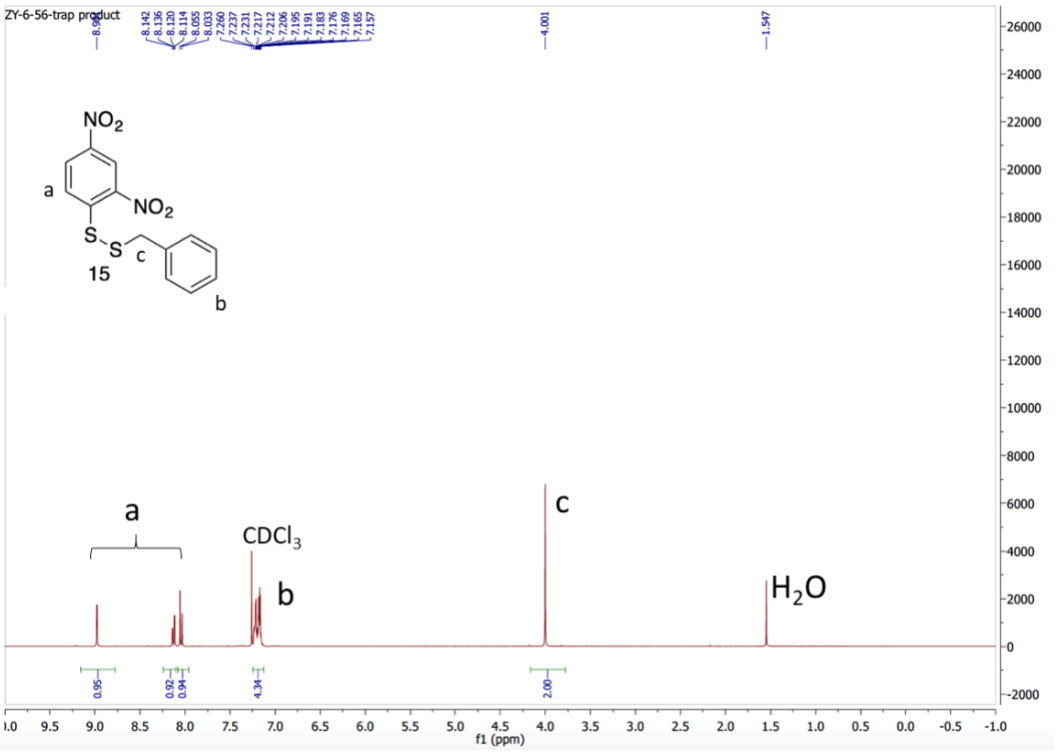
ZY-6-56-trap product
NO2
NO2
a
S
S
c
15
b
a
CDCl3
b
c
H2O
f1 (ppm)

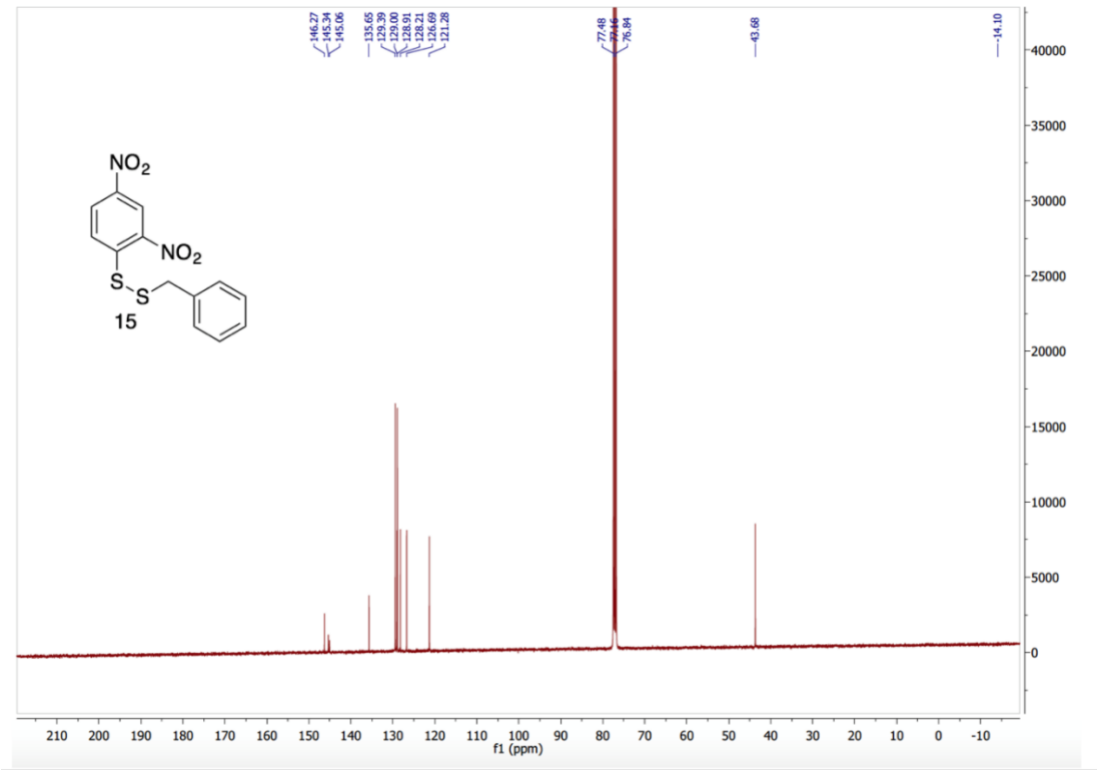
NO2
NO2
S
S
15
f1 (ppm)

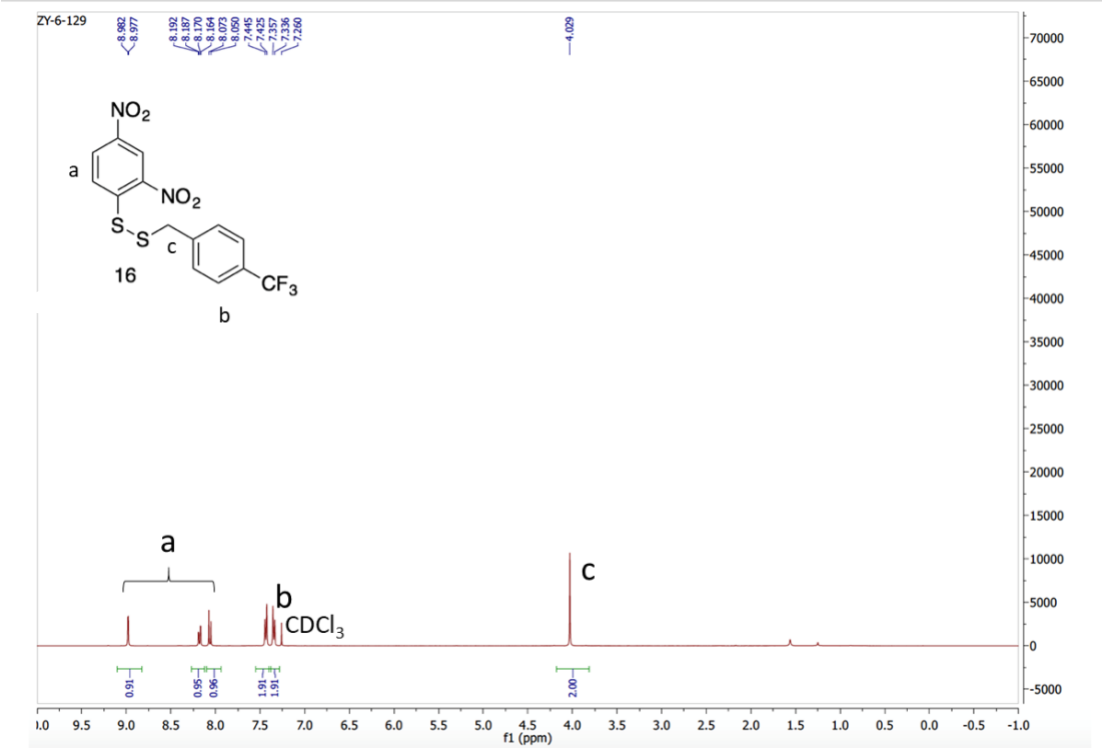
ZY-6-129
8.982
8.977
8.192
8.187
8.170
8.164
8.073
8.050
7.445
7.425
7.337
7.336
7.260
4.029
NO2
NO2
a
S
S
c
16
CF3
b
a
b
CDCl3
c
0.91
0.95
0.96
1.91
1.91
2.00
f1 (ppm)

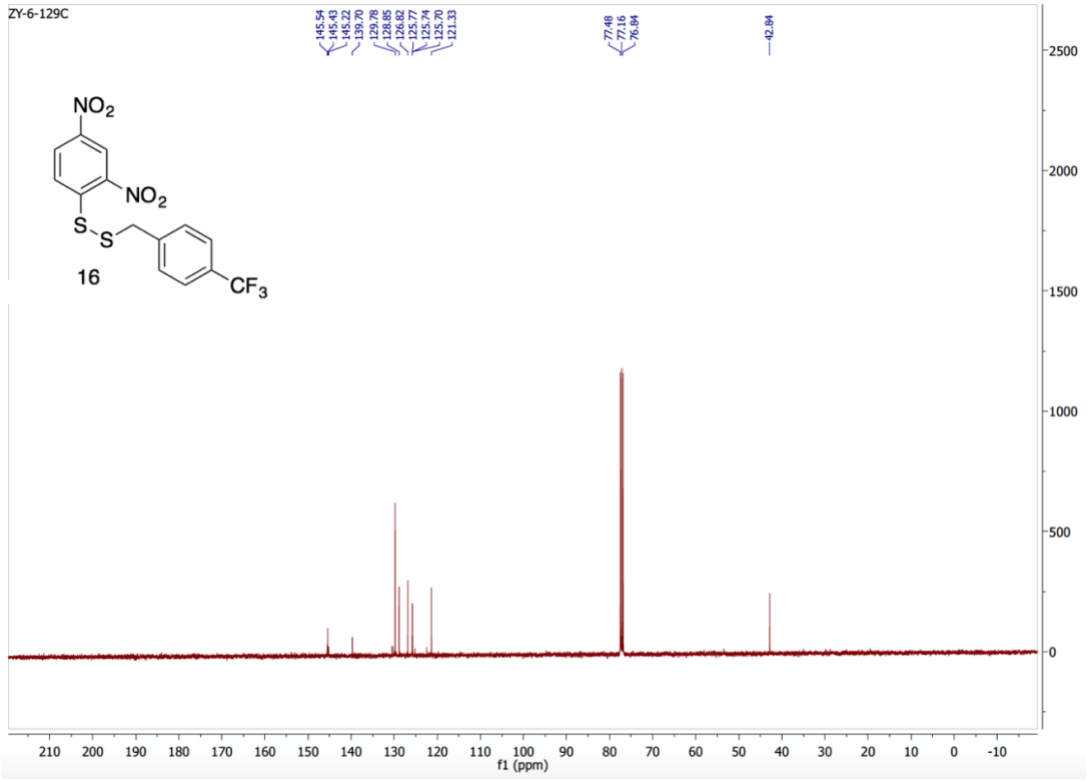
ZY-6-129C
145.54
145.43
145.22
139.70
129.78
128.85
126.82
125.77
125.74
125.70
121.33
77.48
77.16
76.84
42.84
NO2
NO2
S
S
16
CF3
f1 (ppm)

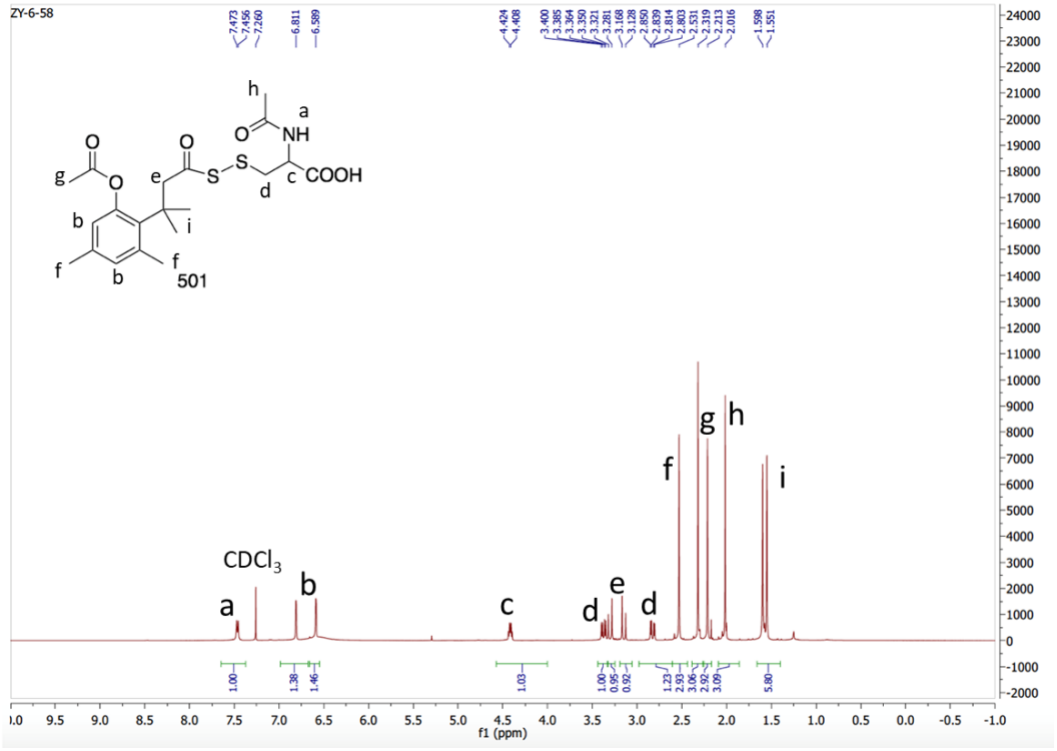
ZY-6-58
CDCl3
501
f1 (ppm)

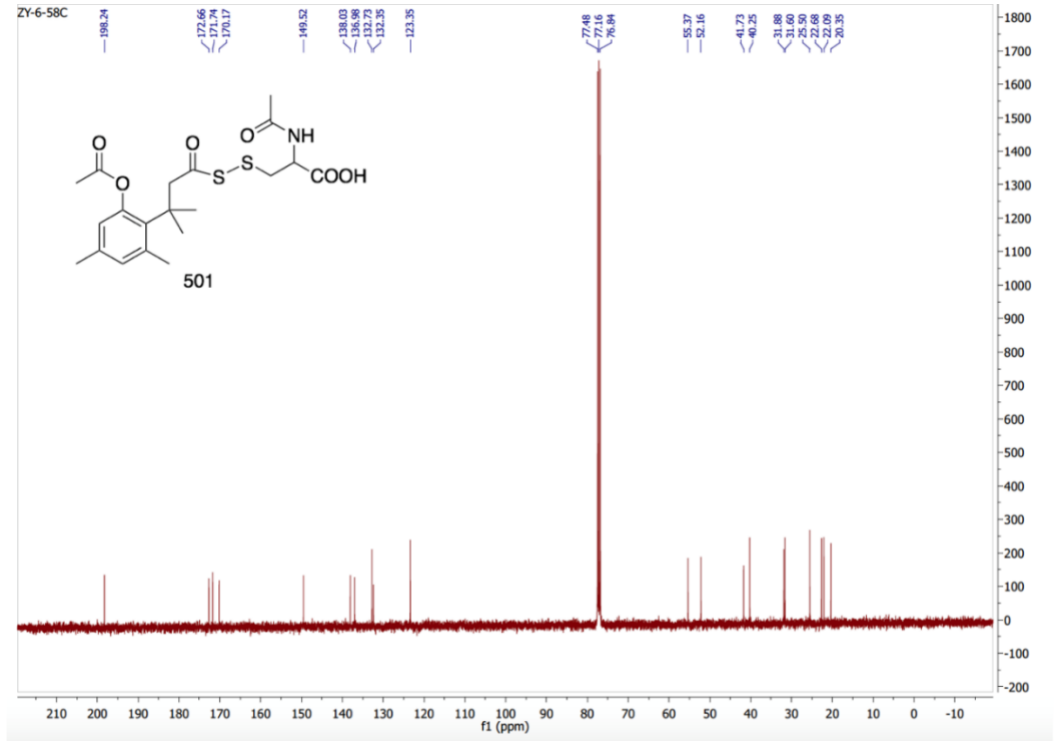
ZY-6-58C
501
f1 (ppm)

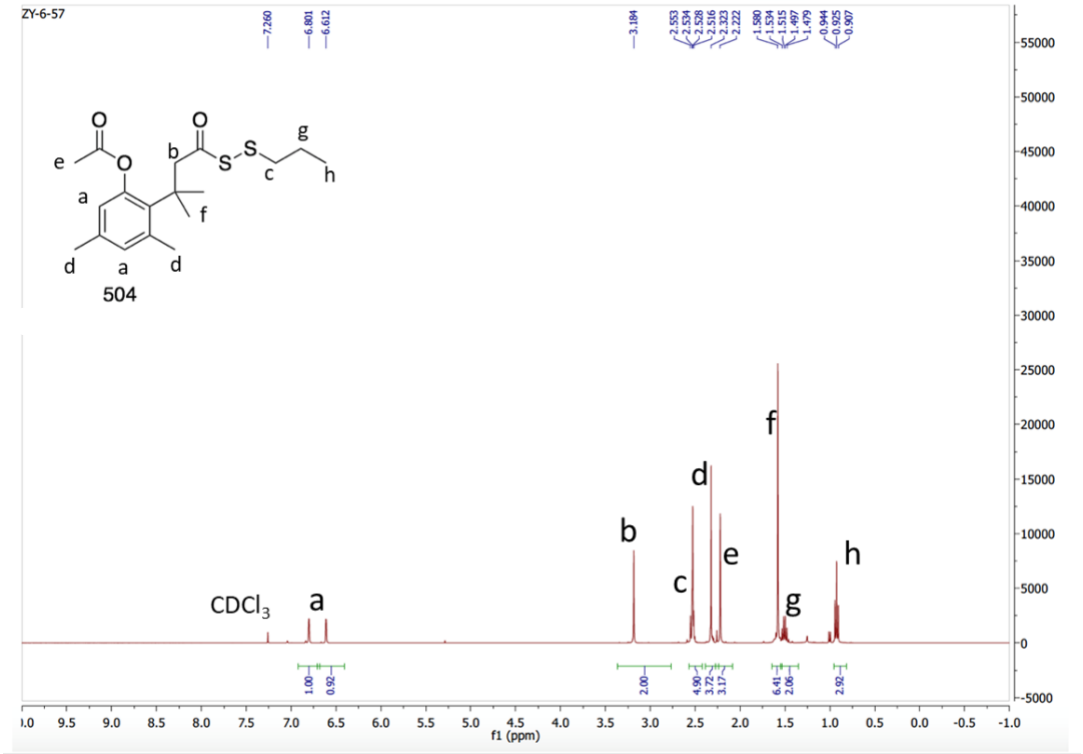
ZY-6-57
504
CDCl3
a
b
c
d
e
f
g
h
f1 (ppm)

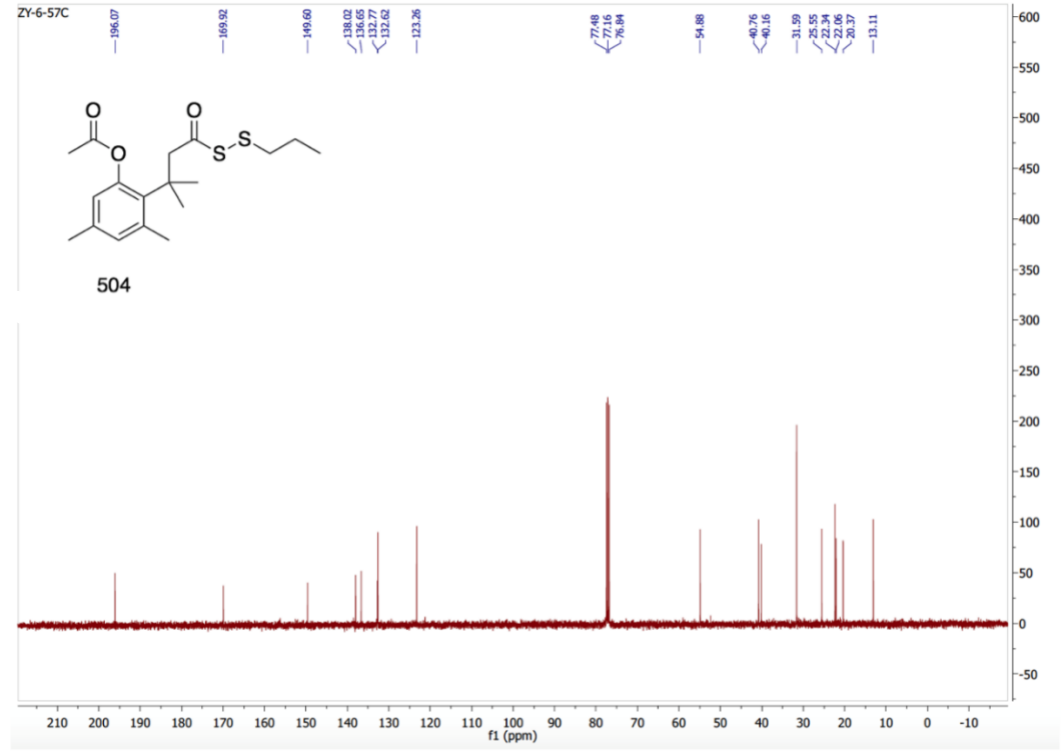
ZY-6-57C
504
f1 (ppm)

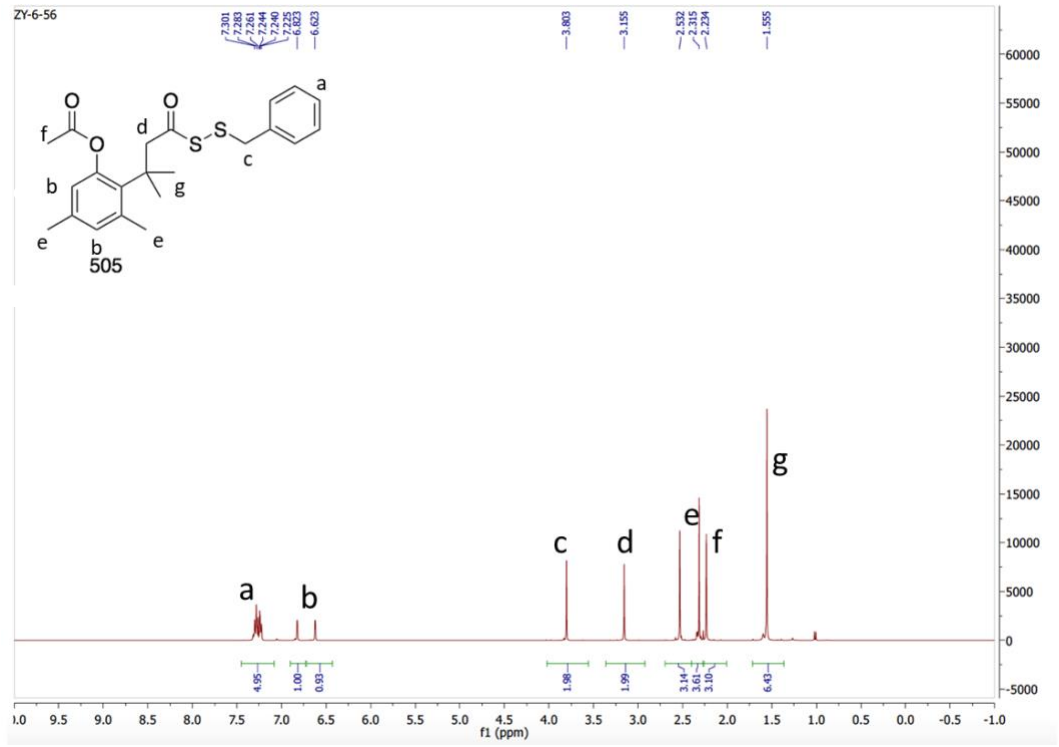
ZY-6-56
505
a
b
c
d
e
f
g
f1 (ppm)

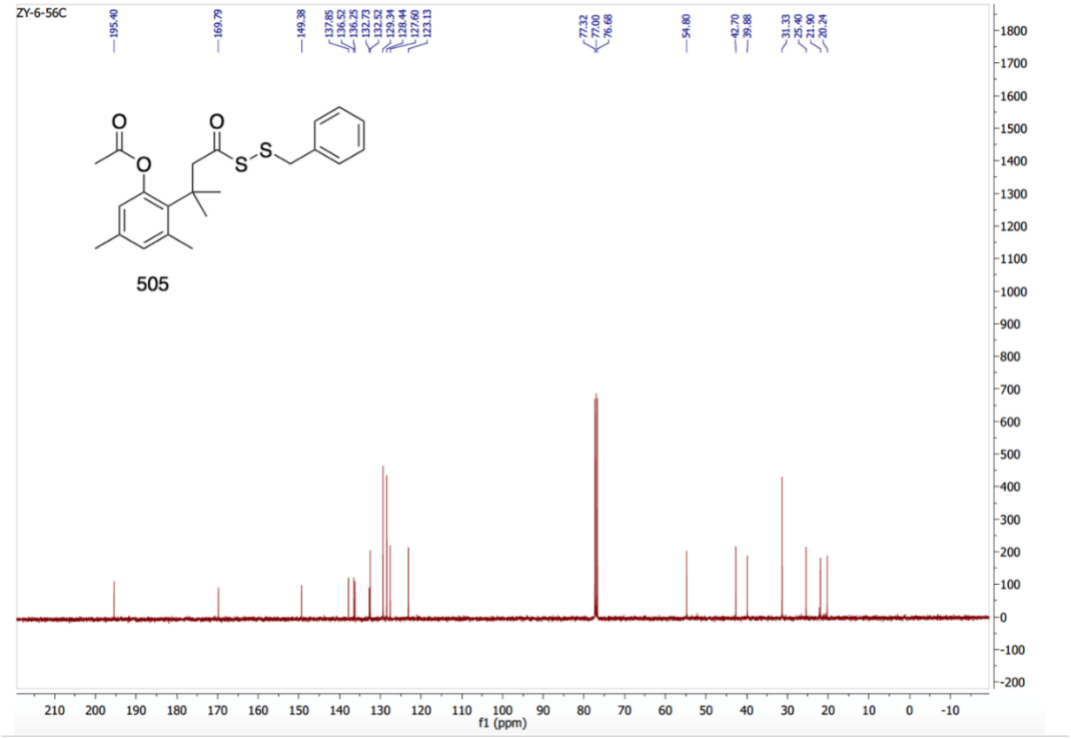
ZY-6-56C
505
f1 (ppm)

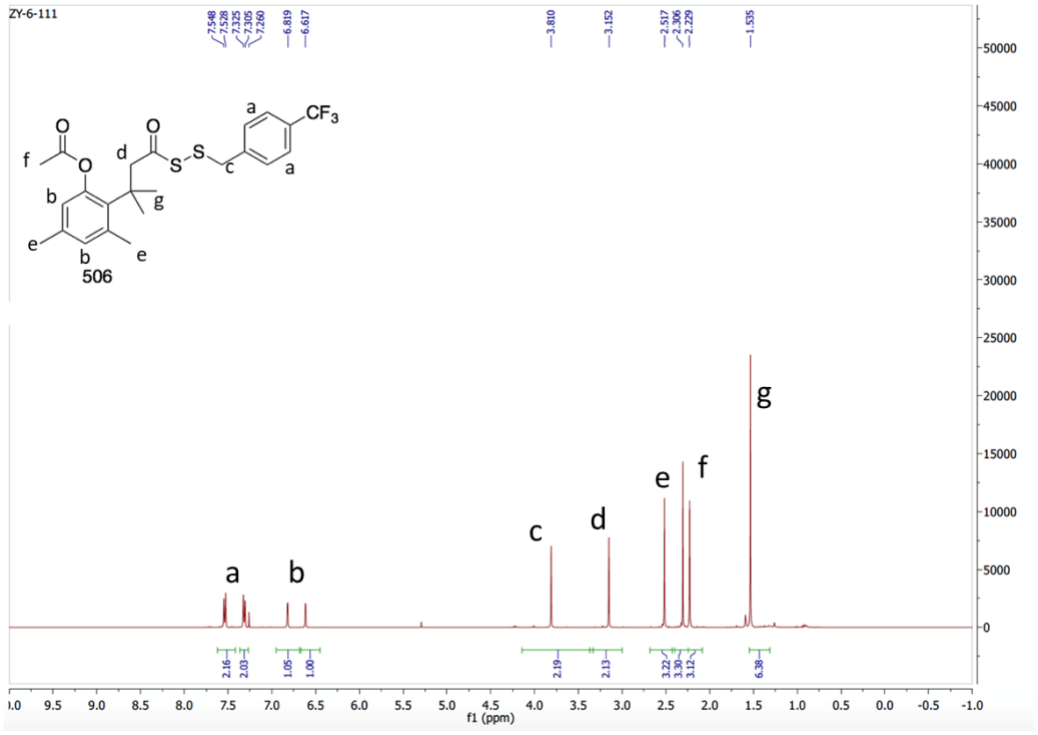
ZY-6-111
506
a
b
c
d
e
f
g
f1 (ppm)

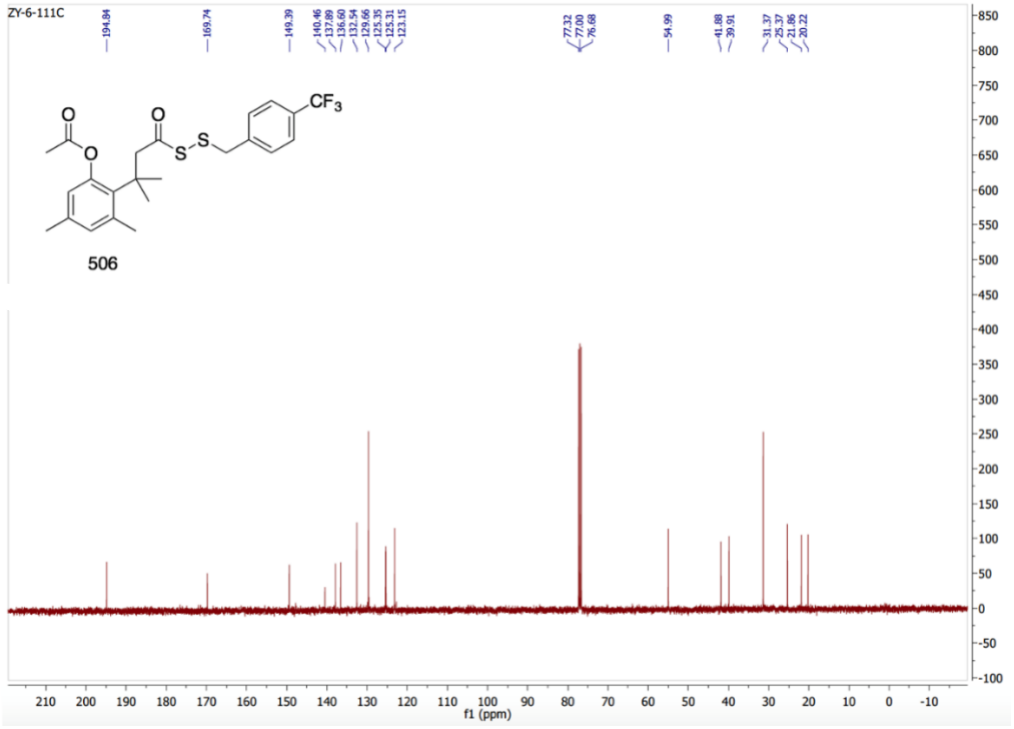
ZY-6-111C
506
f1 (ppm)

Appendix C NMR Spectrum of nitro-based CO probes

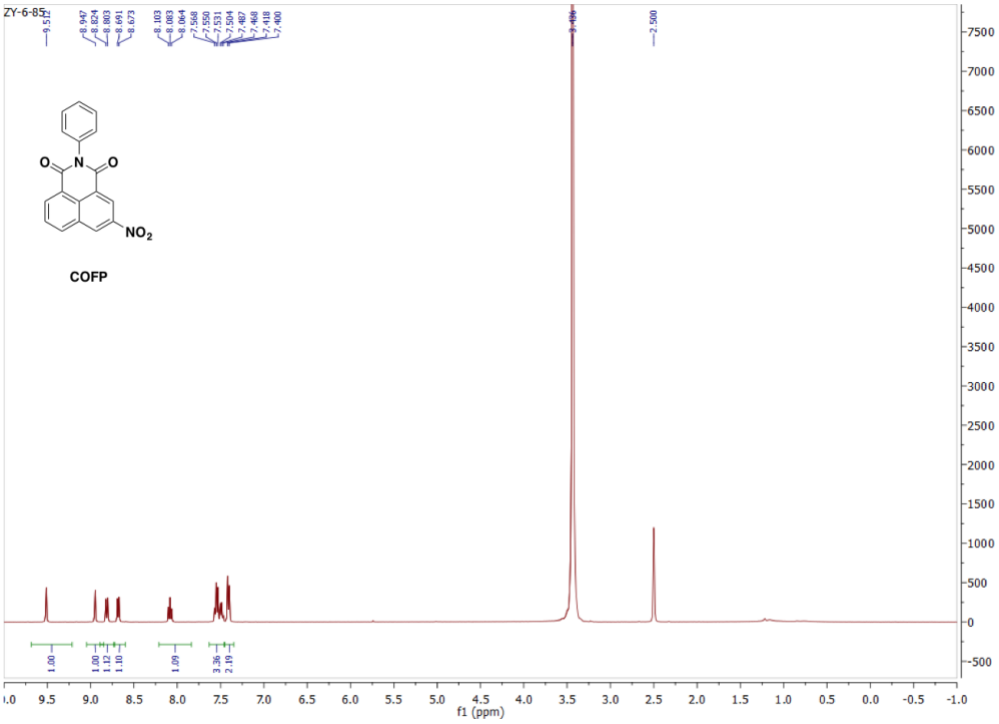

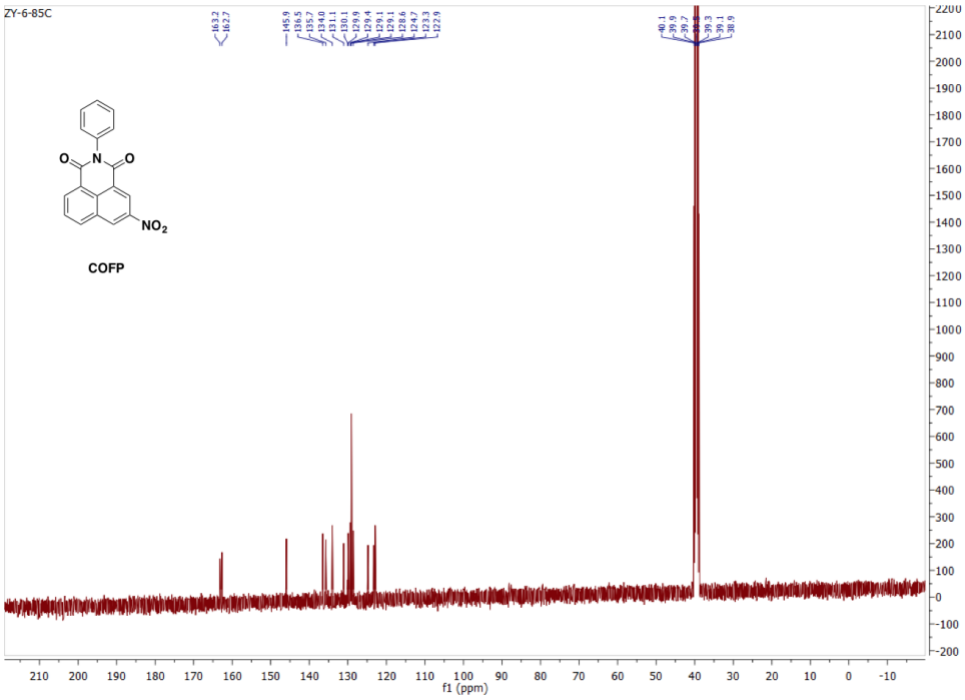

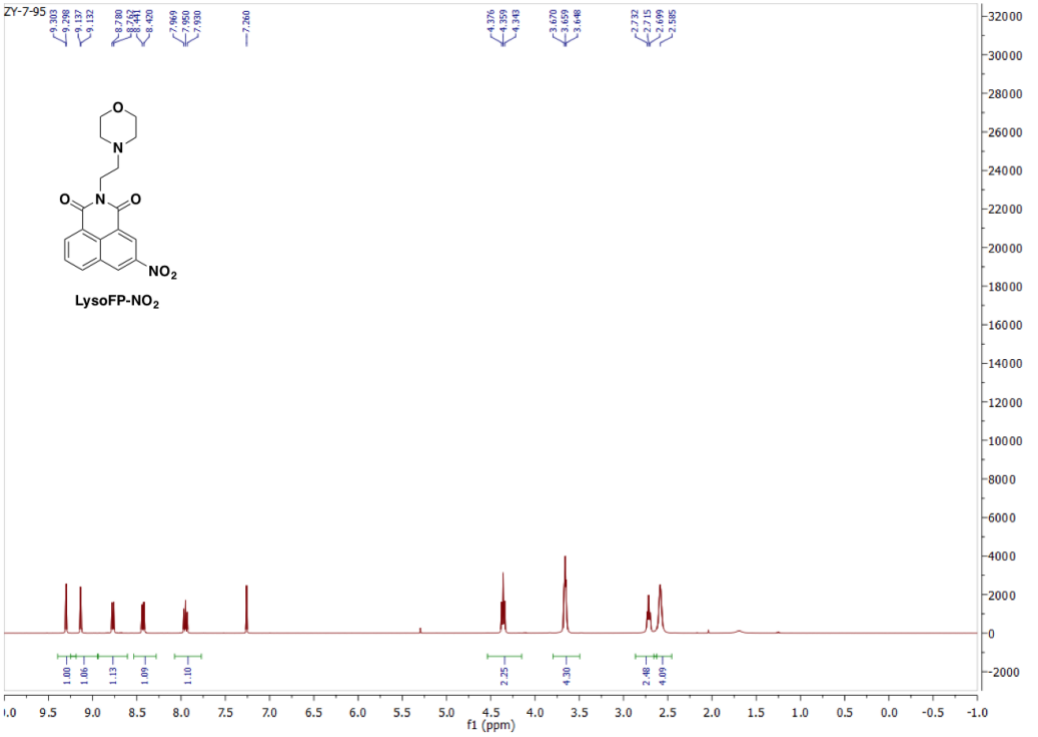
ZY-7-95
LysoFP-NO2
f1 (ppm)

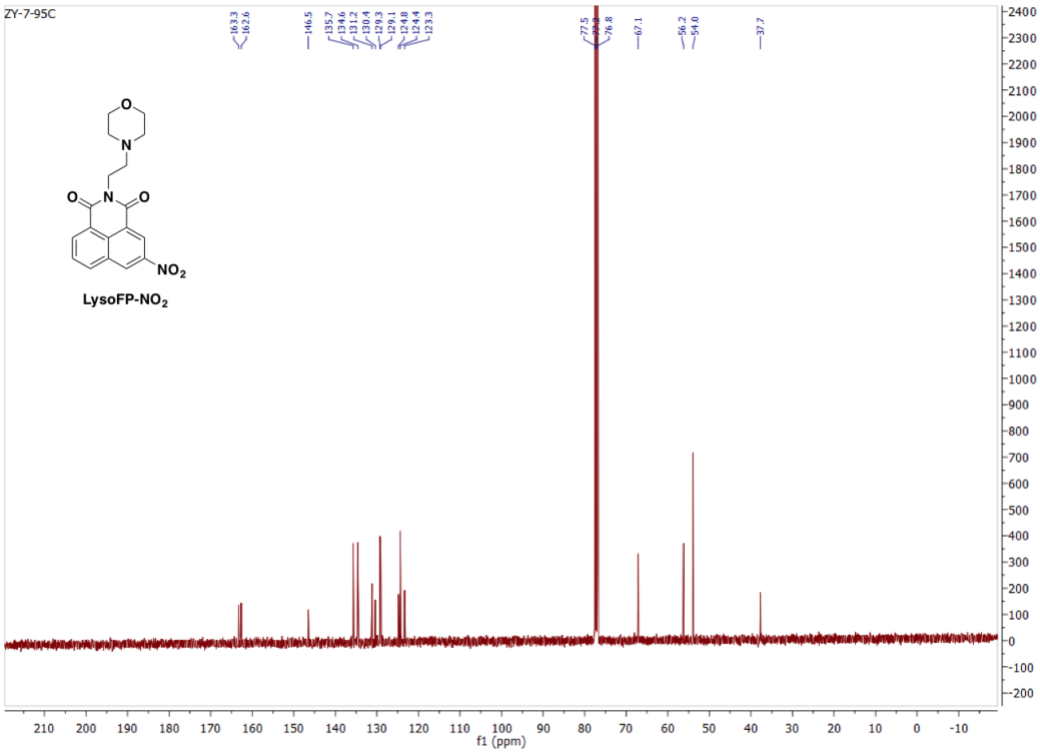
ZY-7-95C
LysoFP-NO2
f1 (ppm)

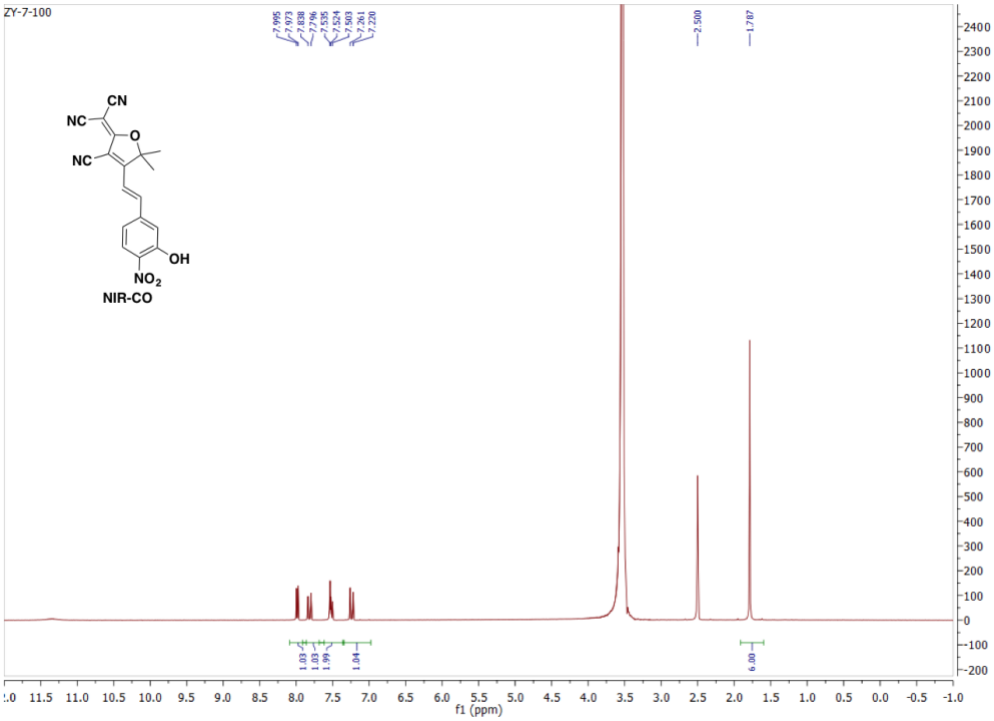
ZY-7-100
7.995
7.973
7.838
7.796
7.535
7.524
7.303
7.261
7.220
2.500
1.787
CN
NC
O
NC
OH
NO2
NIR-CO
1.03
1.03
1.99
1.04
6.00
f1 (ppm)

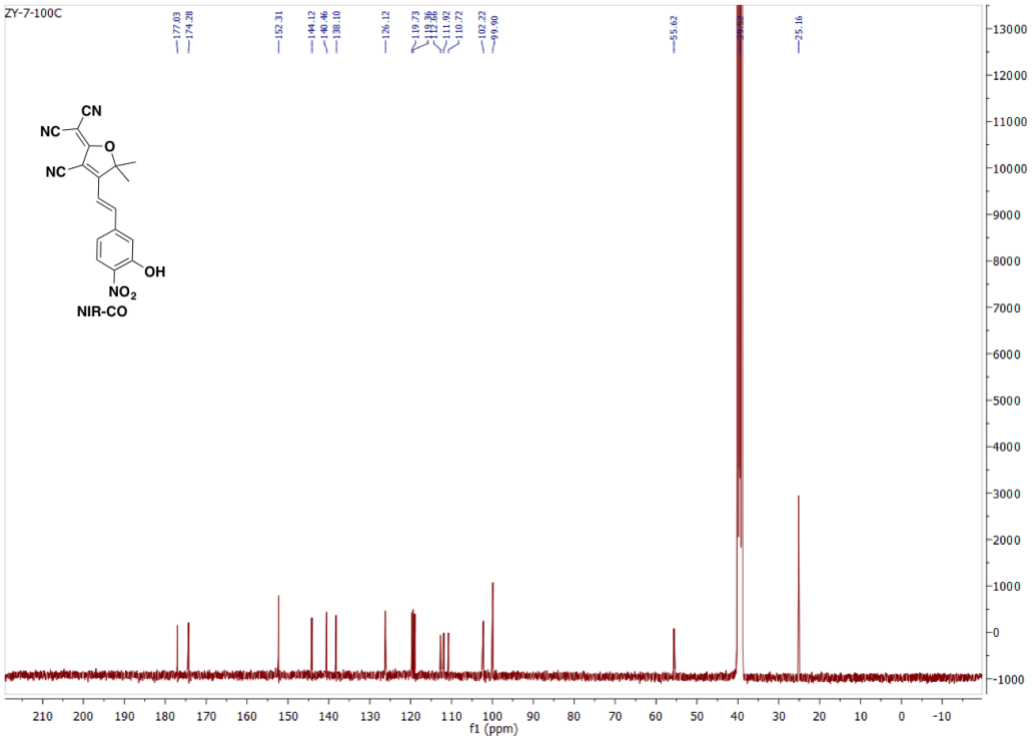
ZY-7-100C
177.03
174.28
152.31
144.12
140.46
138.10
126.12
119.73
115.88
111.92
110.72
102.22
99.90
55.62
39.52
25.16
CN
NC
O
NC
OH
NO2
NIR-CO
f1 (ppm)

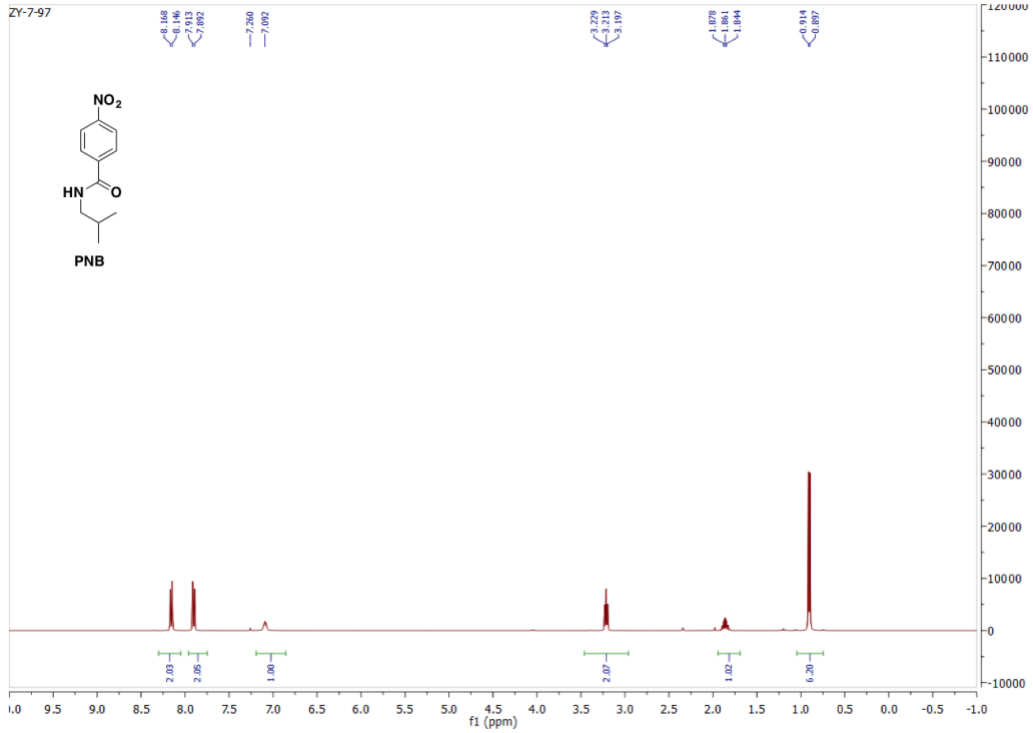
ZY-7-97
8.168
8.146
7.913
7.892
7.260
7.092
3.229
3.213
3.197
1.878
1.861
1.844
0.914
0.897
NO2
HN
O
PNB
2.03
2.05
1.00
2.07
1.02
6.20
f1 (ppm)

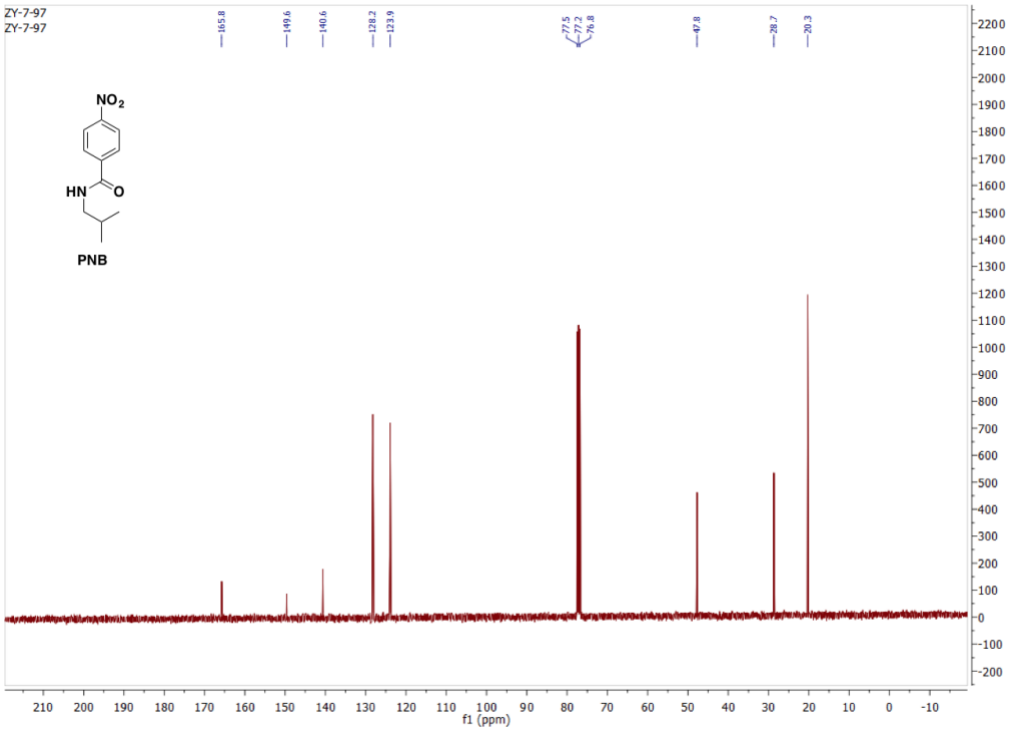
ZY-7-97
ZY-7-97
165.8
149.6
140.6
128.2
123.9
77.5
77.2
76.8
47.8
28.7
20.3
NO2
HN
O
PNB
f1 (ppm)

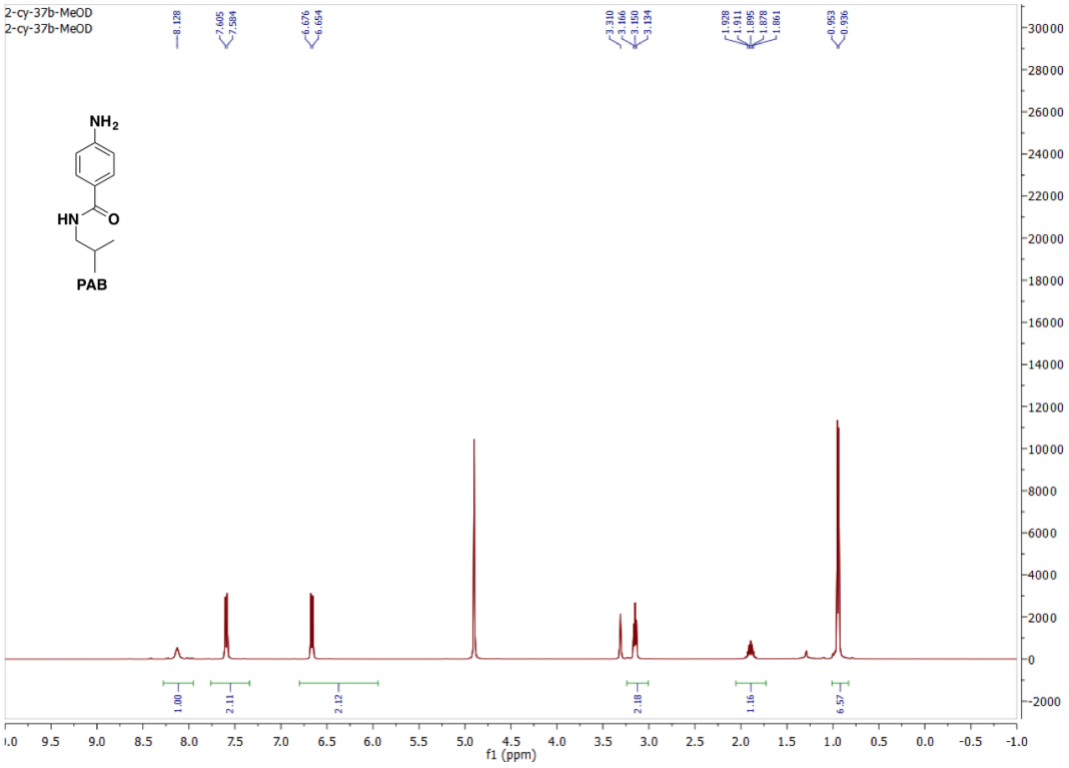
2-cy-37b-MeOD
2-cy-37b-MeOD
NH2
HN
O
PAB
f1 (ppm)

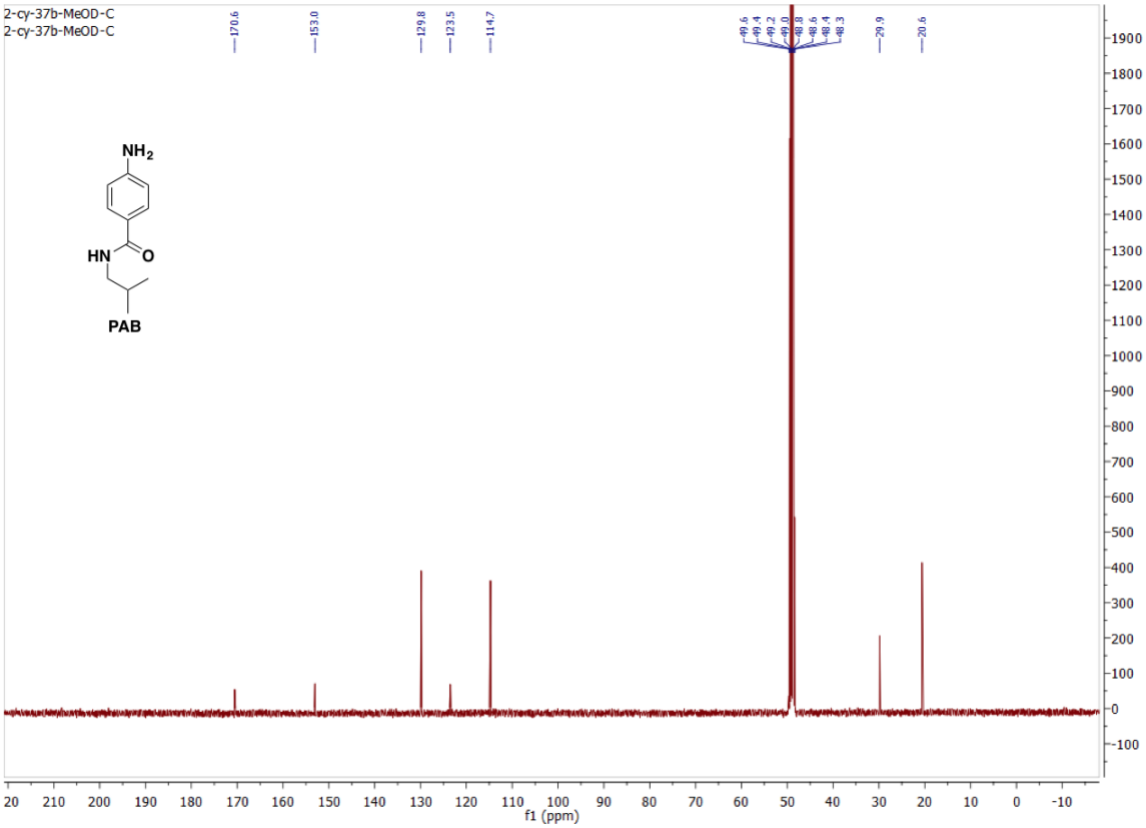
2-cy-37b-MeOD-C
2-cy-37b-MeOD-C
NH2
HN
O
PAB
f1 (ppm)

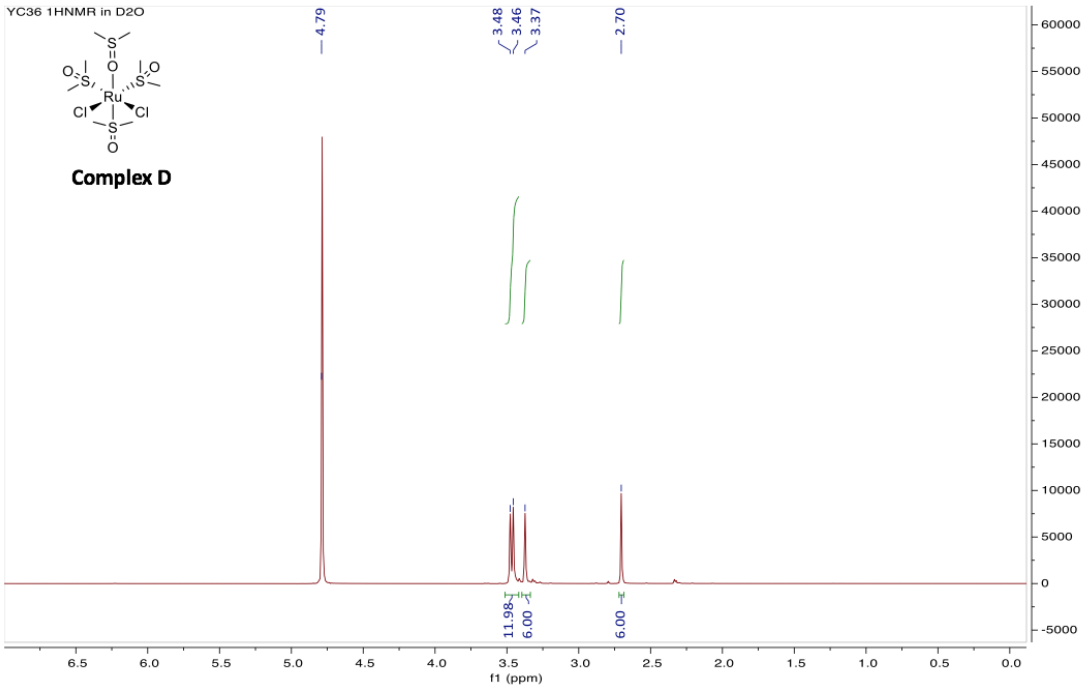
YC36 1HNMR in D2O
Complex D
4.79
3.48
3.46
3.37
2.70
11.98
6.00
6.00
f1 (ppm)

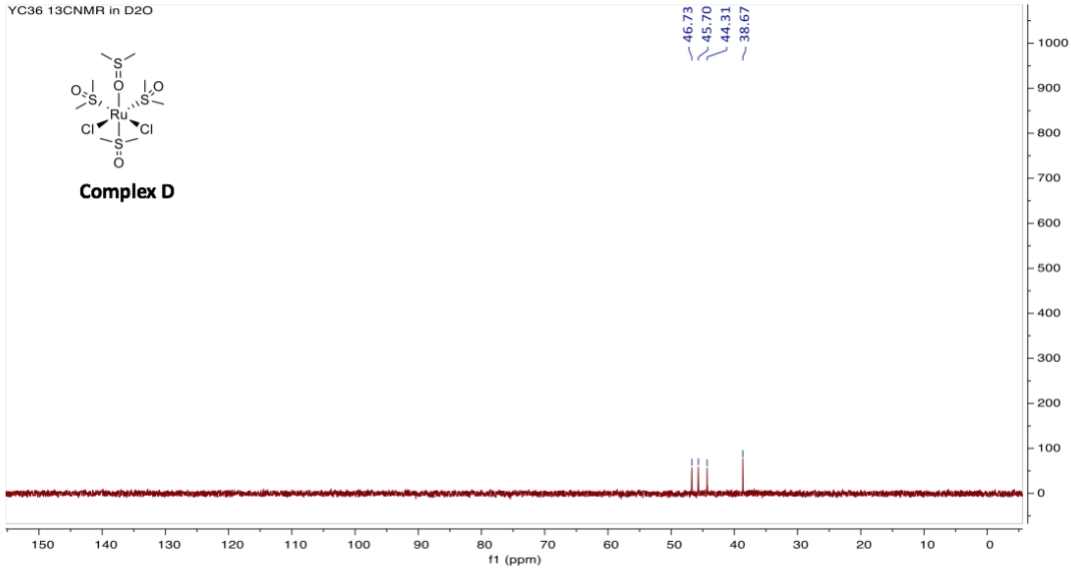
YC36 13CNMR in D2O
Complex D
46.73
45.70
44.31
38.67
f1 (ppm)